EUROPEAN ORGANIZATION FOR NUCLEAR RESEARCH

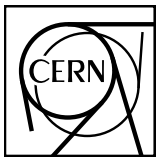

ALICE-ANA-2019-xxx
December 12, 2020

Measurement of an excess in the yield of J/ψ at very low p_T in Pb-Pb collisions at $\sqrt{s_{NN}} = 5.02$ TeV

O. Bugnon[1], M. Guilbaud[1]

1. SUBATECH, IMT Atlantique, Université de Nantes, CNRS-IN2P3, Nantes, France

Email: ophelie.bugnon@cern.ch, m.guilbaud@cern.ch

Abstract

In this note, we report on the excess of J/ψ yield at very low transverse momentum ($p_T < 0.3$ GeV/c) in the forward rapidity region ($2.5 < y < 4$). The analysis is performed from peripheral to more central events using the full Pb–Pb $\sqrt{s_{NN}} = 5.02$ TeV sample from 2015 and 2018 data taking. Therefore, the presented results extend greatly previous studies performed at $\sqrt{s_{NN}} = 2.76$ TeV and $\sqrt{s_{NN}} = 5.02$ TeV in peripheral Pb–Pb collisions. In this study, the coherent photoproduction is assumed to be the driving physics mechanism to explain such a J/ψ yield excess and the results are shown as a function of centrality. In light of the obtained results, new theoretical motivations and implications will be discussed.

Contents

1 Introduction **4**

2 Detector description **4**

3 Data and event selection **4**

3.1 Data sample . . . 4

3.2 Event selection . . . 5

3.3 Muon track cuts . . . 5

4 Monte-Carlo productions **6**

5 Luminosity and normalization factor **8**

5.1 Offline method . . . 8

5.2 Online method . . . 8

5.3 Pile-up factor . . . 9

5.4 Results . . . 9

5.5 Luminosity . . . 9

6 Raw signal extraction **10**

6.1 Systematic tests . . . 10

6.2 Invariant mass fit . . . 11

6.3 Combination of systematic tests . . . 17

6.4 Results . . . 17

7 Acceptance Efficiency correction **24**

7.1 Hadronic Acceptance Efficiency . . . 24

7.1.1 Sytematic uncertainty on MC inputs . . . 25

7.2 J/ψ coherent photoproduction Acceptance Efficiency . . . 25

8 Modelization of the hadronic contamination in the low p_{T} J/ψ production **31**

8.1 Measurement of the $R_{\mathrm{AA}}^{\mathrm{h\ J/\psi}}$ . . . 31

8.2 Parametrisation of the $R_{\mathrm{AA}}^{\mathrm{h\ J/\psi}}$ . . . 36

8.3 Parametrisation of the pp reference cross section . . . 38

8.4 Parametrization of the hadronic Acceptance Efficiency . . . 39

8.5 Results hadronic J/ψ at very low p_{T} . . . 39

9 J/ψ coherent photoproduction cross section **49**

9.1 Systematic uncertainties 50

9.2 Results 50

A Run lists **59**

B Fit Functions **60**

C Tails set for signal extraction **61**

D Results signal extraction **64**

E Results differential pp cross **68**

F Results J/ψ acceptance efficiency **69**

G Results J/ψ R_{AA} **78**

H Additionnal check with the corrected yield **82**

Presentations

PAG presentaions

7 June 2019 : https://indico.cern.ch/event/826269/
4 March 2020 : https://indico.cern.ch/event/872377/
10 April 2020 : https://indico.cern.ch/event/908527/
5 June 2020 : https://indico.cern.ch/event/926496/
4 September 2020 : https://indico.cern.ch/event/951477/
2 Octber 2020 : https://indico.cern.ch/event/961738/
6 November 2020 : https://indico.cern.ch/event/971941/

PWG-DQ meeting

17 November 2020 : https://indico.cern.ch/event/973352/
1 December 2020 : https://indico.cern.ch/event/976436/

Physics Forum

23 November 2020 : https://indico.cern.ch/event/971860/
9 December 2020 : https://indico.cern.ch/event/979254/

ALICE mini week

17 June 2020 : https://indico.cern.ch/event/925992/
21 October 2020 : https://indico.cern.ch/event/963856/

ALICE week

7 July 2020 : https://indico.cern.ch/event/929805/

1 Introduction

Properties of the color-deconfined quark gluon plasma (QGP) created in sufficiently high energy collisions of heavy nuclei can be studied using heavy-quark resonances produced in initial hard scatterings. Yields of various quarkonium states, which have a short formation time in their rest frames and can typically escape the QGP before they decay, encode information on the evolution of the plasma from its early stages to the hadronization. In particular, quarkonia yields in heavy ion collisions are expected to be modified with respect to proton-proton (pp) collisions, which serve as a Quantum ChromoDynamics (QCD) vacuum reference. On the one hand, according to Debye screening and glu-dissociation, quarkonia are suppressed sequentially depending on the binding energy of a particular state and the medium temperature. On the other hand, at LHC energies, a competing mechanism known as regeneration can enhance quarkonia production via recombination of charm quarks during or at the end of the deconfined phase. In addition, any collision involving a heavy nucleus in the initial state experiences cold nuclear matter (CNM) effects. Therefore the modification of measured yields of quarkonia in heavy ion collisions result from CNM effects as well as effects of the QGP. The nuclear modification factor ($R_{\rm AA}$) measurement in lead-lead (Pb–Pb) and proton-lead (p–Pb) collisions and the anisotropic flow measurement of quarkonia in Pb–Pb, p–Pband proton-proton (pp) collisions are crucial to understand the relative contributions of the various physics mechanism involved in the quarkonia production. These observables have been extensively studied by ALICE, CMS or LHCb experiments in Pb–Pb, p–Pb and pp collisions at various center-of-mass energies.

Nevertheless, an excess in the J/ψ (the charmonia vector state with the lower mass) with respect to expectations in the hadronic production (suppression/regeneration) scenario was reported by the ALICE collaboration at very low transverse momentum ($p_{\rm T}$) in Pb–Pb collisions at $\sqrt{s_{\rm NN}} = 2.76$ TeV. One of the most plausible explanation for this excess is the coherent photoproduction of J/ψ. Indeed, in Ultra-Peripheral Collisions (UPC), the J/ψ coherent photoproduction has been measured but this contribution was expected to be largely dominated by the J/ψ hadronic production in more central events. This is generally true except in the low $p_{\rm T}$ region. Therefore, to fully understand the J/ψ production in Pb–Pb collisions, the coherent photoproduction of J/ψ has to be studied in details to be able to disentangle the hadronic and electromagnetic contributions and potential QGP like effects affecting their production rates. The phenomenon is interesting on its own since it opens more fundamental questions on how the coherence with an entire nucleus can survive in collisions with nuclear overlap assuming that coherent photoproduction of J/ψ is at the origin of the excess. In addition, the J/ψ photoproduction might be helpful to constrain gluon distribution in nucleus and its potential as a new probe of the QGP must be explored.

In this note, we report on the measurement of J/ψ production in Pb–Pb collisions at $\sqrt{s_{\rm NN}} = 5.02$ TeV at very low $p_{\rm T}$ ($p_{\rm T} < 300$ MeV/c) and forward rapidity. Following the hypothesis that coherent J/ψ photoproduction mechanism is at the origin of the observed excess, the corresponding cross-section is measured as a function of the collision centrality using the full data sample collected in 2015 and 2018. For centrality bins in where the significance of the excess is too low, an upper limit on the cross section is given. This new study greatly enlarge the precision and the centrality reach of the previous measurements and will be a stepping stone for future more differential studies.

2 Detector description

3 Data and event selection

3.1 Data sample

The data sample analised in this work corresponds to three periods of Pb–Pb collisions at $\sqrt{s_{\rm NN}} =$ 5.02 TeV during LHC run-2 : LHC15o, LHC18q and LHC18r. The 365 runs that passed the QA se-

Period	AOD	Pass	Nb runs	Luminosity	Nb of CMUL events after PS
LHC15o	AOD229	muon_calo_pass1	137	$\sim 225\ \mu\mathrm{b}^{-1}$	126395768
LHC18q	AOD225	muon_calo_pass3	130	$\sim 215\ \mu\mathrm{b}^{-1}$	111006434
LHC18r	AOD225	muon_calo_pass3	98	$\sim 320\ \mu\mathrm{b}^{-1}$	162979305

Table 1: Information about data samples

lection are listed in appendix A.

QA for LHC15o : https://twiki.cern.ch/twiki/bin/view/ALICE/MuonPbPbQA2015.
QA for LHC18q and LHC18r : https://twiki.cern.ch/twiki/bin/viewauth/ALICE/MuonPbPbQA2018.

The AOD sets used are AOD229 for the 2015 period and AOD225 for the 2018 periods. The reconstruction passes used are muon_calo_pass1 for 2015 and muon_calo_pass3 for 2018.

We select only events that passed the Physics Selection to ensure a clean data sample. The Physics Selection task used is the standard one. (((AliInputEventHandler*)(AliAnalysisManager::GetAnalysisManager()->GetInputEventHandler()))->IsEventSelected()) & AliVEvent::kMuonUnlikeLowPt7

A summary of these informations are reported in the table 1 with the number of CMUL events that passed the physic selection.

3.2 Event selection

The triggers used for the analysis are listed below.

- Minimum Bias trigger (CINT7) corresponding to a logical AND between signals in V0-A and V0-C. The name of the trigger class used is CINT7-B-NOPF-MUFAST. It was used for the offline normalization of the LHC15o period.
- Minimum Bias trigger (CINT7ZAC) corresponding to a combination of CINT7 and 1ZAC triggers. 1ZAC is a trigger on ZNA and ZNC detectors to remove EM contribution. The name of the trigger class used is CINT7ZAC-B-NOPF-CENTNOPMD. It was used for the offline normalization of the LHC18q and LHC18r periods.
- Minimum Bias trigger (C0V0M) corresponding to the sum of the V0-A and V0-C triggers in addition to a threshold. Depending on the run considered, the name of the trigger class used is CINT7ZAC-B-NOPF-CENTNOPMD or C0V0M-B-NOPF-MUFAST. It was used for the online normalization.
- Dimuon Unlike Low trigger (CMUL7) requires a muon pair of opposite charge sign, each with $p_T \geq 1$ GeV/c in addition to the MB trigger. The name of the trigger class used is CMUL7-B-NOPF-MUFAST.
- Single Muon Low trigger (CMSL7) requires only one muon track fired in the trigger system with $p_T \geq 1$ GeV/c in addition to the MB trigger. The name of the trigger class used is CMSL7-B-NOPF-MUFAST.

3.3 Muon track cuts

Offline cuts are applied to select muon tracks from events that passed the event selection. The muon track selection in the present analysis corresponds to the standard one for quarkonium studies.

- **Matched tracks :** ensure that a track in the tracking system match a track in trigger chambers considering the low p_{T} trigger threshold.

- **Selection on the pseudo-rapidity :** $-4 < \eta < -2.5$ on single muon tracks to ensure that they are in the spectrometer acceptance.

- **Selection on the angle at the end of the front absorber :** must be $2^{\circ} < \theta_{abs} < 10^{\circ}$ to remove tracks crossing the high-Z material part of the absorber, involving multiple scattering.

- $p \times DCA$ **cut** $< 6\sigma$**:** which is the product of the track momentum with its closest distance approach (DCA). It is used to remove tracks which are not coming from the interaction vertex such as beam-gas interactions.

The J/ψ candidates are formed by combining all pairs of opposite sign (OS) tracks that satisfied the above criteria. We operate a selection on the rapidity of the muon pair after reconstruction to stay within the acceptance of the spectrometer : $-4.0 < y_{lab} < -2.5$.

Figure 1 shows the opposite sign dimuon distribution as a function of p_{T} for 5 centrality classes in two invariant mass ranges : $2.8 < m_{\mu\mu} < 3.4$ corresponding to the J/ψ region and $1.5 < m_{\mu\mu} < 2.8$ to compare with pure background distribution, where the $\gamma\gamma \to \mu^{+}\mu^{-}$ could also be present. The curve corresponding to the backgound distribution is normalized to the integral of the "corresponding" J/ψ distribution between 0.65 and 2 GeV/c. One can see that, from 50% centrality, the red distribution, corresponding to the J/ψ invariant mass range, differs significantly from the other at very low p_{T}, i.e. $p_{\mathrm{T}} < 0.3$ GeV/c. It is also interesting to note the presence of the $\gamma\gamma \to \mu^{+}\mu^{-}$ process at very low p_{T} mostly in the 70-90% centrality class. This process peaks at very low p_{T} as for the J/ψ photoproduction while other background contributions should fall to 0 going down to 0 p_{T}.

4 Monte-Carlo productions

Simulations for hadroproduced J/ψ based on the embedding technique. This technique consists of adding real data events to each simulated signal in order to recreate the detector response. One MC J/ψ signal is embedded in each CINT7-B-NOPF-MUFAST event triggered in the data to recreate the most realistic occupancy of the detector. Then we perform the reconstruction of the J/ψ as it's performed for real data. The simulation is performed run by run following kinematics distributions over p_{T} and rapidity tuned on real data events in the centrality class 0-90% and taking into account the detector status at each run. The same generated distributions are used for all centrality classes.

LHC16e2 and LHC16e2_plus embedding MC simulations anchored to LHC15o.

LHC19a2 embedding MC simulations anchored to LHC18q and LHC18r.

Simulations for photoproduced J/ψ are using the STARLIGHT generator. The transport of the muons in the detector is performed using GEANT3. The simulations are performed run-by-run to take into account the detector status over the time. In contrast to the simulations for the hadronic contribution, STARLIGHT simulations do not use the embedding technique, not allowing a centrality dependent study.

LHC18c2 STARLIGHT simulations anchored to LHC15o.

LHC20a6 STARLIGHT simulations anchored to LHC18q and LHC18r.

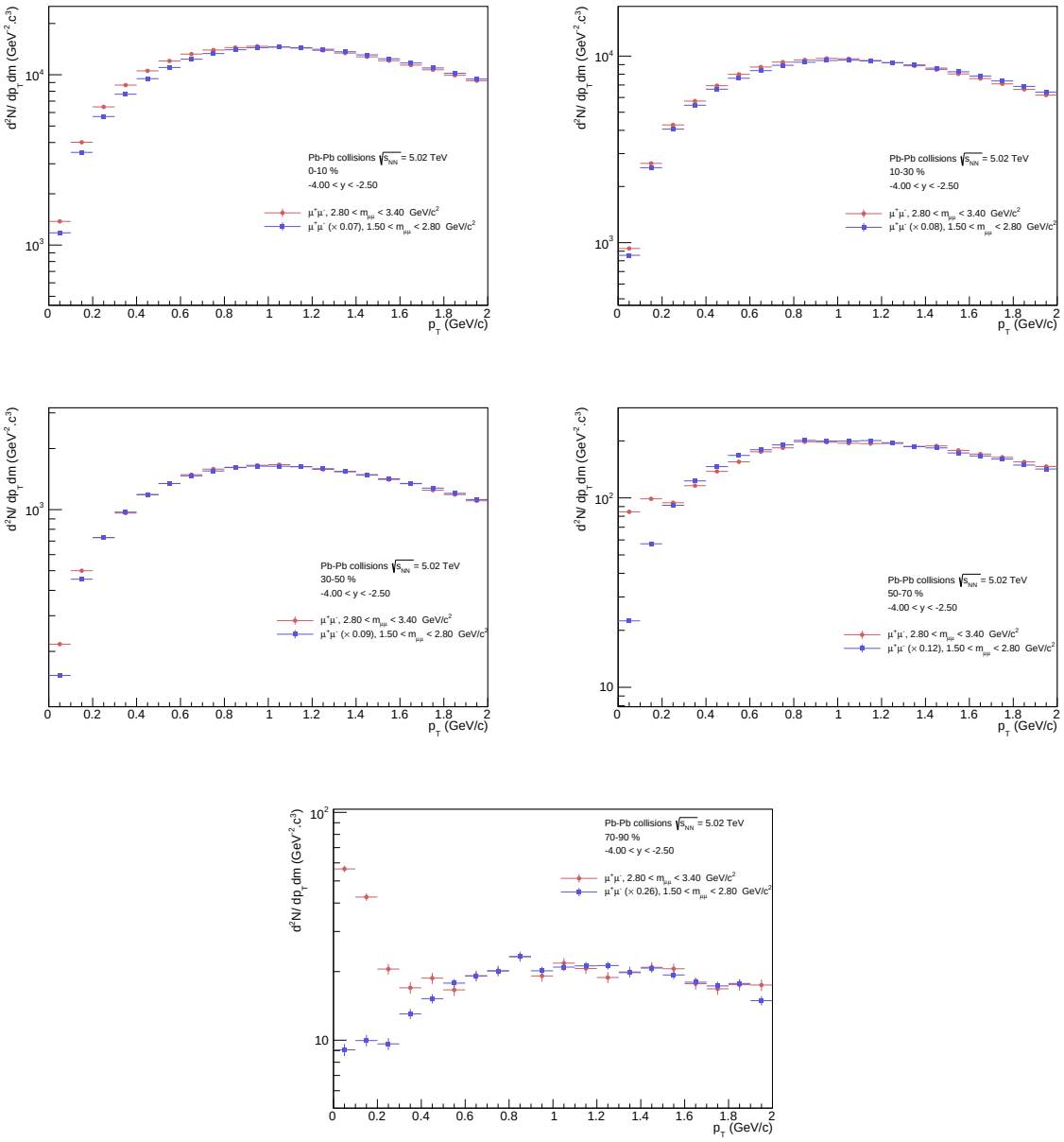

Fig. 1: OS dimuon distribution as a function of p_{T} for 5 centrality classes (0-10%, 10-30%, 30-50%, 50-70% and 70-90%) in two invariant mass ranges : $2.8 < m_{\mu\mu} < 3.4$ (red curve) and $1.5 < m_{\mu\mu} < 2.8$ (blue curve).

NEW : Simulations for photoproduced J/ψ with signal from STARLIGHT embedded in real events.

LHC20g13 embedding STARLIGHT simulations anchored to LHC15o.

LHC20j4 embedding STARLIGHT simulations anchored to LHC18q and LHC18r.

5 Luminosity and normalization factor

The current analysis is based on events containing two opposite sign muons in the rapidity range of the muon spectrometer. Consequently, observables calculated with these selections are biased. In order to compare our results to other data samples or results from other experiments, we need the number of minimum bias events associated to the set of events from the selected trigger of this analysis.

The number of minimum bias events is computed according to the number of CMUL7 events as :

$$N_{\mathrm{MB}}^{\mathrm{eq}} = F_{\mathrm{Norm}}^{i} \times N_{\mathrm{CMUL7}} \tag{1}$$

where F_{Norm} is the normalization factor integrated on the period. A short description of the methods is given in this note. The online method uses C0V0M trigger and the offline method uses the CINT7ZAC trigger. The normalization factor corresponding to the Pb–Pb at 5.02 TeV data sample has been evaluated in [1]. The cited analysis note provides more details on the choice of the MB triggers used.

5.1 Offline method

The first method is based on recorded triggers from offline data (AOD). We compute the offline normalization factor for each run i with the formula below.

$$F_{\mathrm{Norm}}^{\mathrm{off1},i} = \frac{N_{\mathrm{MB}}^{i}}{N_{\mathrm{MB\&0MUL}}^{i}} \tag{2}$$

where N_{MB}^{i} is the total number of minimum bias events and $N_{\mathrm{MB\&0MUL}}^{i}$ is the total number of minimum bias events where a 0MUL input was recorded.

This method can be calculated in two steps to improve the precision by using an intermediate trigger with higher statistics. Using CMSL trigger, the offline factor becomes :

$$F_{\mathrm{Norm}}^{\mathrm{off2},i} = \frac{N_{\mathrm{MB}}^{i}}{N_{\mathrm{MB\&0MSL}}^{i}} \times \frac{N_{\mathrm{CMSL}}^{i}}{N_{\mathrm{CMSL\&0MUL}}^{i}} \tag{3}$$

where N_{CMSL}^{i} is the total number of events and $N_{\mathrm{MB\&0MSL}}^{i}$ ($N_{\mathrm{CMSL\&0MUL}}^{i}$) are respectively the number of minimum bias events (CMSL events) where a 0MSL (0MUL) input was recorded.

5.2 Online method

This method is using the online L0b trigger scalers. It corresponds to L0 inputs sent from the trigger to the CTP. The normalization factor is computed for each run as :

$$F_{\mathrm{Norm}}^{\mathrm{on},i} = \frac{P_{\mathrm{MB}}^{i} \times L0b_{\mathrm{MB}}^{i}}{P_{\mathrm{MUL}}^{i} \times L0b_{\mathrm{MUL}}^{i}} \tag{4}$$

	Offline direct CINT7ZAC	Offline indirect CINT7ZAC	Online C0V0M	F_{Norm}
15o	11.845 ± 0.012	11.851 ± 0.007	11.8754 ± 0.0010	11.88 ± 0.03
18q	13.488 ± 0.006	13.504 ± 0.006	13.5496 ± 0.0012	13.55 ± 0.06
18r	13.633 ± 0.008	13.639 ± 0.006	13.6511 ± 0.0010	13.65 ± 0.02

Table 2: Normalization factors from [1].

where $L0b^i_{\mathrm{MB}}$ and $L0b^i_{\mathrm{MUL}}$ are the L0b inputs for MB and MUL triggers. P_{MB} and P_{MUL} are the purity factors computed offline in order to correct the $L0b$ taken directly from the OCDB where the physics selection is not yet applied. They are calculated as the fraction of events that passed the physics selection and the centrality selection (0-90%) for each trigger.

$$P^i_{\mathrm{trigger}} = \frac{N^i_{\mathrm{trigger}}(\mathrm{PS})}{N^i_{\mathrm{trigger}}(\mathrm{ALL})} \tag{5}$$

5.3 Pile-up factor

The pile-up factor (PU^i) is a correction applied to all the F_{Norm} factors in order to take into account the probability to have more than one interaction in an event. It can be estimated as

$$PU^i = \frac{\mu^i}{1 - e^{-\mu^i}} \tag{6}$$

where μ^i is the mean number of bunch crossing for the run i.

$$\mu^i = -ln\left(1 - \frac{P^i_{\mathrm{MB}} \times L0b^i_{\mathrm{MB}}}{N^i_{\mathrm{colliding}} \times f_{\mathrm{LHC}}}\right) \tag{7}$$

where $N^i_{\mathrm{colliding}}$ is the number of colliding bunches and f_{LHC} the revolutionnary frequency at the LHC.

5.4 Results

The resulting normalization factor for each method is obtained as the weighted average of the factors computed run-by-run :

$$F_{\mathrm{Norm}} = \frac{\sum_i F^i_{\mathrm{Norm}} * N^i_{\mathrm{CMUL}}}{\sum_i N^i_{\mathrm{CMUL}}} \tag{8}$$

Table 2 summarizes the numerical values for the three data taking periods for each method.

The F_{Norm} value used to compute the equivalent number of MB events is chosen as the one with the smallest statistical error, the online method.

The systematic uncertainty is the largest difference between the online C0V0M and either offline methods using CINT7ZAC (or CINT7 for 15o). The statistical error is neglected because the uncertainty is dominated by the systematic uncertainty.

5.5 Luminosity

The integrated luminosity corresponding to the CMUL events is computed as :

$$L_{\mathrm{int}} = \frac{N^{0-90\%}_{\mathrm{MB}}}{0.9 * \sigma_{\mathrm{Pb-Pb}}} \tag{9}$$

with the equivalent number of MB events associated with the number of CMUL triggered events $N^{0-90\%}_{\mathrm{MB}} = F_{\mathrm{Norm}} \times N_{\mathrm{CMUL}}$.

	F_{Norm}	$N_{\text{MB}}^{0-90\%}$	$\mathscr{L}_{\text{int}}$
15o	11.88 ± 0.03	$1\,501\,581\,724 \pm 3\,791\,873$	$\sim 225\ \mu\text{b}^{-1}$
18q	13.55 ± 0.06	$1\,504\,137\,181 \pm 6\,660\,386$	$\sim 215\ \mu\text{b}^{-1}$
18r	13.65 ± 0.02	$2\,224\,667\,513 \pm 3\,259\,586$	$\sim 320\ \mu\text{b}^{-1}$
Total	$\sim$	$5\,230\,386\,418 \pm 13\,711\,845$	$758 \pm 38.4\ (5\%)\ \mu\text{b}^{-1}$

Table 3: Normalization factors, number of MB events and integrated luminosity for each period.

$\sigma_{\text{Pb-Pb}}$ is the nucleon-nucleon inelastic cross section given by [2]. The value adopted is $\sigma_{\text{Pb-Pb}} = 7.67 \pm 0.16$ b

The number of equivalent MB events has been evaluatd for the each period using the value reported in table 2 and the number of CMUL events reported in table 1. The total number of MB events for the three periods is $N_{\text{MB}} = 5.2303864.10^9 \pm 13711845\ (syst.)$.

6 Raw signal extraction

The signal extraction is performed by fitting the dimuon OS invariant mass distribution. The function is a sum of two functions describing the resonance peaks of the two lowest charmonia states (J/ψ and ψ(2S)) and one function describing the background shape.

We performed several tests to extract the raw number of J/ψ and the associated statistical and systematic uncertainties. These tests are a combination of several functions, fitting ranges and function parameters as detailed below.

6.1 Systematic tests

Signal : Functions used to describe the signal shape are presented in [3]. One signal function per ψ state with excited-state parameters constrained with J/ψ parameters: $m_{\psi(2S)} = m_{\text{J}/\psi} + (m_{\psi(2S)} - m_{\text{J}/\psi})_{\text{PDG}}$ and $\sigma_{\psi(2S)} = \sigma_{\text{J}/\psi} * 1.05$.

- Double Cristal Ball extended : Gaussian core with power law tails (CB2)
- Function used by the NA60 experiment (NA60)

Background : The background was fitted either with :

- A quadratic variable width gaussian (qVWG)
- A ratio of second order polynomial over a third order polynomial (Pol2/Pol3)

Two invariant mass fitting ranges were tested :

- $2.2 < m_{\mu\mu} < 4.5$ GeV/c^2
- $2.4 < m_{\mu\mu} < 4.7$ GeV/c^2

Signal tails : Tails for the CB2 and NA60 functions are extracted for the three p_{T} ranges used in this analysis. In the p_{T} bin 0-0.3 GeV/c, three hypothesis are assumed on the production process : hadronic, coherent and incoherent photoproduction. In the p_{T} bin 0.3-1 GeV/c, the hypothesis are constrained to hadronic and incoherent photoproduction while in the p_{T} bin 1-8 GeV/c, we assume that only the hadronic production is at the origin of the J/ψ production. The simulation productions are weighted

run-by-run with respect to the number of CMUL events in the data. Tails from simulations are extracted from a fit to the pure signal invariant mass in the range [1;5] GeV/c^2. The tails parameters are p_{T} and y dependent but are not the centrality dependent.

- tails obtained by fitting the hadronic J/ψ production from embedding MC simulations. Results in table C.1.
- tails obtained by fitting the hadronic J/ψ production from pp data at $\sqrt{s_{\mathrm{NN}}} = 13$ TeV. Tails extracted only for the CB function for each fitting range and for each background function. Results in table C.4.
- tails obtained by fitting the coherent J/ψ photoproduction from STARLIGHT simulations (without embedding) for the lowest p_{T} bin. Results in table C.3.
- tails obtained by fitting the incoherent J/ψ photoproduction from STARLIGHT simulations (without embedding) for the two lowest p_{T} bins. Results in table C.3.

The tails are then fixed for the signal extraction.

6.2 Invariant mass fit

For each test, the fit is performed with a log likelihood method. The likelihood approach allows to properly take into account the empty bins, when fitting histograms with low statistics. A fit is assumed to be valid if the three conditions below are satisfied :

- the fit status must be 0, meaning that the fit converged.
- $\chi^2/\mathrm{NDF} < 2.5$.
- the covariance matrix status must be 3, meaning that the covariance matrix has been successfully calculated.

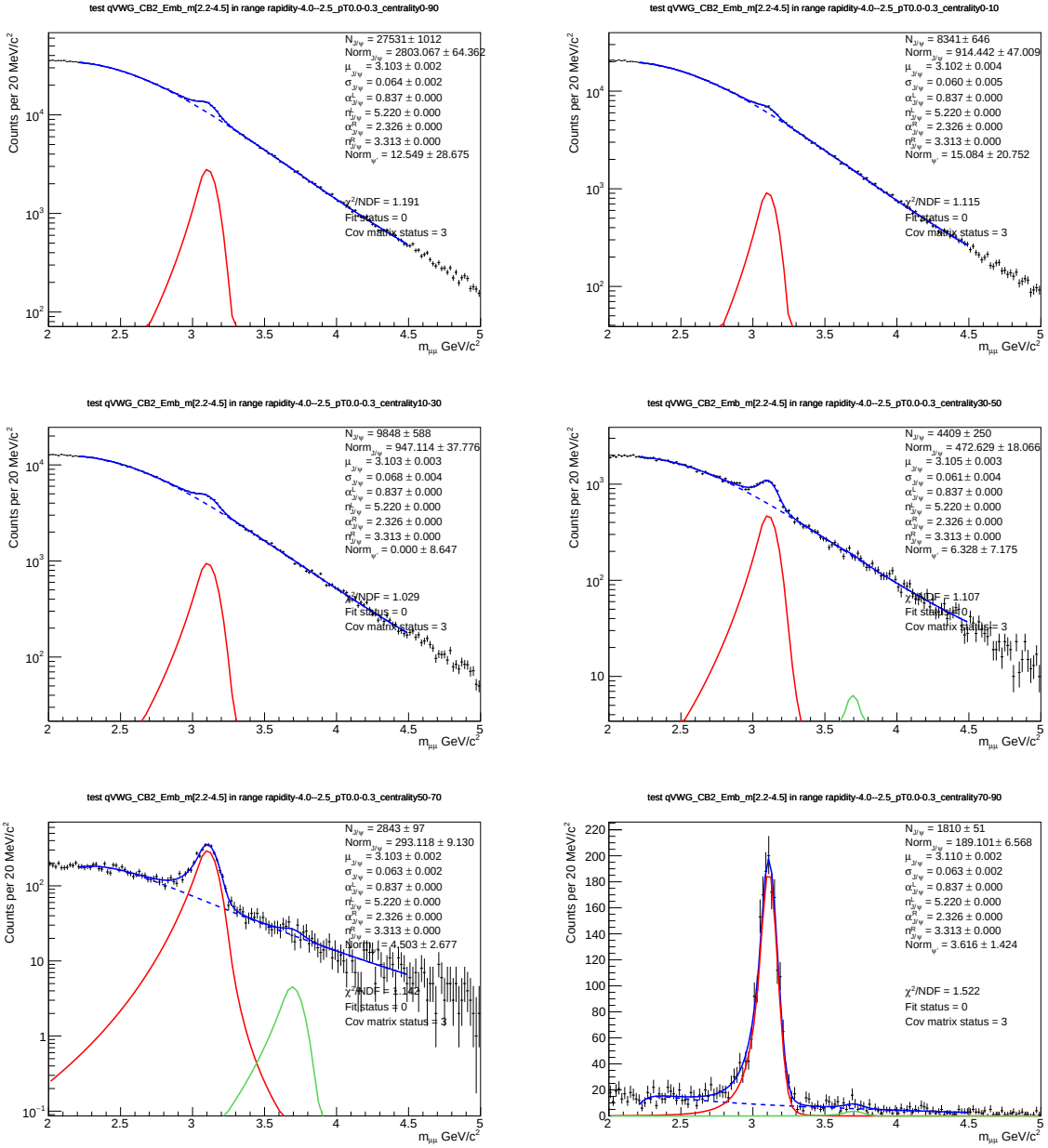

Fig. 2: OS dimuon invariant mass distribution fit, in $0 < p_{\mathrm{T}} < 0.3$ GeV/c for the centrality ranges: 0-90%(top left), 0-10%(top right), 10-30% (middle left), 30-50% (middle right), 50-70% (bottom left), 70-90% (bottom right)

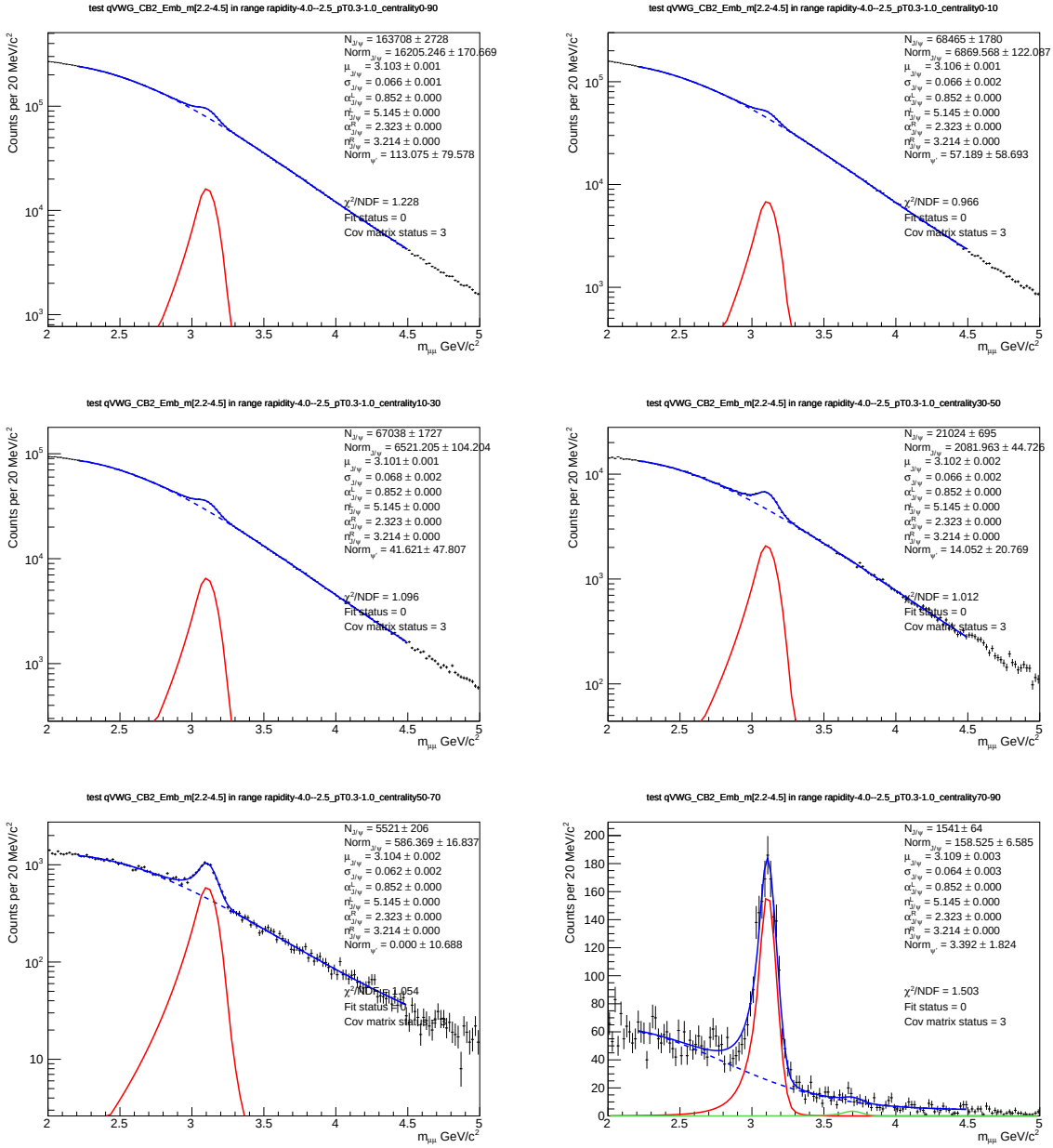

Fig. 3: OS dimuon invariant mass distribution fit, in $0.3 < p_{\mathrm{T}} < 1.0$ GeV/c for the centrality ranges: 0-90%(top left), 0-10%(top right), 10-30% (middle left), 30-50% (middle right), 50-70% (bottom left), 70-90% (bottom right)

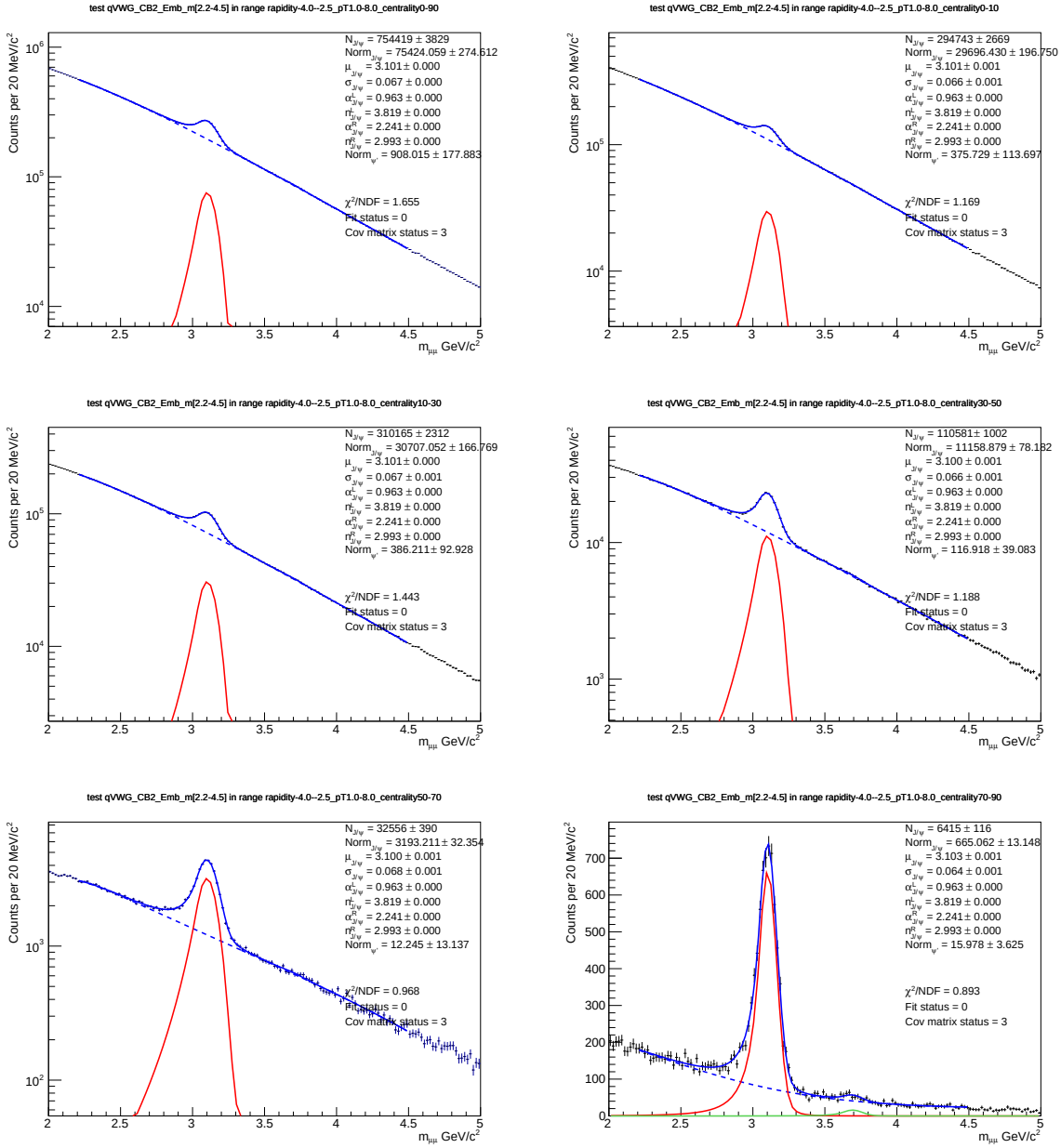

Fig. 4: OS dimuon invariant mass distribution fit, in $1.0 < p_{\mathrm{T}} < 8.0$ GeV$/c$ for the centrality ranges: 0-90%(top left), 0-10%(top right), 10-30% (middle left), 30-50% (middle right), 50-70% (bottom left), 70-90% (bottom right)

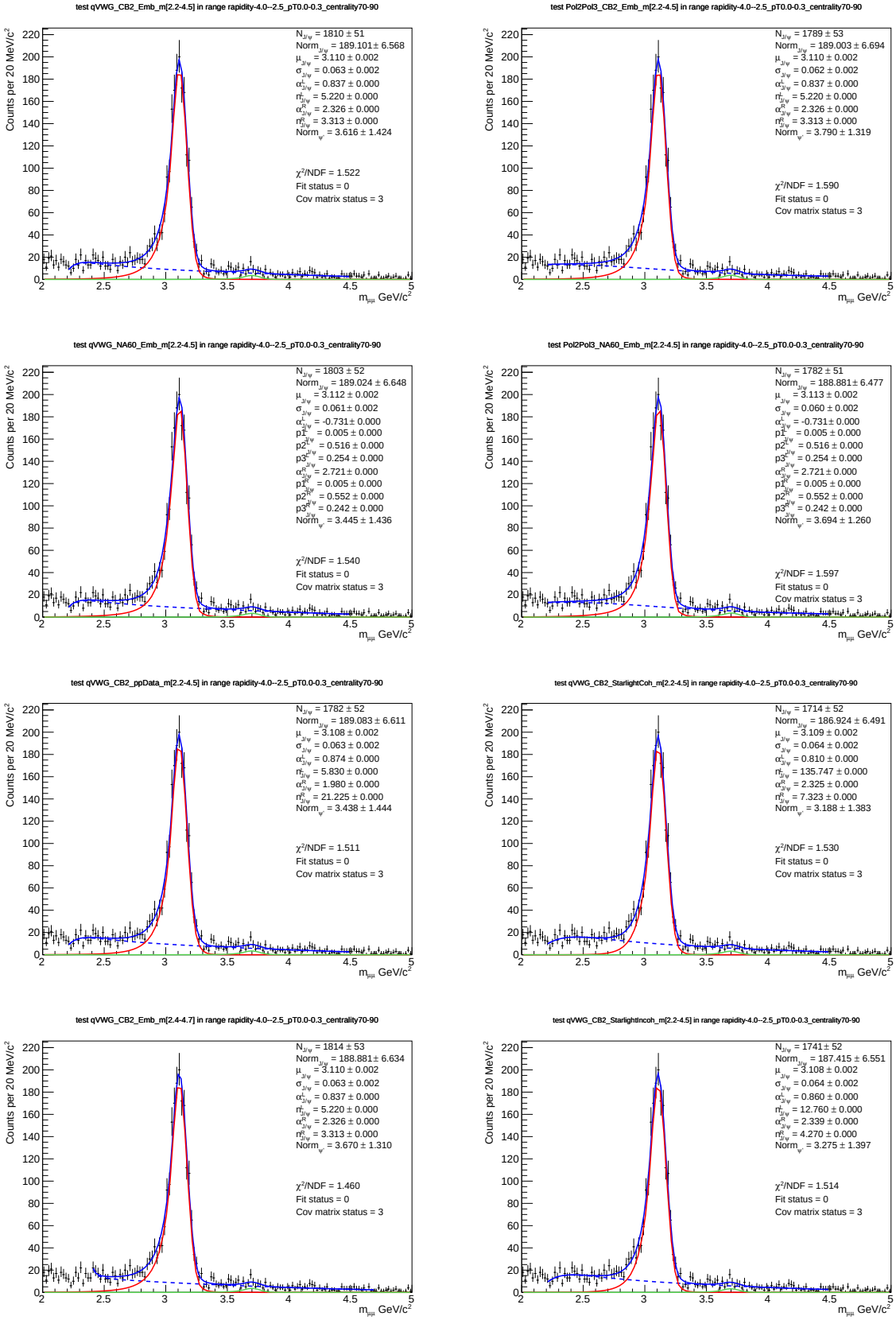

Fig. 5: OS dimuon invariant mass distribution fit in the mass range $2.2 < m_{\mu\mu} < 4.5$ GeV/c^2, in $0 < p_{\mathrm{T}} < 0.3$ GeV/c and for the centrality class 70-90%. Fit with a qVWG+CB2 and tails from embedding MC (top left), Pol2/Pol3+CB2 and tails from embedding MC (top right), qVWG+NA60 and tails from embedding MC (middle top left), Pol2/Pol3+NA60 and tails from embedding MC (middle top right), qVWG+CB2 and tails from pp data (middle bottom left), qVWG+CB2 and tails from STARLIGHT coherent J/ψ production (middle bottom right), qVWG+CB2 in the interval $2.4 < m_{\mu\mu} < 4.7$ GeV/c^2 and tails from embedding simulations (bottom left), qVWG+CB2 and tails from STARLIGHT incoherent J/ψ production (bottom right).

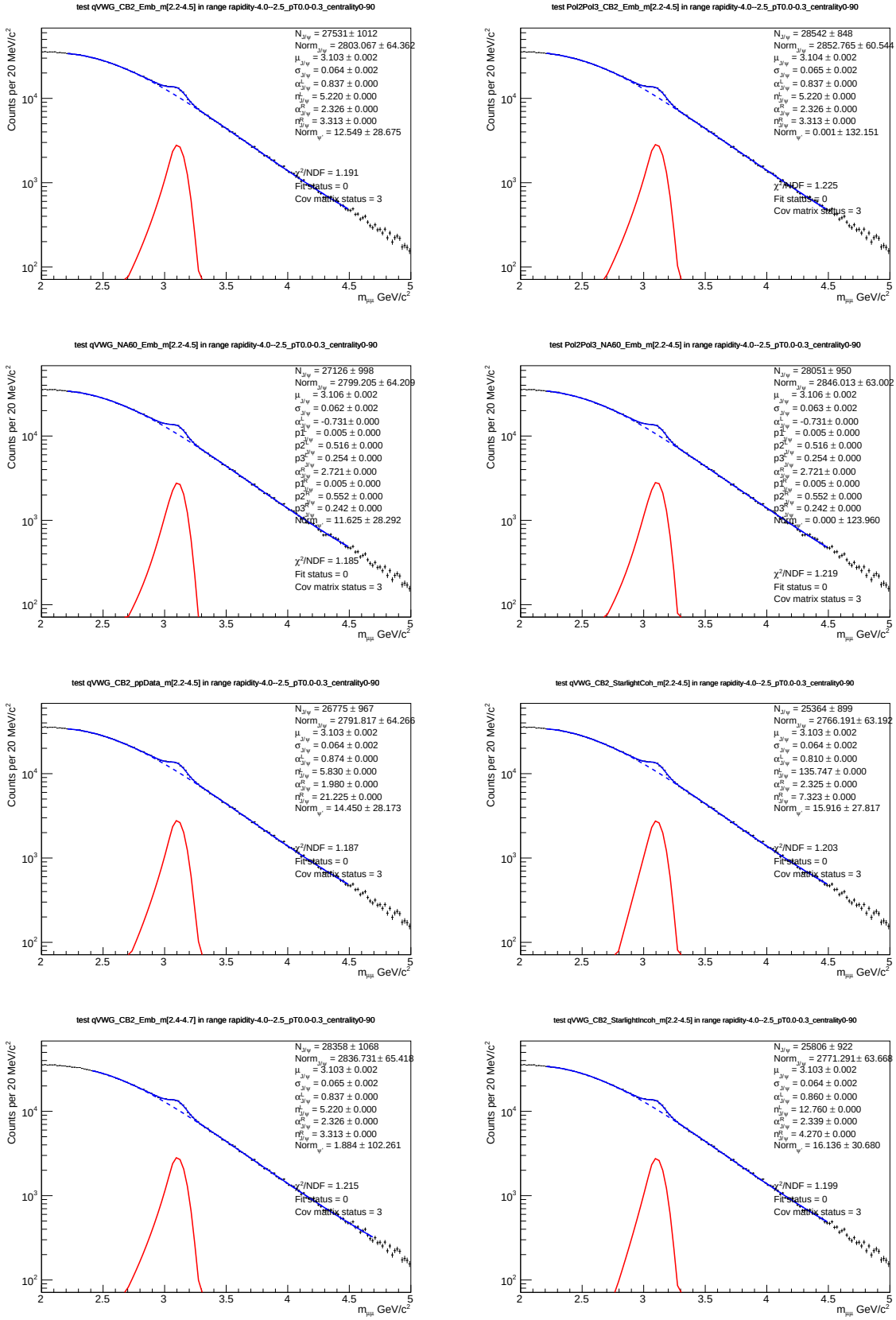

Fig. 6: OS dimuon invariant mass distribution fit in the mass range $2.2 < m_{\mu\mu} < 4.5$ GeV/c^2, in $0 < p_{\rm T} < 0.3$ GeV/c and for the centrality class 0-90%. Fit with a qVWG+CB2 and tails from embedding MC (top left), Pol2/Pol3+CB2 and tails from embedding MC (top right), qVWG+NA60 and tails from embedding MC (middle top left), Pol2/Pol3+NA60 and tails from embedding MC (middle top right), qVWG+CB2 and tails from pp data (middle bottom left), qVWG+CB2 and tails from STARLIGHT coherent J/ψ production (middle bottom right), qVWG+CB2 in the interval $2.4 < m_{\mu\mu} < 4.7$ GeV/c^2 and tails from embedding simulations (bottom left), qVWG+CB2 and tails from STARLIGHT incoherent J/ψ production (bottom right).

	0-0.3 GeV/c	0.3-1 GeV/c	1-8 GeV/c
0-90%	26925 ± 957 ± 726	160490 ± 2501 ± 3013	731279 ± 3695 ± 20322
0-10%	8351 ± 762 ± 312	67969 ± 1840 ± 1494	285842 ± 2807 ± 7675
10-30%	9624 ± 571 ± 278	65644 ± 1636 ± 1265	299523 ± 2174 ± 7934
30-50%	4280 ± 225 ± 105	20358 ± 636 ± 452	107119 ± 974 ± 2790
50-70%	2763 ± 98 ± 68	5519 ± 192 ± 185	31455 ± 366 ± 831
70-90%	1758 ± 57 ± 32	1506 ± 64 ± 23	6258 ± 119 ± 169

Table 4: Number of J/ψ obtained in each $p_{\rm T}$ range and centrality class by combining the results of the various tests. The quoted uncertainties are statistical and systematic.

6.3 Combination of systematic tests

The total number of tests by centrality class is 28 for $p_{\rm T} < 0.3$ GeV/c, 20 for $0.3 < p_{\rm T} < 1$ GeV/c and 12 for $p_{\rm T} > 1$ GeV/c.

The final number of J/ψ is calculated as the weighted average of all test results.

$$N_{\rm J/\psi} = \frac{\sum_{i=0}^{N_{\rm test}} \omega^i N^i_{\rm J/\psi}}{\sum_{i=0}^{N_{\rm test}} \omega^i} \tag{10}$$

with ω^i the weight applied to the test i such as tests using data inputs have the same weight as those using MC inputs.

The combined statistical uncertainty is given by the weighted average of the individual statistical uncertainties.

$$\sigma^{\rm stat}_{\rm J/\psi} = \frac{\sum_{i=0}^{N_{\rm test}} \omega^i \sigma^{i,\ \rm stat}_{\rm J/\psi}}{\sum_{i=0}^{N_{\rm test}} \omega^i} \tag{11}$$

The systematic uncertainty is taken as the standard deviation of the results.

$$\sigma^{\rm syst}_{\rm J/\psi} = \frac{\sum_{i=0}^{N_{\rm test}} \omega^i}{\sum_{i=0}^{N_{\rm test}} \omega^i - 1} \times \sqrt{\frac{\sum_{i=0}^{N_{\rm test}} \omega^i N^{2,\ i}_{\rm J/\psi}}{\sum_{i=0}^{N_{\rm test}} \omega^i} - \left(\frac{\sum_{i=0}^{N_{\rm test}} \omega^i N^i_{\rm J/\psi}}{\sum_{i=0}^{N_{\rm test}} \omega^i} \right)^2} \tag{12}$$

A display of the systematic tests are shown figures 7, 8 and 9 for $0 < p_{\rm T} < 0.3$ GeV/c, figures 10, 11 and 12 for $0.3 < p_{\rm T} < 1$ GeV/c and figures 13, 14 and 15 for $1 < p_{\rm T} < 8$ GeV/c.

6.4 Results

The raw number of J/ψ for each centrality classes in the three $p_{\rm T}$ ranges are reported in the table 4.

The signal extraction has been performed for $p_{\rm T}$ from 0 to 15 GeV/c in order to compute the nuclear modification factor ($R_{\rm AA}$) used to estimate the hadronic contribution at low $p_{\rm T}$ in section 8.

The same tests has been performed but considering only tails obtained by fitting the hadronic production

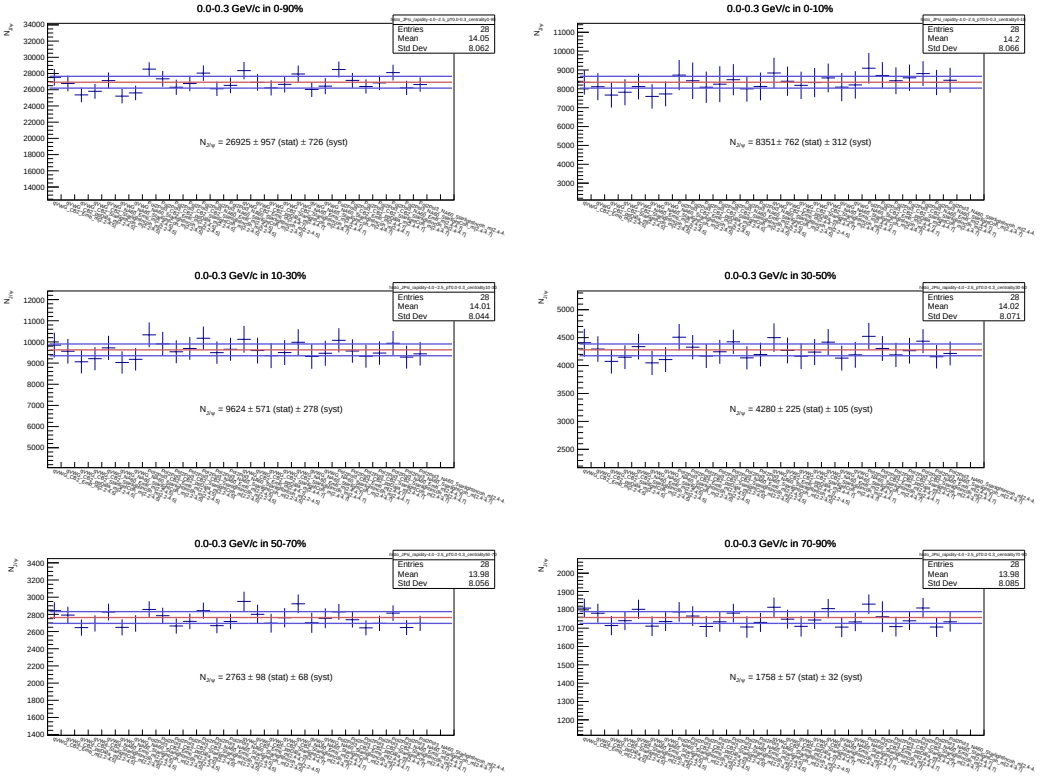

Fig. 7: Number of J/ψ for several systematic tests in $p_T < 0.3$ GeV/c and for centrality class 0-90% (top left), 0-10% (top right), 10-30% (middle left), 30-50% (middle right), 50-70% (bottom left), 70-90% (bottom right).

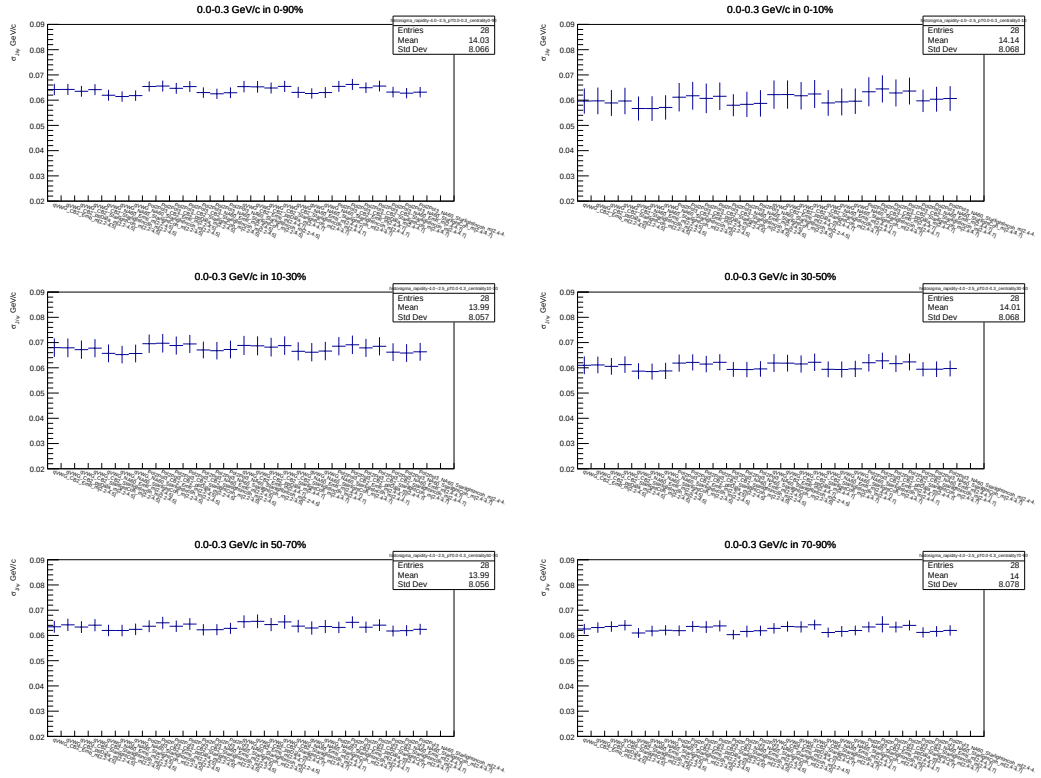

Fig. 8: J/ψ width for several systematic tests in $p_T < 0.3$ GeV/c and for centrality class 0-90% (top left), 0-10% (top right), 10-30% (middle left), 30-50% (middle right), 50-70% (bottom left), 70-90% (bottom right).

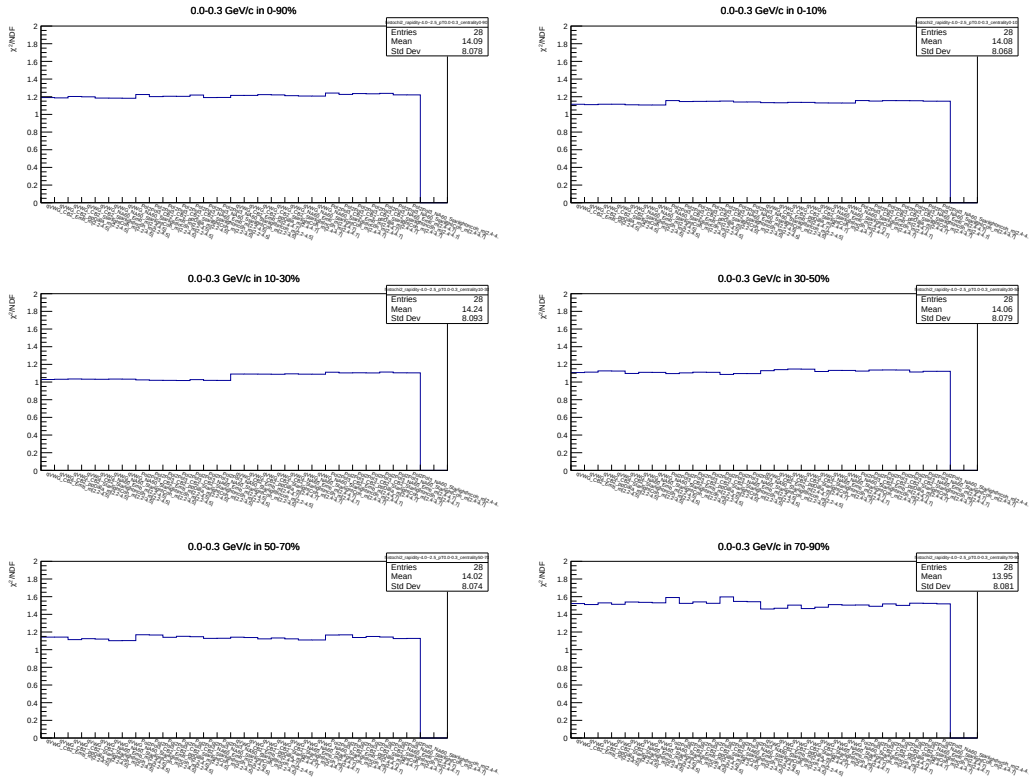

Fig. 9: χ^2/NDF for each systematic tests in $p_{\mathrm{T}} < 0.3$ GeV/c and for centrality class 0-90% (top left), 0-10% (top right), 10-30% (middle left), 30-50% (middle right), 50-70% (bottom left), 70-90% (bottom right).

from embedding MC simulations and pp data. The tails extracted with hadronic MC simulations are evaluated in each p_{T} intervals of this analysis (see table C.2). The raw J/ψ yield is presented figure 16 and values can be found in appendix D. Looking at the results for the most peripheral class table D.6, we found a yield of J/ψ in 0.3 to 1 GeV/c higher than in 1 to 2 GeV/c that does not reproduce the trend in other centrality classes. To investigate a possible contribution of the incoherent photoproduction that may affect the R_{AA}, this p_{T} range has been split in two.

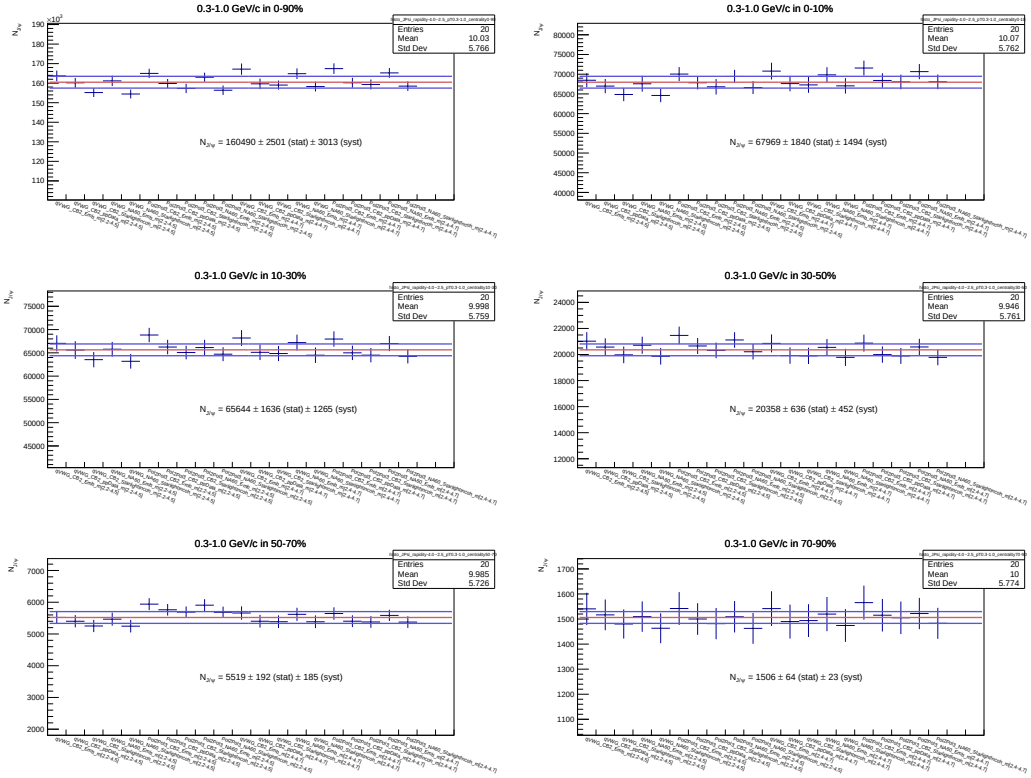

Fig. 10: Number of J/ψ for several systematic tests in $0.3 < p_{\mathrm{T}} < 1$ GeV$/c$ and for centrality class 0-90% (top left), 0-10% (top right), 10-30% (middle left), 30-50% (middle right), 50-70% (bottom left), 70-90% (bottom right).

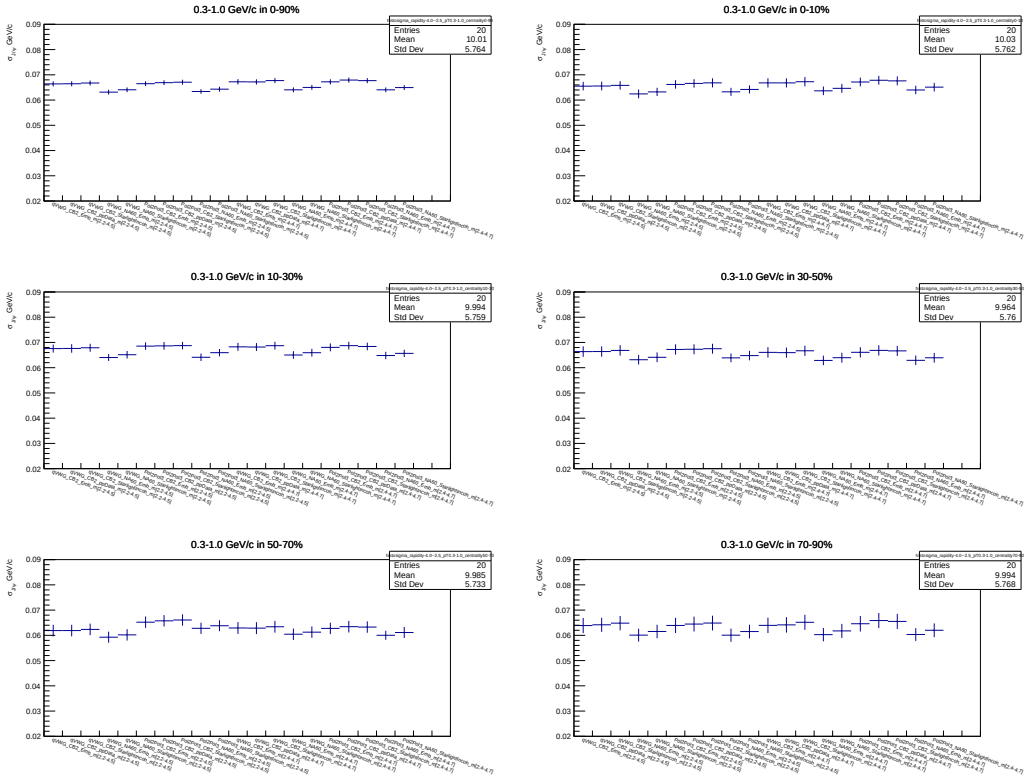

Fig. 11: J/ψ width for several systematic tests in $0.3 < p_{\mathrm{T}} < 1$ GeV/c and for centrality class 0-90% (top left), 0-10% (top right), 10-30% (middle left), 30-50% (middle right), 50-70% (bottom left), 70-90% (bottom right).

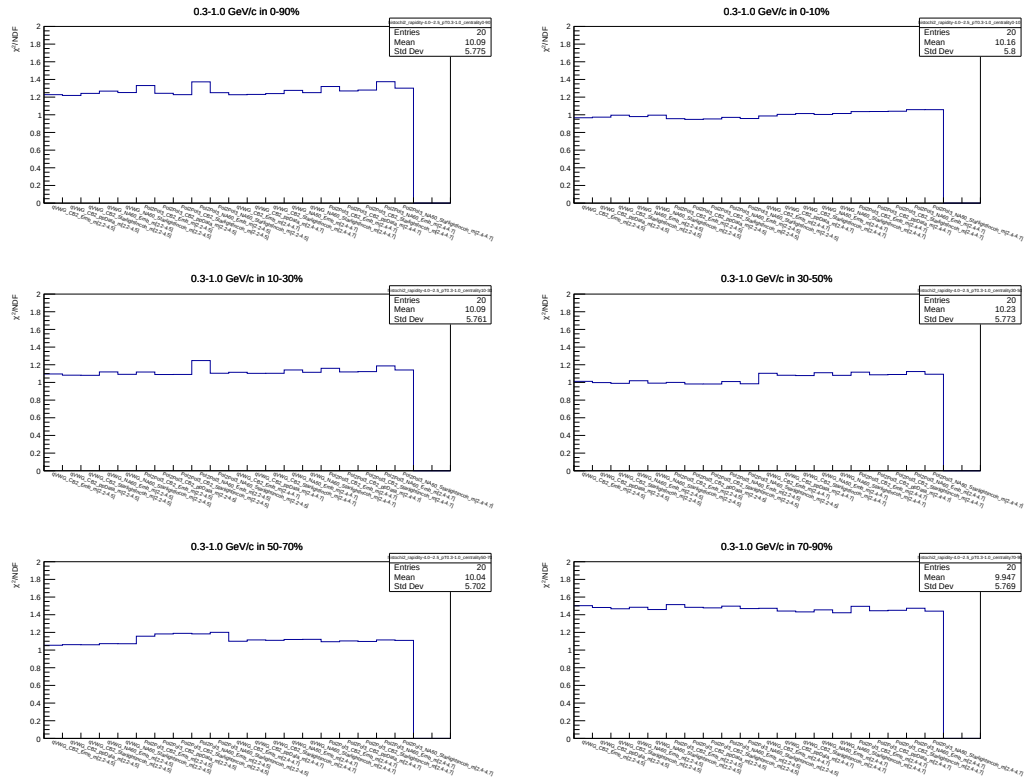

Fig. 12: χ^2/NDF for each systematic tests in $0.3 < p_{\mathrm{T}} < 1$ GeV/c and for centrality class 0-90% (top left), 0-10% (top right), 10-30% (middle left), 30-50% (middle right), 50-70% (bottom left), 70-90% (bottom right).

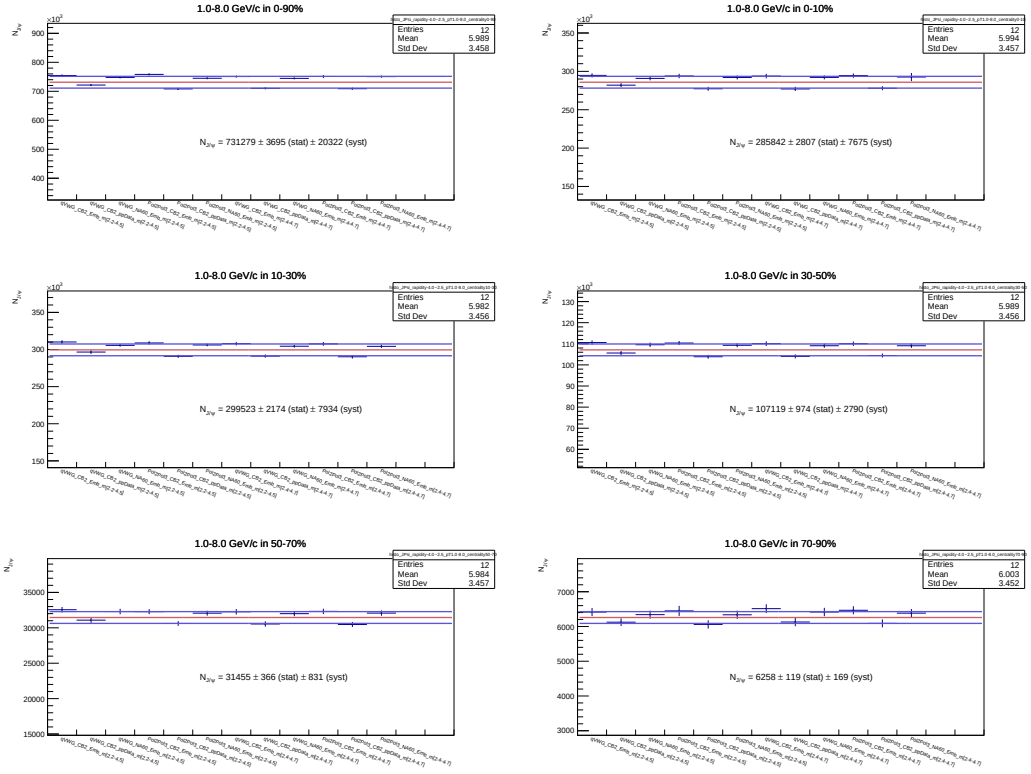

Fig. 13: Number of J/ψ for several systematic tests in $1 < p_T < 8$ GeV/c and for centrality class 0-90% (top left), 0-10% (top right), 10-30% (middle left), 30-50% (middle right), 50-70% (bottom left), 70-90% (bottom right).

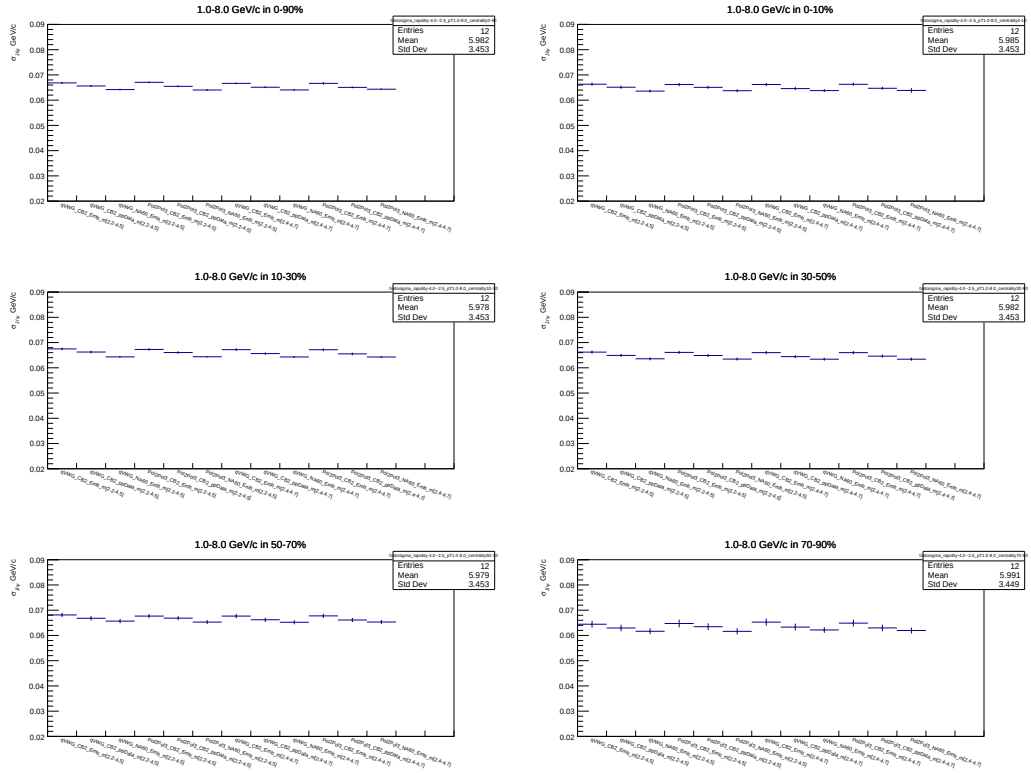

Fig. 14: J/ψ width for several systematic tests in $1 < p_T < 8$ GeV/c and for centrality class 0-90% (top left), 0-10% (top right), 10-30% (middle left), 30-50% (middle right), 50-70% (bottom left), 70-90% (bottom right).

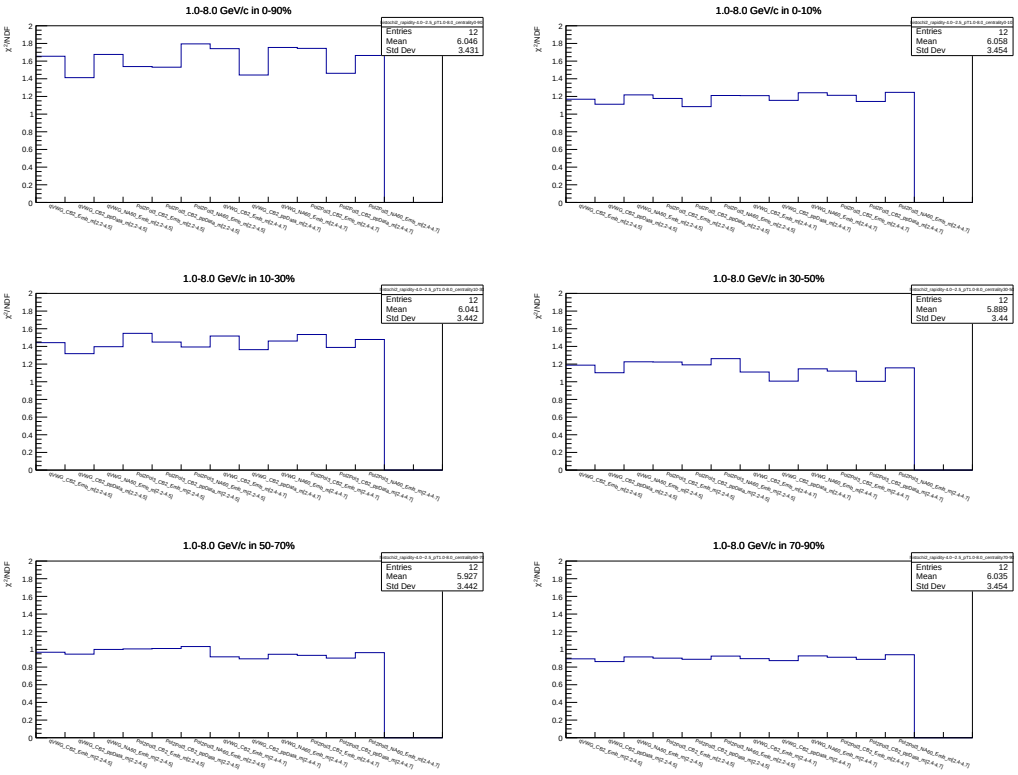

Fig. 15: χ^2/NDF for each systematic tests in $1 < p_{\mathrm{T}} < 8$ GeV/c and for centrality class 0-90% (top left), 0-10% (top right), 10-30% (middle left), 30-50% (middle right), 50-70% (bottom left), 70-90% (bottom right).

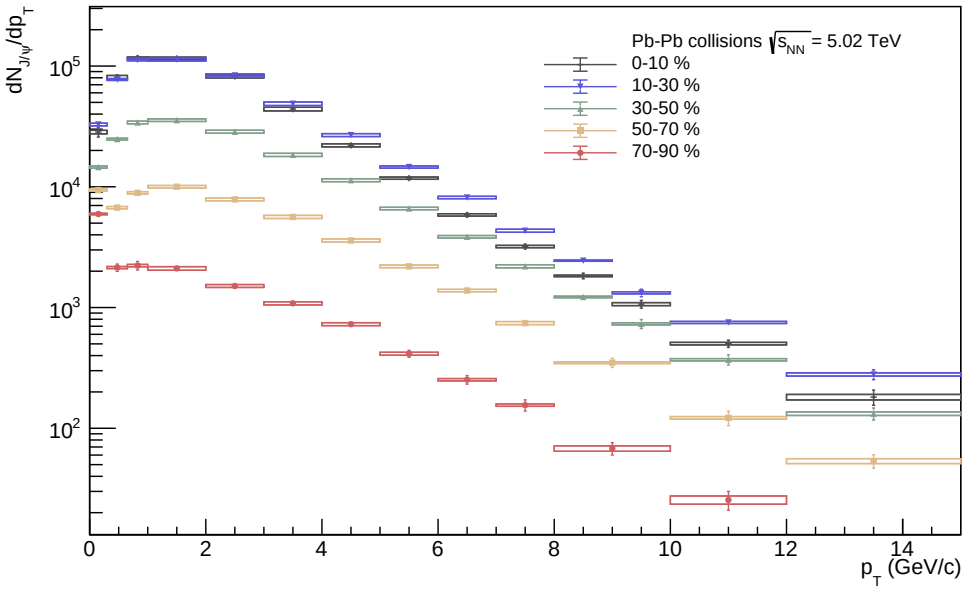

Fig. 16: $\mathrm{d}N_{\mathrm{J}/\psi}/\mathrm{d}p_{\mathrm{T}}$ as a function of p_{T} for each centrality class.

7 Acceptance Efficiency correction

The Acceptance Efficiency of the detector is extracted using the set of simulations reported section 4. For both hadronic J/ψ and coherently photoproduced J/ψ, the acceptance efficiency correction is defined as the number of reconstructed J/ψ over the number of generated J/ψ in the MC production. We applied the same kinematic cuts on on the generated and reconstructed MC data as it was done for the tracks selection in the data sample.

7.1 Hadronic Acceptance Efficiency

The acceptance efficiency correction of the detector for the hadronic contribution $((\mathscr{A} \times \varepsilon)^{J/\psi}_{AA}(\Delta y, \Delta p_T))$ was estimated from the offical Monte Carlo (MC) production of each period using the embedding technique. The physics selection was applied to the CINT7 trigger for the reconstructed simulation.

In order to make the number of MC J/ψ proportional to the number of analysed CMUL7 events and reconstructed J/ψ and to account for the evolution of the detector status with time, some weights were considered:

The run number weighting is a weight proportional to the number of CMUL7 events triggered in each run to take into account the time evolution on the acceptance efficiency.

The centrality weighting is a weight proportional to the raw number of J/ψ extracted in $0.3 < p_T < 15$ GeV/c (excluding the region of the excess) in each centrality subranges (ranges of 10%) to take into account the evolution of the yield of J/ψ per MB event as a function of the centrality.

MC kinematic inputs. Since the J/ψ $(\mathscr{A} \times \varepsilon)$ is not constant over p_T and rapidity, the J/ψ generator needs input functions for each centrality class. These inputs are obtained using a data-driven method. At the first step, the $(\mathscr{A} \times \varepsilon)$ is obtained using the embedded simulations with a generator using a set of input functions without centrality dependence.

The generated MC distribution are fitted and the resulting functions are used as a baseline for the weight of the next iterations ($f_0^{MC}(p_T^{gen})$ and $f_0^{MC}(y^{gen})$). These functions are very closed to those used by the generator.

The p_T and y shapes of the J/ψ distribution are described by these functions for each centrality class, where A, B, n_1 and n_2 are free parameters:

$$f(p_T) = A \times \frac{p_T}{\left(1 + \left(\frac{p_T}{B}\right)^{n_1}\right)^{n_2}} \tag{13}$$

$$f(y) = A \times e^{-0.5 \times \left(\frac{y}{B}\right)^2} \tag{14}$$

For iterations $i > 0$, the acceptance efficiency is applied to the raw J/ψ distributions to provide an equivalent generated distribution for the data. These corrected data distributions are then fitted to provide the genereted function at the iteration i ($f_i^{data}(p_T^{eq.\ gen})$ and $f_i^{data}(y^{eq.\ gen})$). It allows us to evaluate a weight that will be applied to both generated et reconstructed MC distributions before evaluating the new $(\mathscr{A} \times \varepsilon)$. Since we do not save the weighted MC distributions at each step, the weight calculated at a given iteration i is

$$w_i(p_T) = \frac{f_i^{data}(p_T^{eq.\ gen})}{f_0^{MC}(p_T^{eq.\ gen})} \tag{15}$$

$$w_i(y) = \frac{f_i^{\mathrm{data}}(y^{\mathrm{eq.\ gen}})}{f_0^{\mathrm{MC}}(y^{\mathrm{gen}})} \tag{16}$$

Finally, the weight applied to the generated and reconstructed MC distributions is the product of the p_{T} weight and the rapidity weight. The acceptance efficiency obtained with the weighted distributions is compared to the one from the previous iteration. The procedure is performed until the functions from two consecutive iterations converged, i.e. the ratio of $(\mathscr{A} \times \varepsilon)$ is under 0.2%.

Two iterations were sufficient to obtain converging results in all the centrality classes, expect in the 50-70% centrality class where a third iteration was necessary. The generated distributions obtained at each iteration are shown in Figures 19 and 20. The $(\mathscr{A} \times \varepsilon)$ values obtained in the last iteration are those used for the correction of the J/ψ yield in the analysis. Results of the $(\mathscr{A} \times \varepsilon)$ are shown in Figures 17 and 18 as a function of p_{T} and y, respectively. Numerical values can be found in F. The statistical error is taken as the largest value between $1/N_{\mathrm{gen}}$ and the binomial error given by

$$\sigma = \sqrt{\frac{N_{\mathrm{rec}}}{N_{\mathrm{gen}}} * \frac{1 - N_{\mathrm{rec}}/N_{\mathrm{gen}}}{N_{\mathrm{gen}}}} \tag{17}$$

7.1.1 Sytematic uncertainty on MC inputs

Update : The tuning method used to obtain the centrally dependent generation functions as a function of p_{T} and y is done separately for the two quantities. But this method therefore neglects the possible p_{T}-y correlations of the functional forms. To estimate the associated systematic uncertainty, we use a double differential tuning method based on the generation functions versus p_{T} (y) for 6 (12) bins in y (p_{T}) obtained in the pp analysis at 13 TeV [4] assuming that the order of magnitude of the uncertainty related to the correlations is the same order of magnitude in both collision systems and for both energies. For each combination of p_{T} and y distributions used to correct the simulations, we take the ratio of the resulting $(\mathscr{A} \times \varepsilon)$ to the mean value. Results are shown figures F.1 and F.2. The systematic uncertainty from this contribution is taken as the largest deviation observed in each p_{T} interval of the analysis figure F.1 with a negligible centrality dependence.

We also considered the systematic uncertainty related to the limited statistic when fitting the p_{T} and y data yields to get the generation distributions. To estimate this uncertainty, we obtained 50 generation functions by fitting the distributions versus p_{T} and y after varying the values of the data randomly in their statistical uncertainties. The generations fonctions for all these tests are shown figures F.3 and F.4. All these functions are then used to weight the simulations and obtain a value. The dispersion of these results provides the systematic uncertainty associated with the limited data statistics. The dispersion of the results are shown for each centrality class on figures F.5 and F.6. We took a conservative systematic uncertainty of 0.4% which is the largest value observed on figure F.5.

7.2 J/ψ coherent photoproduction Acceptance Efficiency

The Acceptance Efficiency correction of the detector for coherently photoproduced J/ψ ($(\mathscr{A} \times \varepsilon)^{\mathrm{J}/\psi}_{\mathrm{coh}}$) was estimated using STARLIGHT simulations of each period as reported section 4.

The $(\mathscr{A} \times \varepsilon)_i$ is evaluated for each run i as the fraction of the number reconstructed J/ψ over the number of generated J/ψ integrated in rapidity (i.e. $-4 < y < -2.5$) and for $p_{\mathrm{T}} < 0.3$ GeV/c.

The figure 21 shows the $(\mathscr{A} \times \varepsilon)^{\mathrm{J}/\psi}_{\mathrm{coh}}$) as a function of the run number in $-4 < y < -2.5$ from STARLIGHT simulations. As for the hadronic $(\mathscr{A} \times \varepsilon)$, we must apply a weight to each run proportional to the number

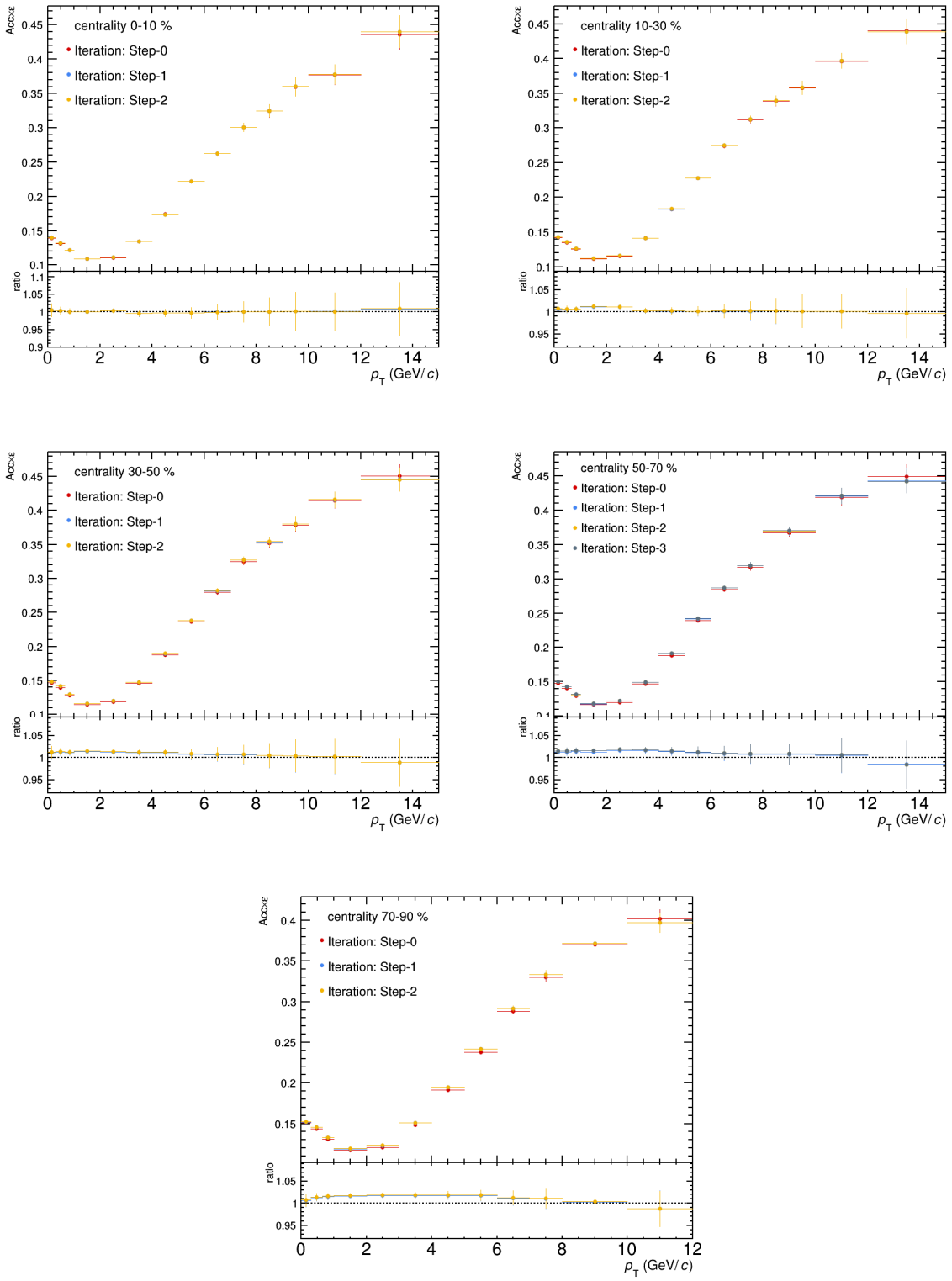

Fig. 17: $J/\psi(\mathscr{A} \times \varepsilon)$ for each iteration as a function of p_T for the full data sample of Pb–Pb collisions at 5 TeV. The ratio of each bottom panel corresponds to the ratio of the $(\mathscr{A} \times \varepsilon)$ from le last step over the step 0.

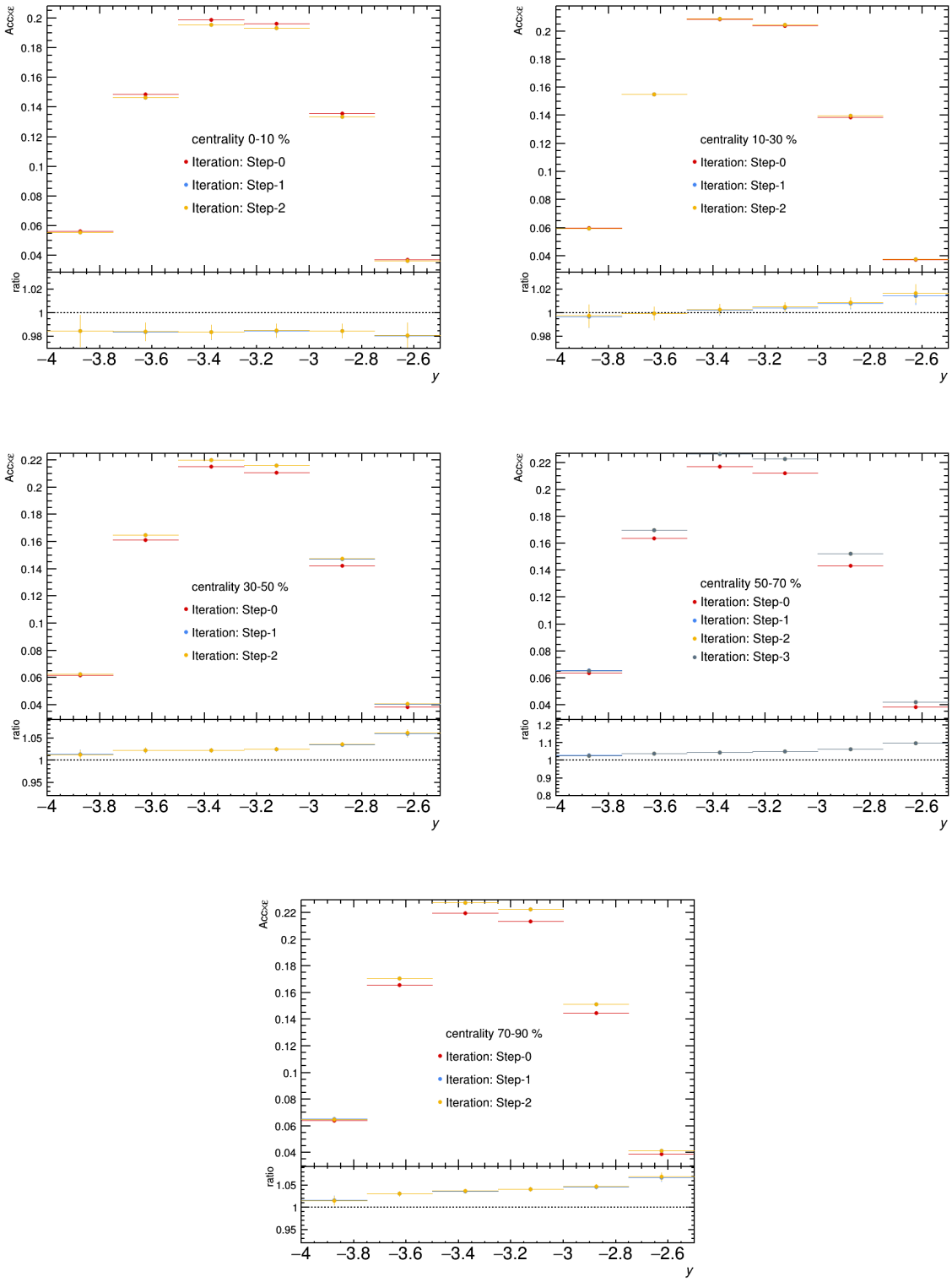

Fig. 18: J/$\psi(\mathscr{A} \times \varepsilon)$ for each iteration as a function of y for the full data sample of Pb–Pb collisions at 5 TeV. The ratio of each bottom panel corresponds to the ratio of the $(\mathscr{A} \times \varepsilon)$ from le last step over the step 0.

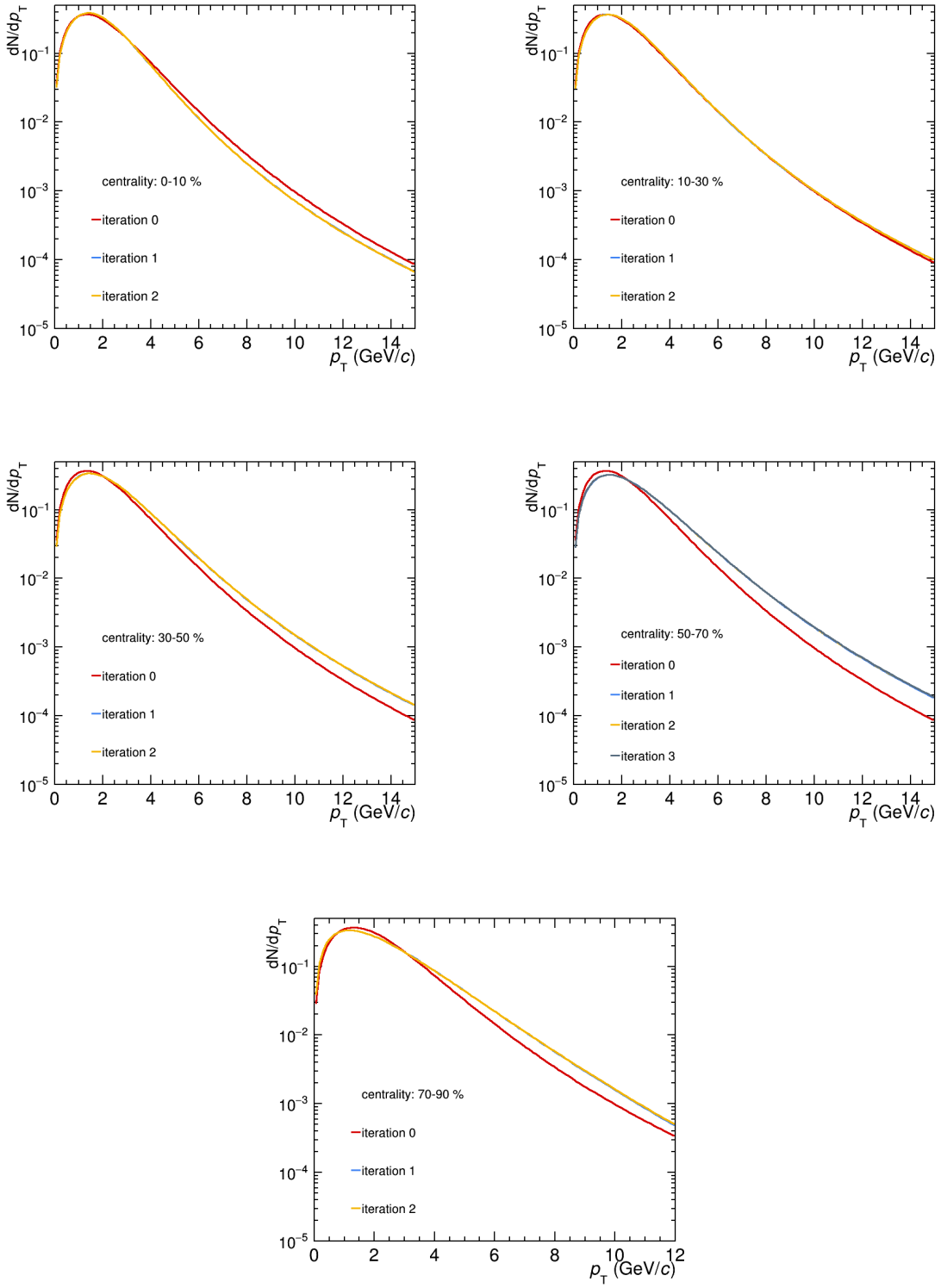

Fig. 19: Generated p_{T}distribution function for each iteration for the full data sample of Pb–Pb collisions at 5 TeV.

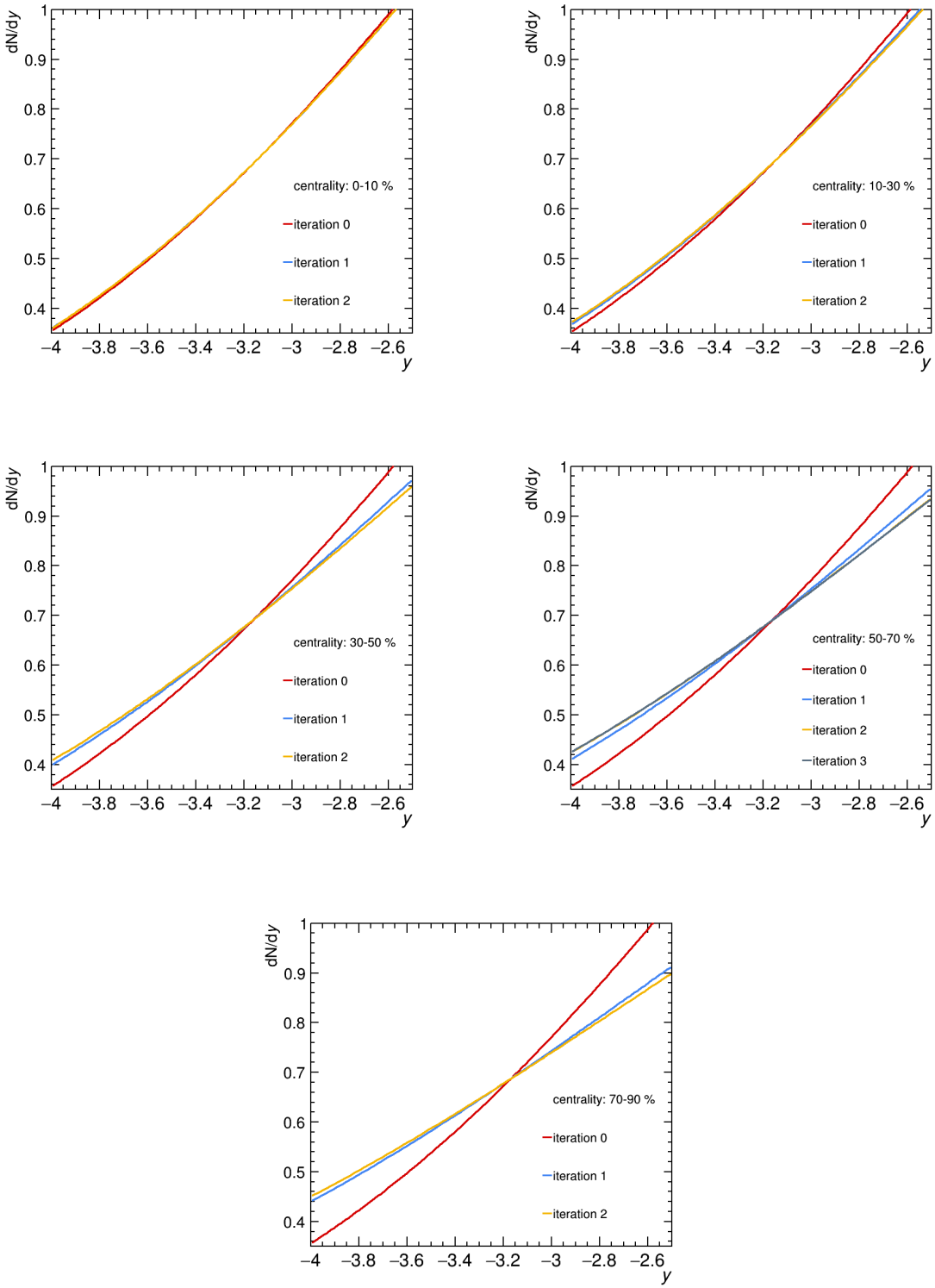

Fig. 20: Generated y distribution function for each iteration for the full data sample of Pb–Pb collisions at 5 TeV.

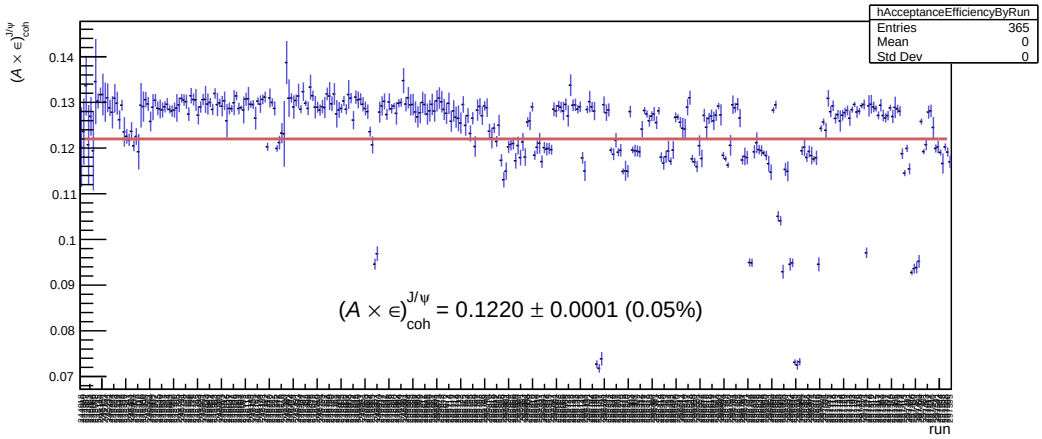

Fig. 21: $((\mathscr{A} \times \varepsilon)^{\mathrm{J}/\psi}_{\mathrm{coh}})$ as a function of the run number in $-4 < y < -2.5$ from STARLIGHT simulations. The straight line correponds to the average value weighted by the number of CMUL7 events recorded in each run.

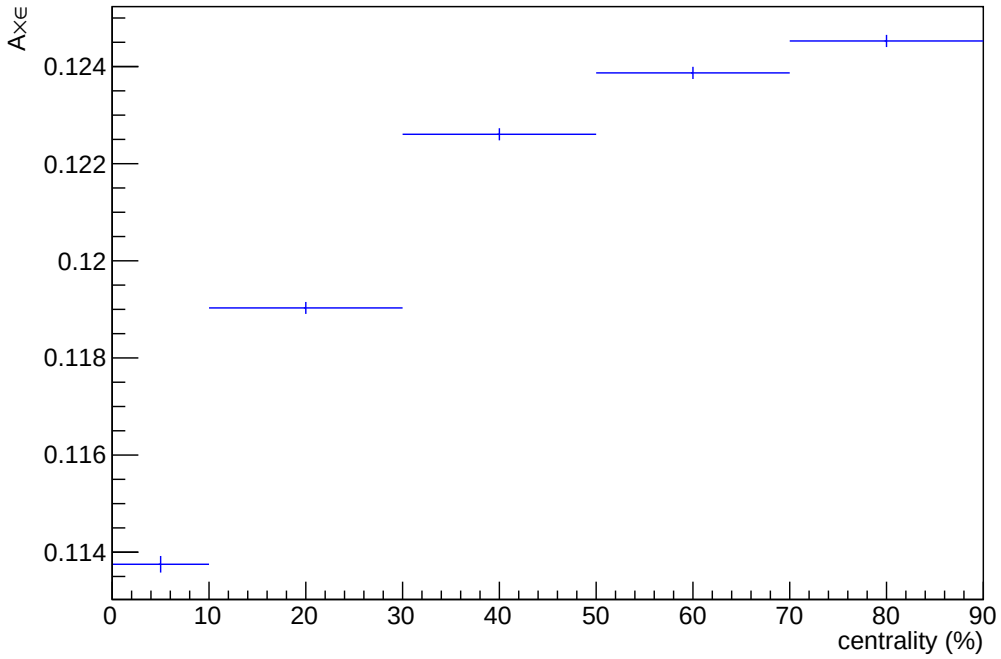

Fig. 22: $((\mathscr{A} \times \varepsilon)^{\mathrm{J}/\psi}_{\mathrm{coh}})$ as a function of the centrality in $-4 < y < -2.5$ and $p_{\mathrm{T}} < 0.3$ GeV/c from embedding STARLIGHT simulations.

of CMUL events triggered in the data. The straight line correponds to the weighted average value that will be used to correct the coherent photoproduction cross section.

Update : as reported in section 4, embedding STARLIGHT simulations are now available for the full data sample : LHC20g13 (LHC20j4) for the 2015 (2018) period. The $(\mathscr{A} \times \varepsilon)$ for coherent J/ψ has been extracted for $p_{\mathrm{T}} < 0.3$ GeV/c and $-4 < y < -2.5$ in each centrality class.

Results are shown figure 22 and numerical values are reported in table F.6. The statistical error is taken as the largest value between $1/N_{\mathrm{gen}}$ and the binomial error.

8 Modelization of the hadronic contamination in the low $p_{\rm T}$ J/ψ production

In order to isolate the excess yield of J/ψ at very low $p_{\rm T}$ we propose a method to model the expected number of J/ψ from hadroproduction assuming a smooth evolution of the hadronic nuclear modification factor ($R_{\rm AA}^{\rm h}$). The expected hadronic number of J/ψ in a given $p_{\rm T}$ interval can be obtained by integrating the following equation.

$$\int_{p_{\rm T1}}^{p_{\rm T2}} \frac{{\rm d}N_{\rm AA}^{\rm h\ J/\psi}}{{\rm d}p_{\rm T}} {\rm d}p_{\rm T} = \mathscr{N} \times \int_{p_{\rm T1}}^{p_{\rm T2}} \frac{{\rm d}\sigma_{\rm pp}^{\rm h\ J/\psi}}{{\rm d}p_{\rm T}} \times R_{\rm AA}^{\rm h\ J/\psi}(p_{\rm T}) \times (\mathscr{A} \times \varepsilon)_{\rm AA}^{\rm h\ J/\psi}(p_{\rm T}) {\rm d}p_{\rm T} \tag{18}$$

$\frac{{\rm d}\sigma_{\rm pp}^{\rm h\ J/\psi}}{{\rm d}p_{\rm T}}$ is parametrization of the J/ψ cross section measured by ALICE in pp collisions at $\sqrt{s_{\rm NN}} =$ 5.02 TeV [5]. Numerical values can be found in E.

$R_{\rm AA}^{\rm h\ J/\psi}(p_{\rm T})$ is a modelization of the J/ψ nuclear modification factor measured in the section 8.1.

$(\mathscr{A} \times \varepsilon)_{\rm AA}^{\rm h\ J/\psi}(p_{\rm T})$ is a parameterization of the acceptance times efficiency of hadronic J/ψ determined from embedding MC simulations as described section 7.

$\mathscr{N}$ is a normalization factor corresponding to the number of J/ψ in the $p_{\rm T}$ range $1-8$ GeV/c where the hadronic component is expected to be dominant.

$$\mathscr{N} = N_{\rm J/\psi}(1-8\ {\rm GeV}/c) / \int_{1\ {\rm GeV}/c}^{8\ {\rm GeV}/c} \frac{{\rm d}\sigma_{\rm pp}^{\rm h\ J/\psi}}{{\rm d}p_{\rm T}} \times R_{\rm AA}^{\rm h\ J/\psi}(p_{\rm T}) \times (\mathscr{A} \times \varepsilon)_{\rm AA}^{\rm h\ J/\psi}(p_{\rm T}) {\rm d}p_{\rm T} \tag{19}$$

8.1 Measurement of the $R_{\rm AA}^{\rm h\ J/\psi}$

The J/ψ invariant yield in AA collisions is defined by

$$Y_{\rm AA}^{\rm J/\psi} = \frac{N_{\rm J/\psi \to \mu^+\mu^-}(\Delta y, \Delta p_{\rm T})}{BR({\rm J/\psi \to \mu^+\mu^-}) \times N_{\rm MB} \times (\mathscr{A} \times \varepsilon)_{\rm AA}^{\rm J/\psi}(\Delta y, \Delta p_{\rm T})} \tag{20}$$

Where $N_{\rm J/\psi \to \mu^+\mu^-}(\Delta y, \Delta p_{\rm T})$ is the raw J/ψ yield for a given $p_{\rm T}$ and y range. $BR = 5.961 \pm 0.033$ % [6] is the branching ratio of J/ψ decaying into dimuon. $N_{\rm MB}$ is the equivalent number of minimum bias events corresponding to the analyzed data sample and $(\mathscr{A} \times \varepsilon)_{\rm AA}^{\rm J/\psi}(\Delta y, \Delta p_{\rm T})$ is the J/ψ acceptance times efficiency determined from embedding MC simulations as described section 7.

The equivalent number of minimum bias events can be computed for each centrality class i using the following formula.

$$N_{\rm MB}^{i} = \frac{N_{\rm CMUL}^{0-90} \times F_{\rm Norm}^{0-90} \times \Delta{\rm cent}^{i}}{90} \tag{21}$$

Finally, the nuclear modification factor of inclusive J/ψ can be calculated for each centrality class and $p_{\rm T}$ range as

$$R_{\rm AA}^{\rm J/\psi} = \frac{Y_{\rm AA}^{\rm J/\psi}}{\langle T_{\rm AA} \rangle \times \sigma_{\rm pp}^{\rm J/\psi}} \tag{22}$$

Centrality class	$\langle T_{AA} \rangle$ (mb^{-1})	$\langle N_{part} \rangle$
0-10%	23.26 ± 0.168 (0.72%)	357.3 ± 0.753
10-30%	11.5835 ± 0.1135 (0.98%)	224.95 ± 1.245
30-50%	3.9165 ± 0.065 (1.66%)	108.97 ± 1.129
50-70%	0.9756 ± 0.02335 (2.39%)	42.655 ± 0.686
70-90%	0.161165 ± 0.00365 (2.26%)	11.3475 ± 0.15695

Table 5: Mean nuclear overlap function and mean number of participant in each centrality class with their associated systematic uncertainties

	0-10%	10-30%	30-50%	50-70%	70-90%
N_{MB}	0.3*				
Signal extraction	1.4 - 5.1	1.2 - 3.3	1.5 - 3.1	1.7 - 4.1	1.4 - 6.6
Centrality limits	0.4*	0.1*	0.9*	2*	3.5*
MC input	0.4 + 1.1 - 2.5				
MCH	3 + 1*	3 + 0.5*	3 + 0.5*	3	3
MTR	1.5 - 2.8 + 1*	1.5 - 2.8 + 1*	1.5 - 2.8 + 0.5*	1.5 - 2.8	1.5 - 2.8
Matching	1				
T_{AA}	0.72*	0.98*	1.66*	2.39*	2.26*
pp cross section	3.5 - 5.6 + 1.8*				

Table 6: Systematic uncertainties on the R_{AA} measurement versus p_T in %. The values marked with an * correspond to uncertainties correlated over p_T.

	0-0.3 GeV/c	0.3-1 GeV/c	1-2 GeV/c
N_{MB}	0.3*		
Signal extraction	1.8 - 3.7	1.5 - 3.4	2.4 - 3.4
Centrality limits	0.1 - 3.5		
MC input	2.5 + 0.4		
MCH	3* + 0 - 1		
MTR	2.8* + 0 - 1	2.0* + 0 - 1	1.5* + 0 - 1
Matching	1*		
T_{AA}	0.72 - 2.39		
pp cross section	5.8*	5.4*	5.1*

Table 7: Systematic uncertainties on the R_{AA} measurement versus centrality in %. The values marked with an * correspond to uncertainties correlated over the centrality.

where $Y_{AA}^{J/\psi}$ is the invariant J/ψ yield given in equation 20, $\langle T_{AA} \rangle$ is the nuclear overlap function given by [2] and reported in table 5 and $\sigma_{pp}^{J/\psi}$ is the J/ψ cross section measured by ALICE in pp collisions at $\sqrt{s_{NN}} = 5.02$ TeV [5] and reported in table E.1.

Systematic uncertainties

The systematic uncertainties on the R_{AA} as a function of p_T reported in table 6 are discussed in this section.

The systematic uncertainties on the R_{AA} as a function of the centrality reported in table 7 are discussed in this section.

448

449 **Monte Carlo parametrisation**

450 The systematic uncertainty on Monte Carlo parametrisation is discussed in section 7.1.1.

451 **Tracking Efficiency**

452 The tracking efficiency has been measured in [7] for 2018 data samples, it was found to be the same as
453 the 2015 data sample. The systematic uncertainty is 1.5% for single muon and thus 3% for dimuons.
454 This sytematic is fully correlated as a function of the centrality but not as a function of p_{T} and y.
455 An additionnal systematic to account for the centrality efficiency loss is applied : 1% for central colli-
456 sions and 0.5% for semi-central collisions, this contribution is correlated as a function of p_{T} and y.

457

458 **Trigger Efficiency**

459 Systematic uncertainties on the trigger efficiency comprise the uncertainty on the intrinsic trigger effi-
460 ciency, the uncertainty on the trigger response and the efficiency loss as a function of the centrality.
461 The intrinsic trigger efficiency has been measured for 2015 data sample in [8] and for 2018 data sample
462 in [1]. A systematic uncertainty of 1.5% and 1% for 2015 and 2018 is found, respectively. We take 1.5%
463 as a conservative systematic on the full data sample. This contribution is fully correlated as a function of
464 centrality but not as a function of p_{T} and y.
465 The systematic uncertainty on the shape of the trigger response has been determined by comparing the
466 influence of two different trigger response distributions on the acceptance efficiency of J/ψ, using data
467 and MC. This systematic uncertainty correlated as a function of centrality but not as a function of p_{T} and
468 y and have been taken from [9].
469 An additionnal systematic to account for the centrality efficiency loss is applied : 1% for central colli-
470 sions and 0.5% for semi-central collisions, this contribution is correlated as a function of p_{T} and y.

471 **Matching**

472 Uncertainty on the matching trigger-tracker track efficiency amouts to 1% for Run2 analysis [10].

473

474 **Others**

475 The systematic uncertainty on the signal extraction are discussed in section 6 and reported in tables D.2,
476 D.3, D.4, D.5 and D.6.

477

478 The systematic uncertainty on the equivalent number of MB events is discussed section 5.

479

480 The systematic on the T_{AA} is obtained with a Glauber model in [2]. The value obtained for each centrality
481 class is reported in table 5.

482

483 **The uncertainty on the centrality limits has been valuated for the 2015 period in [10]. It should**
484 **be the same for the complete data sample. It is avaluated by comparing the number of J/ψ with**
485 **several centrality estimator (V0Mplus05 and V0Mminus05) in each centrality class.The result is**
486 **shown in figure G.1. This systematics has been evaluated in different centrality intervals from those**
487 **in this analysis, the values adopted in each centrality class of this analysis is average weighted by**
488 **the number of J/ψ extracted in each centrality subrange.**

489 The systematic uncertainties on the pp cross sections are taken from [5].

Results

The J/ψ $R_{\rm AA}$ in $-4 < y < -2.5$ as a function of $p_{\rm T}$ is reported in the tables G.1, G.2, G.3, G.4 and G.5 for the centrality class 0-10%, 10-30%, 30-50%, 50-70% and 70-90%, respectively. The J/ψ $R_{\rm AA}$ versus $p_{\rm T}$ is illustrated figure 23 for all centrality classes.

We also performed the evaluation of the J/ψ $R_{\rm AA}$ as a function of the centrality for the two $p_{\rm T}$ intervals of the low $p_{\rm T}$ analysis and one $p_{\rm T}$ range chosen as the reference for hadronic production. Results are reported in table 8 and 9 and 10 for $p_{\rm T} < 0.3$ GeV/c, $0.3 < p_{\rm T} < 1$ GeV/c and $1 < p_{\rm T} < 2$ GeV/c, respectively. The J/ψ $R_{\rm AA}$ versus centrality is illustrated figure 24.

Update after DQ preview : The $p_{\rm T}$ range used to compare with pure hadronic contribution can be chosen as $1 < p_{\rm T} < 2$ GeV/c where regeneration effects in central collisions are closer to the two lowest $p_{\rm T}$ ranges.

Looking at the red distribution (i.e. $p_{\rm T} < 0.3$ GeV/c) of the figure 24, results show a good significance of the excess for peripheral and semi-central collisions down to 30% in centrality. It could allow the first extraction of the cross section of coherently photoproduced J/ψ in the centrality class 30-50%. We can also note that we observed for the first time a $R_{\rm AA}$ larger than the unity in the most peripheral centrality class for $0.3 < p_{\rm T} < 1$ GeV/c (i.e. blue distribution) that could suggest a significant contribution from incoherent J/ψ photoproduction.

0-0.3 (GeV/c)

cent (%)	$R_{\rm AA}^{\rm J/\psi} \pm stat(\%) \pm syst(\%)$
0-10	0.73 ± 0.07 (9.8) ± 0.03 (4.8)
10-30	0.82 ± 0.06 (6.9) ± 0.03 (4.1)
30-50	1.04 ± 0.07 (6.4) ± 0.04 (4.1)
50-70	2.66 ± 0.14 (5.3) ± 0.13 (4.7)
70-90	10.13 ± 0.59 (5.8) ± 0.53 (5.2)

Table 8: J/ψ nuclear modification factor for $0 < p_{\rm T} < 0.3$ GeV/c in $-4 < y < -2.5$ as a function of the centrality. The $R_{\rm AA}$ is evaluated using the results reported in table 4. The quoted errors are statistical and uncorrelated systematic uncertainty. The correlated over the centrality systematic uncertainty (not included) is 7.222% in this $p_{\rm T}$ range.

0.3-1 (GeV/c)

cent (%)	$R_{\rm AA}^{\rm J/\psi} \pm stat(\%) \pm syst(\%)$
0-10	0.75 ± 0.02 (3.0) ± 0.03 (3.7)
10-30	0.70 ± 0.02 (2.8) ± 0.02 (3.4)
30-50	0.62 ± 0.02 (3.4) ± 0.02 (3.9)
50-70	0.67 ± 0.03 (3.8) ± 0.03 (5.2)
70-90	1.09 ± 0.05 (4.6) ± 0.06 (5.1)

Table 9: J/ψ nuclear modification factor for $0.3 < p_{\rm T} < 1$ GeV/c in $-4 < y < -2.5$ as a function of the centrality. The $R_{\rm AA}$ is evaluated using the results reported in table 4. The quoted errors are statistical and uncorrelated systematic uncertainty. The correlated over the centrality systematic uncertainty (not included) is 6.589% in this $p_{\rm T}$ range.

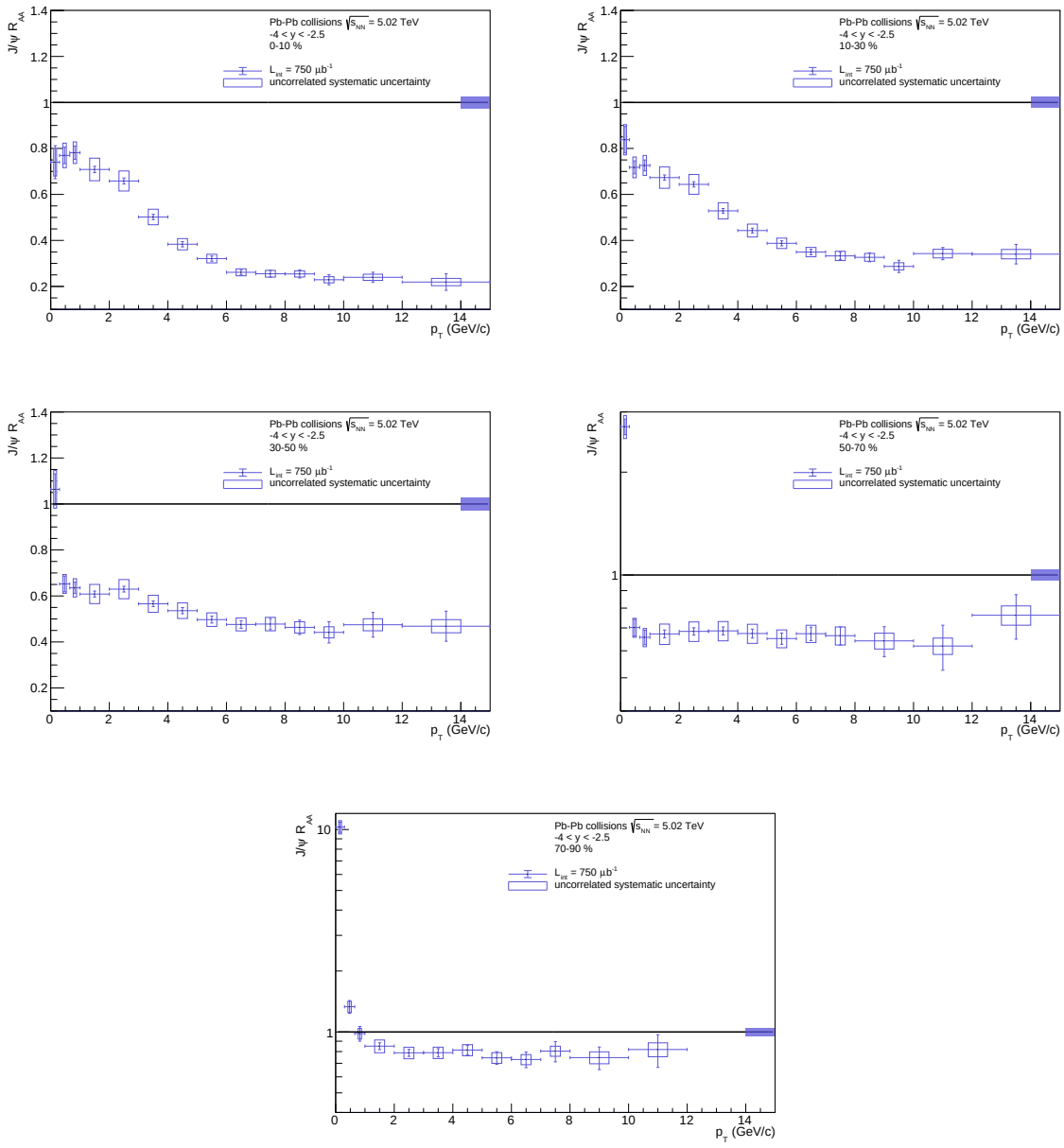

Fig. 23: J/ψ nuclear modification factor distribution as a function of p_{T} in $-4 < y < -2.5$ for each centrality class. The quoted errors are statistical and uncorrelated systematic uncertainty. The correlated over p_{T} systematic uncertainty is represented by a box at the unity.

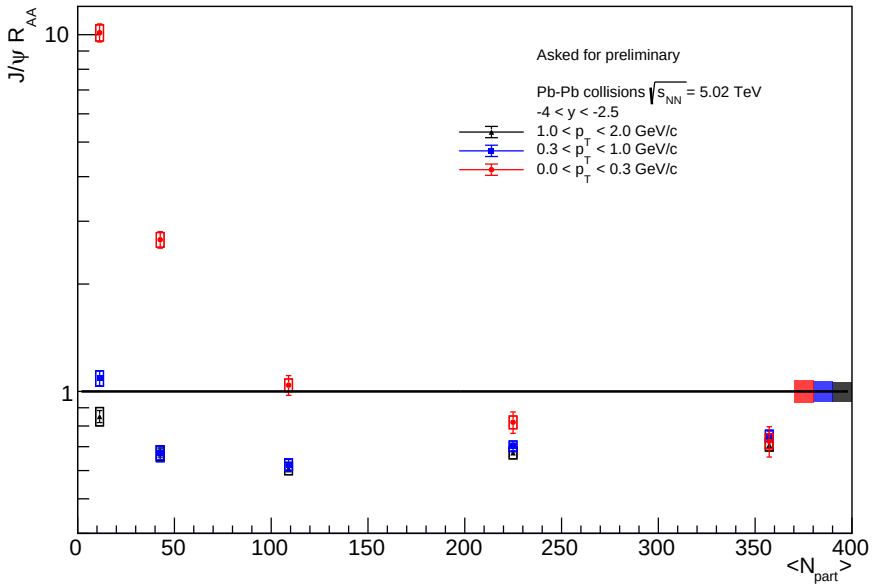

Fig. 24: J/ψ nuclear modification factor distribution as a function of $\langle N_{\rm part}\rangle$ in $-4 < y < -2.5$. The comparison with the hadronic component is performed with the $p_{\rm T}$ range $1 < p_{\rm T} < 2$ GeV/c. The quoted errors are statistical and uncorrelated systematic uncertainty. The correlated over centrality systematic uncertainties are represented by a box at the unity.

1-2 (GeV/c)

cent (%)	$R_{\rm AA}^{J/\psi} \pm stat(\%) \pm syst(\%)$
0-10	0.71 ± 0.01 (1.9) ± 0.03 (3.9)
10-30	0.67 ± 0.01 (1.7) ± 0.03 (3.9)
30-50	0.61 ± 0.01 (2.2) ± 0.02 (4.0)
50-70	0.67 ± 0.02 (2.6) ± 0.03 (4.6)
70-90	0.85 ± 0.03 (3.9) ± 0.05 (5.9)

Table 10: J/ψ nuclear modification factor for $1 < p_{\rm T} < 2$ GeV/c in $-4 < y < -2.5$ as a function of the centrality. The $R_{\rm AA}$ is evaluated using the results reported in table 4. The quoted errors are statistical and uncorrelated systematic uncertainty. The correlated over the centrality systematic uncertainty (not included) is 6.210% in this $p_{\rm T}$ range.

8.2 Parametrisation of the $R_{\rm AA}^{\rm h\ J/\psi}$

The nuclear modification factor was fitted with a Wood-Saxon like function for centrality classes going to 50%. In peripheral collisions, the $R_{\rm AA}$ is described with a straight line, that is either a first degree polynomial or a constant. For the Wood-saxon like function, we tried to fix the $p_{\rm T0}$ parameter to $m_{J/\psi}$, $m_{J/\psi}/2$, $\langle p_{\rm T}\rangle$ and $2 * \langle p_{\rm T}\rangle$. The $\langle p_{\rm T}\rangle$ of hadronic J/ψ was obtained by fitting the invariant yield distribution as described in H. We also tried two different fitting ranges 0.65-15 and 1-15 GeV/c, both of them exclude the region of the excess. **Update : Finally, the uncertainty considered on each point is the quadratic sum of the statistical and uncorrelated systematic uncertainties from the signal extraction and the systematic uncertainties on the $(\mathscr{A} \times \varepsilon)$. In order not to take into account twice the uncertainties on the pp cross section and on the acceptance efficiency (statistical only), these are considered in the parametrizations described in sections 8.3 and 8.4, respectively.** Results of the fits are shown on Fig. 25.

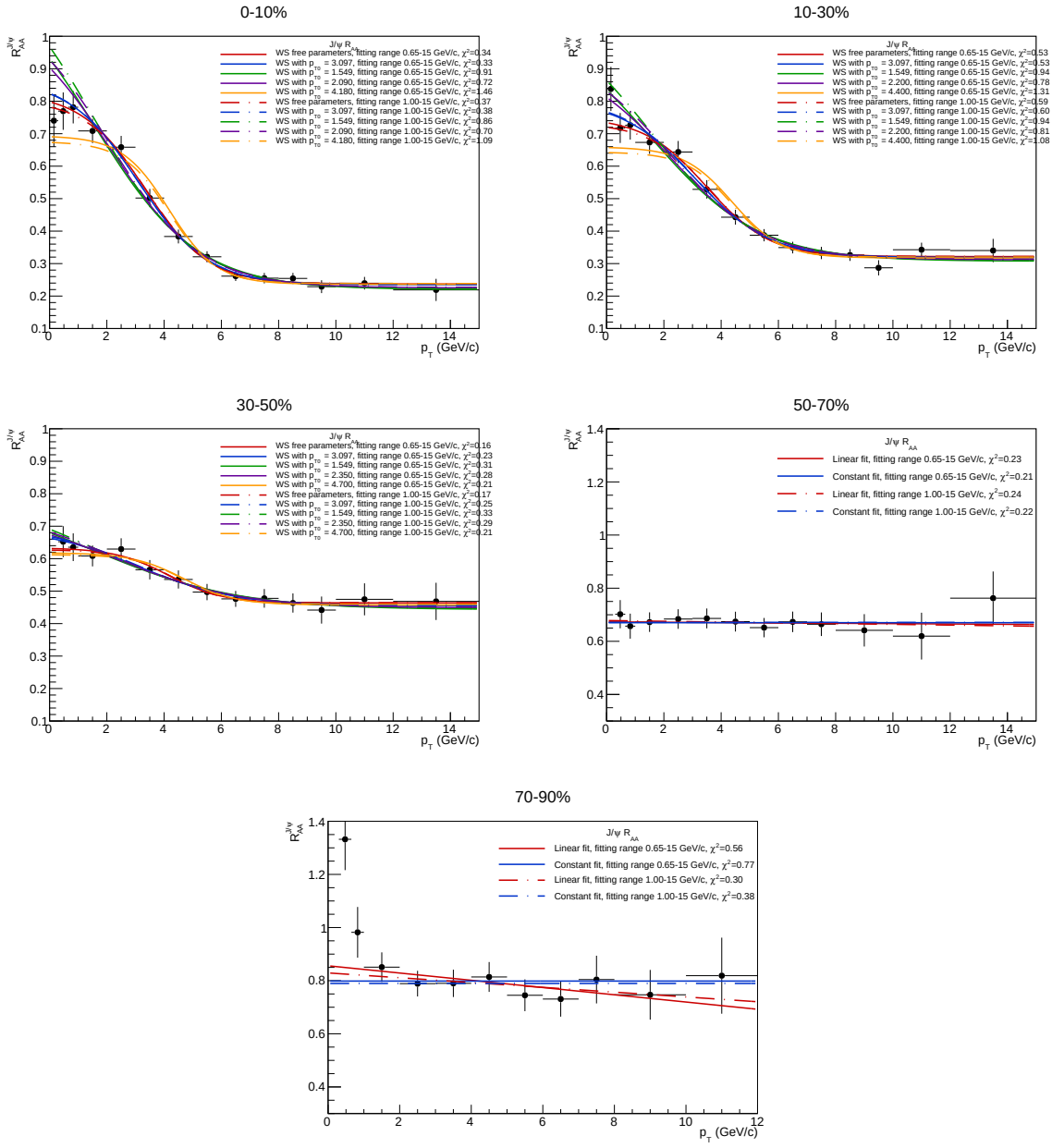

Fig. 25: Fit of the $R_{\mathrm{AA}}^{\mathrm{h\,J/\psi}}$ distribution as a function of p_{T} in $-4 < y < -2.5$ with a Wood-Saxon like function for central and semi-central collisions (0% to 50%) and with a straight line or a linear function for peripheral collisions (50% to 90%). The uncertainty on each data point is the quadratic sum of the statistical and uncorrelated systematic uncertainties not related to the pp cross section and the $(\mathscr{A} \times \varepsilon)$(syst on $(\mathscr{A} \times \varepsilon)$ included).

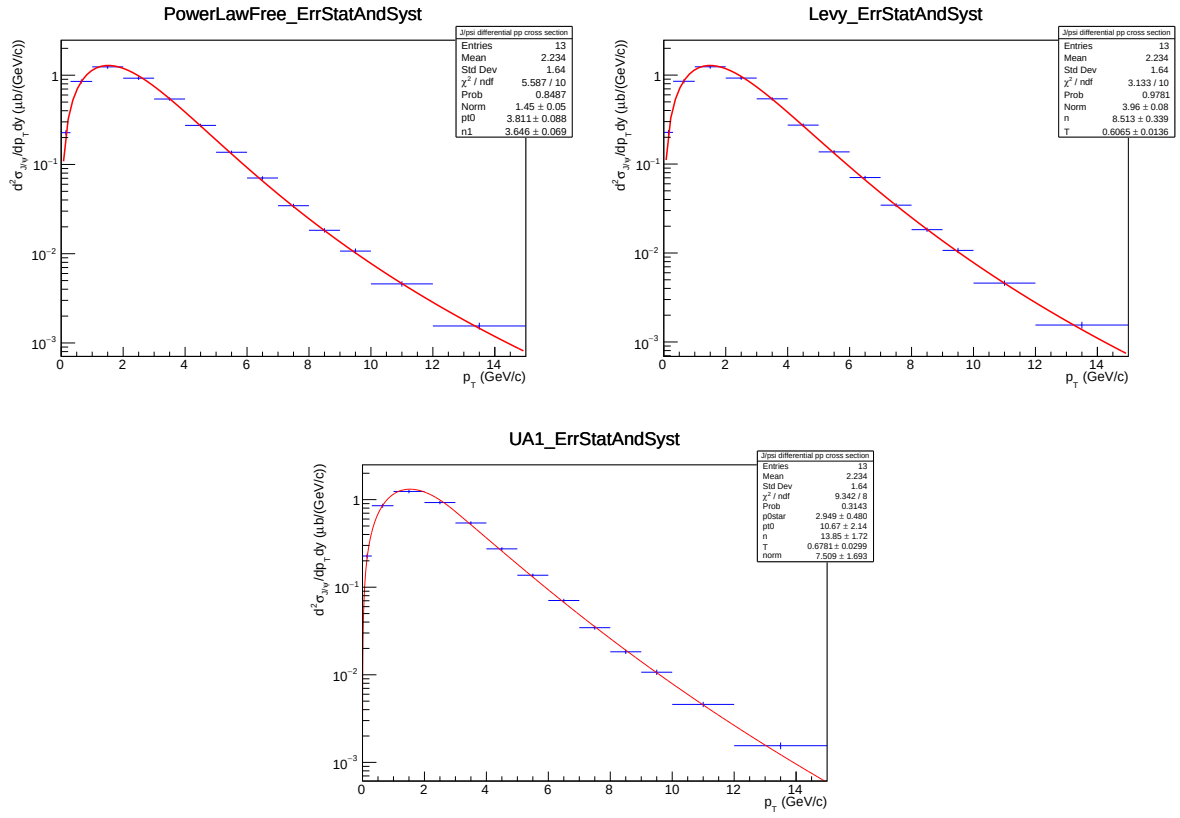

Fig. 26: Fit of $\mathrm{d}\sigma_{\mathrm{pp}}^{\mathrm{h\ J/\psi}}/\mathrm{d}p_{\mathrm{T}}$ distribution from [5] as a function of $p_{\mathrm{T}}$with a power law (left), a Levy function (right) and a UA1 function (bottom). The uncertainty on each data point is the quadratic sum of the statistcal and uncorrelated systematic uncertainties.

8.3 Parametrisation of the pp reference cross section

The J/ψ p_{T} differential cross section was calculated with the data collected in pp collisions at $\sqrt{s_{\mathrm{NN}}} =$ 5.02 TeV with the 2017 dataset [5]. It is parametrized using either a power law function (whose parameter D is free or set to 2), a Levy function or the UA1 function. A description of these function can be found in B.

For the parametrization of eq 18, the uncertainty considered on each point is the quadratic sum of the statistical and uncorrelated systematic uncertainties. Results of the fits are shown on Fig. 26.

At low p_{T} the measurement provides only results for the binning 0-0.3 GeV/c and 0.3-1 GeV/c. For the calculation of the R_{AA} in 0.3-0.65 and 0.65-1 GeV/c, we get the pp cross section by integreting the above-mentionned parametrization. The fitting procedure was thorough by assigning to each data point :

- the quadratic sum of the statistical and uncorrelated systematic uncertainties to extract the cross section and the standard deviation on the results.
- the statistical uncertainty only to get the statistical uncertainty of the test.
- the uncorrelated systematic uncertainty only to get the systematic uncertainty of the test.

The cross section is calculated as the weighted average of all test results. The combined statistical uncertainty is given by the weighted average of the individual statistical uncertainties. And the total uncorrelated systematic uncertainty is given by the quadratic sum of the standard deviation and the combined

	$\frac{{\rm d}\sigma_{\rm pp}^{\rm J/\psi}}{{\rm d}p_{\rm T}{\rm d}y}$ $\pm$ (stat) $\pm$ (syst) measured	$\frac{{\rm d}\sigma_{\rm pp}^{\rm J/\psi}}{{\rm d}p_{\rm T}{\rm d}y}$ $\pm$ (stat) $\pm$ (syst) extracted in this analysis
0-0.3 GeV/c	0.227 $\pm$ 0.00779 $\pm$ 0.0126	0.221 $\pm$ 0.00242 $\pm$ 0.00928
0.3-1 GeV/c	0.852 $\pm$ 0.0108 $\pm$ 0.0433	0.838 $\pm$ 0.00731 $\pm$ 0.0260
0.3-0.65 GeV/c		0.659 $\pm$ 0.00640 $\pm$ 0.0233
0.65-1 GeV/c		1.0163 $\pm$ 0.00829 $\pm$ 0.0294
1-8 GeV/c		0.466 $\pm$ 0.00220 $\pm$ 0.00922

Table 11: J/ψ differential cross section $\frac{{\rm d}\sigma_{\rm pp}^{\rm J/\psi}}{{\rm d}p_{\rm T}{\rm d}y}$ (μb/(GeV/c)) measured by ALICE in pp collisions at $\sqrt{s_{\rm NN}} =$ 5.02 TeV [5] compared to the one extracted from the fitting procedure. The correlated systematic uncertainty of 1.9% is not included here.

systematic uncertainty given by the weighted average of the individual systematic uncertainties. The weight of each test is given in such a way that each function has the same weight. Finally, a correlated systematic uncertainty of 1.9% from the cross section measurement is applied to the values determined here. Results are presented table 11 and are compared to the measured cross section. The values are comptible within $1\sigma_{\rm syst}$.

8.4 Parametrization of the hadronic Acceptance Efficiency

The parametrization of the $(\mathscr{A} \times \varepsilon)$ as a function of $p_{\rm T}$ was done using a third degree polynomial and a ratio of two Levy functions. The fit was performed in $0 < p_{\rm T} < 10$ GeV/c. Above 10 GeV/c the functions used to describe the $p_{\rm T}$ $(\mathscr{A} \times \varepsilon)$ distribution differs from the MC distribution, making the fit difficult, especially with the ratio of Levy functions which is very sensitive to fluctuations. Results of the fits using a ratio of two Levy functions are shown on Fig. 27 and using a third degree polynomial are shown on Fig.28. **Update : the $(\mathscr{A} \times \varepsilon)$ is fitted assigning the statistical. The Pol3 function that does not well describe the $(\mathscr{A} \times \varepsilon)$ at very low $p_{\rm T}$ was not considered in the parametrization. Moreover, it has been studied in previous analysis that the Levy function reproduces well the generated and reconstructed distributions from the simulations. It is therefore coherent to take a ratio of two Levy functions to parameterize the acceptance efficiency.**

8.5 Results hadronic J/ψ at very low $p_{\rm T}$

In each centrality class, several combinations of the foregoing parametrizations were tested in order to extract the expected number of J/ψ from hadronic production at low $p_{\rm T}$ using equation 18. Note that for each parametrization used in the latter, the fit must satisfy status = 0, cov matrix status = 3 and $\chi^2/{\rm NDF} < 2.5$.

A conservative approach is adopted to propagate the uncertainties from each element of the parametrization eq. 18. In order not to take into account twice the uncertainties on the pp cross section and the $(\mathscr{A} \times \varepsilon)$ only the statistical and uncorrelated systematic uncertainties not related to $\frac{{\rm d}\sigma_{\rm pp}^{\rm h\ J/\psi}}{{\rm d}p_{\rm T}}$ and the statistical uncertainty not related to $(\mathscr{A} \times \varepsilon)_{\rm AA}^{\rm h\ J/\psi}(p_{\rm T})$ are considered in the parametrization of the $R_{\rm AA}(p_{\rm T})$. The full uncertainties were considered for the parametrization of $\frac{{\rm d}\sigma_{\rm pp}^{\rm h\ J/\psi}}{{\rm d}p_{\rm T}}$ and only the statistical uncertainty was considered for the parametrization of $(\mathscr{A} \times \varepsilon)_{\rm AA}^{\rm h\ J/\psi}(p_{\rm T})$.

The eq. 18 can be reformulated to propagate the uncertainty on the parametrization taking into account the correlation between the integral and the normalization factor :

$$\int_{p_{\rm T1}}^{p_{\rm T2}} \frac{{\rm d}N_{\rm AA}^{\rm h\ J/\psi}}{{\rm d}p_{\rm T}} {\rm d}p_{\rm T} = N_{\rm J/\psi}(1 - 8\ {\rm GeV}/c) \times R(p_{\rm T}) \tag{23}$$

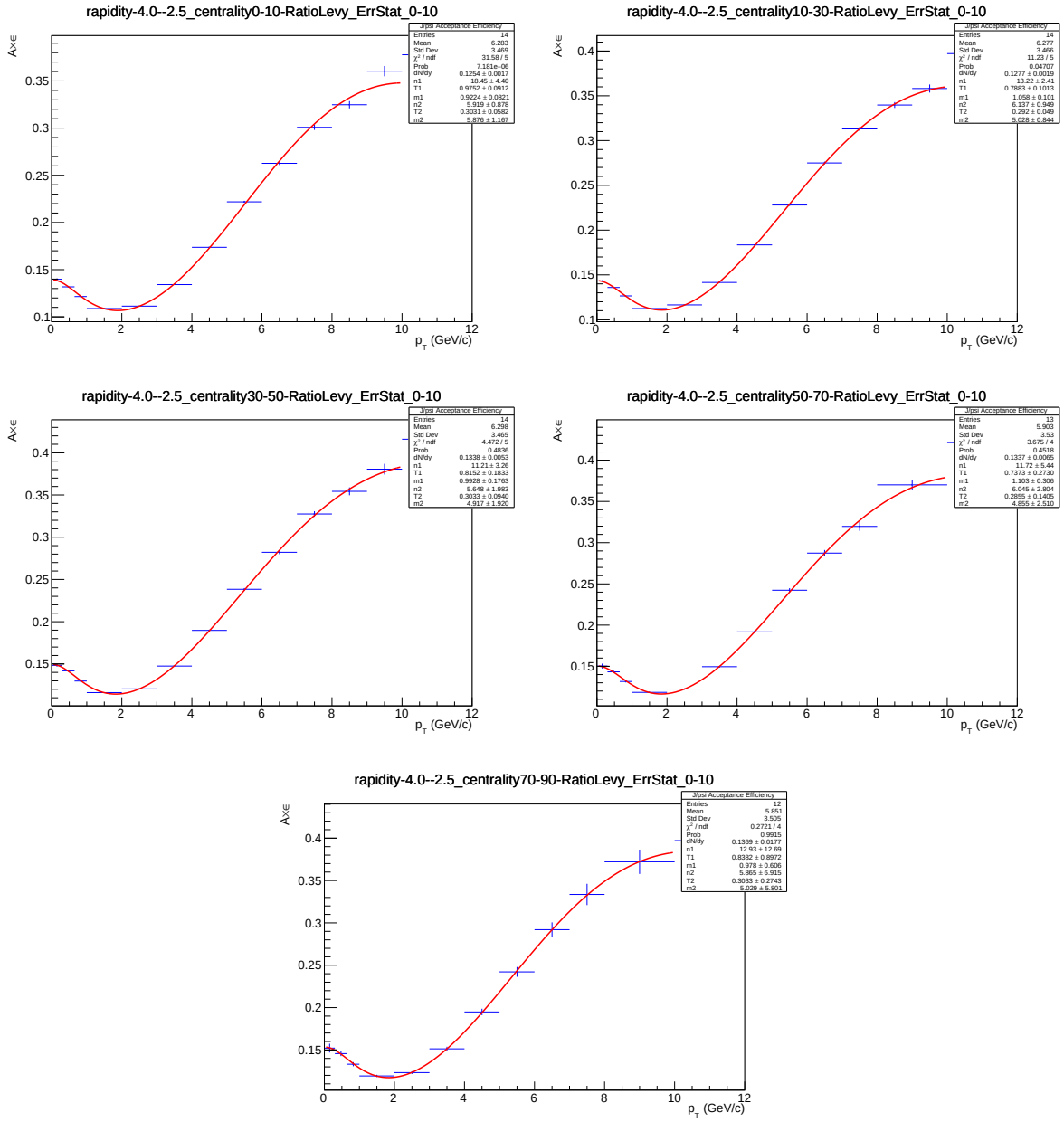

Fig. 27: Fit of $(\mathscr{A} \times \varepsilon)^{\mathrm{J}/\psi}_{\mathrm{AA}}(\Delta y, \Delta p_{\mathrm{T}})$ distribution as a function of p_{T} with a ratio of two Levy functions. The uncertainty on each data point is the quadratic sum of the statistical uncertainty and the uncorrelated systematic uncertainties on the $(\mathscr{A} \times \varepsilon)$.

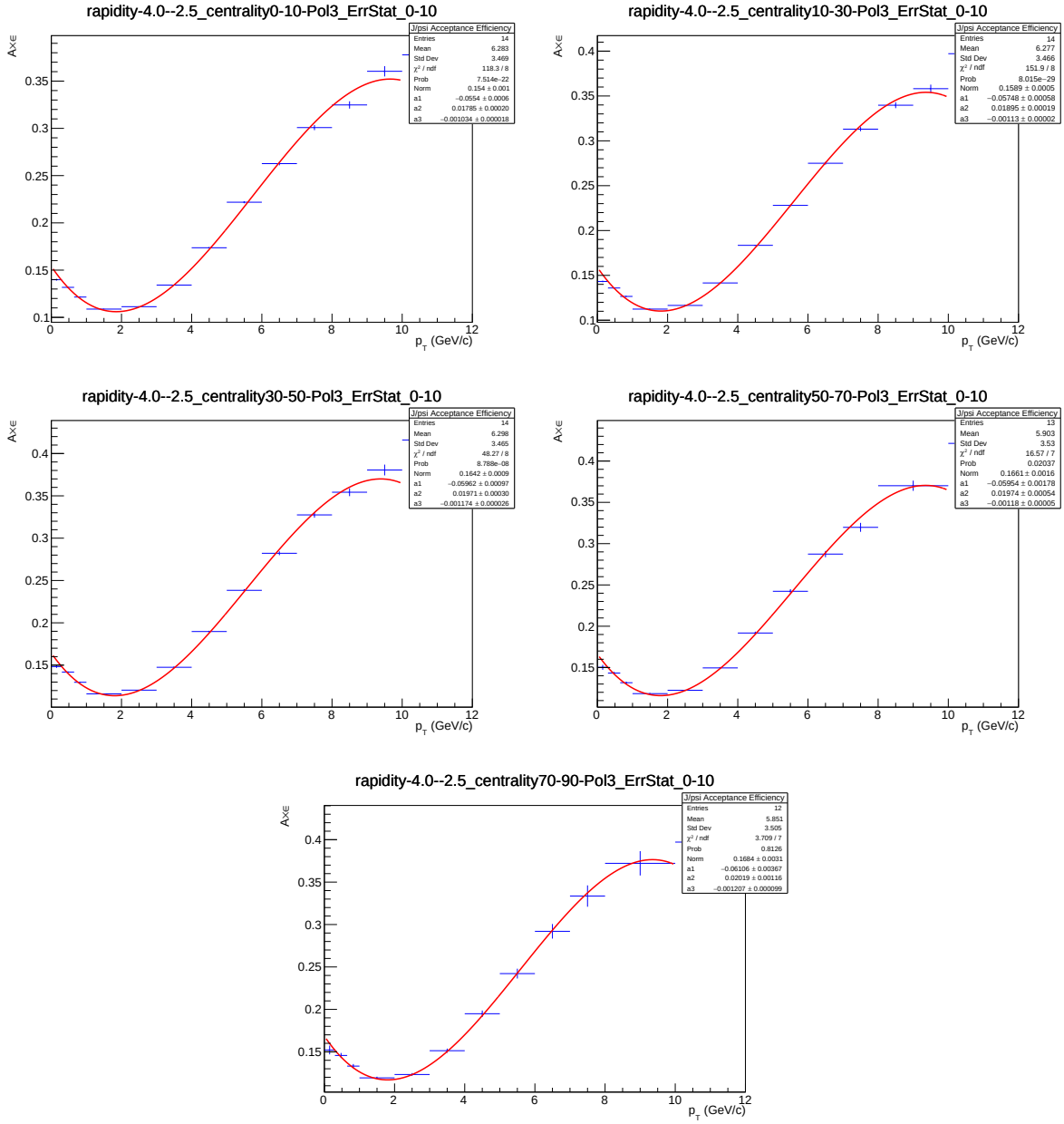

Fig. 28: Fit of $(\mathscr{A} \times \varepsilon)^{\mathrm{J}/\psi}_{\mathrm{AA}}(\Delta y, \Delta p_{\mathrm{T}})$ distribution as a function of p_{T} with a third degree polynomial. The uncertainty on each data point is the quadratic sum of the statistical uncertainty and the uncorrelated systematic uncertainties on the $(\mathscr{A} \times \varepsilon)$.

where $R(p_{\rm T})$ is the ratio of the integral in $[p_{\rm T1}, p_{\rm T2}]$ GeV/c over the integral in $[1,8]$ GeV/c. The uncertainty on $R(p_{\rm T})$ can be evaluated using the covariance matrix on the parametrization filled with the covariance matrix from each term of the parametrization and the jacobian matrix of $R(p_{\rm T})$.

The uncertainty on $R(p_{\rm T})$ is given by :

$$\sigma_R = \sqrt{Jcov J^{\rm T}} \tag{24}$$

The systematic uncertainty on $N_{\rm J/\psi}(1-8$ GeV/$c)$ is then summed in quadrature to σ_R. Only the statistical uncertainty on $N_{\rm J/\psi}(1-8$ GeV/$c)$ contributes to the statistical uncertainty on the parametrization.

Several combinations for the parametrization were considered in each centrality class. Combinations are listed below and results are reported in table 12, 13, 14, 15 and 16.

Tests in the centrality classes 50-70 % and 70-90 %

1. test $R_{\rm AA}$ with Constant fitted in 0.65-15 GeV/c, test pp reference cross section with PowerLawFree and test $(\mathscr{A} \times \varepsilon)$ with RatioLevy.
2. test $R_{\rm AA}$ with Constant fitted in 1-15 GeV/c, test pp reference cross section with PowerLawFree and test $(\mathscr{A} \times \varepsilon)$ with RatioLevy.
3. test $R_{\rm AA}$ with Linear fitted in 0.65-15 GeV/c, test pp reference cross section with PowerLawFree and test $(\mathscr{A} \times \varepsilon)$ with RatioLevy.
4. test $R_{\rm AA}$ with Linear fitted in 1-15 GeV/c, test pp reference cross section with PowerLawFree and test $(\mathscr{A} \times \varepsilon)$ with RatioLevy.
5. test $R_{\rm AA}$ with Constant fitted in 0.65-15 GeV/c, test pp reference cross section with PowerLaw-Fixed and test $(\mathscr{A} \times \varepsilon)$ with RatioLevy.
6. test $R_{\rm AA}$ with Constant fitted in 1-15 GeV/c, test pp reference cross section with PowerLawFixed and test $(\mathscr{A} \times \varepsilon)$ with RatioLevy.
7. test $R_{\rm AA}$ with Linear fitted in 0.65-15 GeV/c, test pp reference cross section with PowerLawFixed and test $(\mathscr{A} \times \varepsilon)$ with RatioLevy.
8. test $R_{\rm AA}$ with Linear fitted in 1-15 GeV/c, test pp reference cross section with PowerLawFixed and test $(\mathscr{A} \times \varepsilon)$ with RatioLevy.
9. test $R_{\rm AA}$ with Constant fitted in 0.65-15 GeV/c, test pp reference cross section with Levy and test $(\mathscr{A} \times \varepsilon)$ with RatioLevy.
10. test $R_{\rm AA}$ with Constant fitted in 1-15 GeV/c, test pp reference cross section with Levy and test $(\mathscr{A} \times \varepsilon)$ with RatioLevy.
11. test $R_{\rm AA}$ with Linear fitted in 0.65-15 GeV/c, test pp reference cross section with Levy and test $(\mathscr{A} \times \varepsilon)$ with RatioLevy.
12. test $R_{\rm AA}$ with Linear fitted in 1-15 GeV/c, test pp reference cross section with Levy and test $(\mathscr{A} \times \varepsilon)$ with RatioLevy.

Tests in the centrality classes 0-10%, 10-30% and 30-50%

test	Syst. Uncorr. on $R(p_{\rm T})$ (%)	Syst. Uncorr. on $N_{\rm J/\psi}(1-8$ GeV/$c)$(%)	Total Syst. Uncorr. (%)	$N^{\rm J/\psi}_{hadro}$ $\pm(stat.)\pm(syst.)$
1	5.60	2.70	6.22	$141\pm3\pm9$
2	5.60	2.70	6.22	$141\pm3\pm9$
3	6.31	2.70	6.86	$148\pm3\pm10$
4	6.43	2.70	6.98	$146\pm3\pm10$
5	3.79	2.70	4.65	$130\pm2\pm6$
6	3.79	2.70	4.65	$130\pm2\pm6$
7	4.74	2.70	5.46	$137\pm3\pm7$
8	4.91	2.70	5.61	$134\pm3\pm8$
9	3.56	2.70	4.47	$134\pm3\pm6$
10	3.56	2.70	4.47	$134\pm3\pm6$
11	4.56	2.70	5.30	$140\pm3\pm7$
12	4.74	2.70	5.46	$138\pm3\pm8$
Total				$138\pm3\pm9$

Table 12: Number of hadronic J/ψ for $p_{\rm T} < 0.3$ GeV/c for each combination of the hadronic parametrization in the centrality class 70-90%.

test	Syst. Uncorr. on $R(p_{\rm T})$ (%)	Syst. Uncorr. on $N_{\rm J/\psi}(1-8$ GeV/$c)$(%)	Total Syst. Uncorr. (%)	$N^{\rm J/\psi}_{hadro}$ $\pm(stat.)\pm(syst.)$
1	5.18	2.64	5.82	$702\pm8\pm41$
2	5.18	2.64	5.82	$702\pm8\pm41$
3	5.57	2.64	6.17	$704\pm8\pm43$
4	5.64	2.64	6.22	$707\pm8\pm44$
5	3.14	2.64	4.11	$649\pm8\pm27$
6	3.14	2.64	4.11	$649\pm8\pm27$
7	3.74	2.64	4.58	$651\pm8\pm30$
8	3.83	2.64	4.65	$653\pm8\pm30$
9	2.86	2.64	3.89	$667\pm8\pm26$
10	2.86	2.64	3.89	$667\pm8\pm26$
11	3.51	2.64	4.39	$669\pm8\pm29$
12	3.60	2.64	4.47	$671\pm8\pm30$
Total				$674\pm8\pm40$

Table 13: Number of hadronic J/ψ for $p_{\rm T} < 0.3$ GeV/c for each combination of the hadronic parametrization in the centrality class 50-70%.

1. test $R_{\rm AA}$ with WoodSaxonLikeFree fitted in 0.65-15 GeV/c, test pp reference cross section with PowerLawFree and test $(\mathscr{A} \times \varepsilon)$ with RatioLevy.
2. test $R_{\rm AA}$ with WoodSaxonLikeFree fitted in 1-15 GeV/c, test pp reference cross section with PowerLawFree and test $(\mathscr{A} \times \varepsilon)$ with RatioLevy.
3. test $R_{\rm AA}$ with WoodSaxonLike fixed to $m_{\rm J/\psi}$ fitted in 0.65-15 GeV/c, test pp reference cross section with PowerLawFree and test $(\mathscr{A} \times \varepsilon)$ with RatioLevy.
4. test $R_{\rm AA}$ with WoodSaxonLike fixed to $m_{\rm J/\psi}$ fitted in 1-15 GeV/c, test pp reference cross section with PowerLawFree and test $(\mathscr{A} \times \varepsilon)$ with RatioLevy.
5. test $R_{\rm AA}$ with WoodSaxonLike fixed to $m_{\rm J/\psi}/2$ fitted in 0.65-15 GeV/c, test pp reference cross section with PowerLawFree and test $(\mathscr{A} \times \varepsilon)$ with RatioLevy.
6. test $R_{\rm AA}$ with WoodSaxonLike fixed to $m_{\rm J/\psi}/2$ fitted in 1-15 GeV/c, test pp reference cross section with PowerLawFree and test $(\mathscr{A} \times \varepsilon)$ with RatioLevy.
7. test $R_{\rm AA}$ with WoodSaxonLike fixed to $\langle p_{\rm T} \rangle$ fitted in 0.65-15 GeV/c, test pp reference cross section with PowerLawFree and test $(\mathscr{A} \times \varepsilon)$ with RatioLevy.
8. test $R_{\rm AA}$ with WoodSaxonLike fixed to $\langle p_{\rm T} \rangle$ fitted in 1-15 GeV/c, test pp reference cross section with PowerLawFree and test $(\mathscr{A} \times \varepsilon)$ with RatioLevy.
9. test $R_{\rm AA}$ with WoodSaxonLike fixed to $2\langle p_{\rm T} \rangle$ fitted in 0.65-15 GeV/c, test pp reference cross section with PowerLawFree and test $(\mathscr{A} \times \varepsilon)$ with RatioLevy.
10. test $R_{\rm AA}$ with WoodSaxonLike fixed to $2\langle p_{\rm T} \rangle$ fitted in 1-15 GeV/c, test pp reference cross section with PowerLawFree and test $(\mathscr{A} \times \varepsilon)$ with RatioLevy.
11. test $R_{\rm AA}$ with WoodSaxonLikeFree fitted in 0.65-15 GeV/c, test pp reference cross section with PowerLawFixed and test $(\mathscr{A} \times \varepsilon)$ with RatioLevy.
12. test $R_{\rm AA}$ with WoodSaxonLikeFree fitted in 1-15 GeV/c, test pp reference cross section with PowerLawFixed and test $(\mathscr{A} \times \varepsilon)$ with RatioLevy.
13. test $R_{\rm AA}$ with WoodSaxonLike fixed to $m_{\rm J/\psi}$ fitted in 0.65-15 GeV/c, test pp reference cross section with PowerLawFixed and test $(\mathscr{A} \times \varepsilon)$ with RatioLevy.
14. test $R_{\rm AA}$ with WoodSaxonLike fixed to $m_{\rm J/\psi}$ fitted in 1-15 GeV/c, test pp reference cross section with PowerLawFixed and test $(\mathscr{A} \times \varepsilon)$ with RatioLevy.
15. test $R_{\rm AA}$ with WoodSaxonLike fixed to $m_{\rm J/\psi}/2$ fitted in 0.65-15 GeV/c, test pp reference cross section with PowerLawFixed and test $(\mathscr{A} \times \varepsilon)$ with RatioLevy.
16. test $R_{\rm AA}$ with WoodSaxonLike fixed to $m_{\rm J/\psi}/2$ fitted in 1-15 GeV/c, test pp reference cross section with PowerLawFixed and test $(\mathscr{A} \times \varepsilon)$ with RatioLevy.
17. test $R_{\rm AA}$ with WoodSaxonLike fixed to $\langle p_{\rm T} \rangle$ fitted in 0.65-15 GeV/c, test pp reference cross section with PowerLawFixed and test $(\mathscr{A} \times \varepsilon)$ with RatioLevy.
18. test $R_{\rm AA}$ with WoodSaxonLike fixed to $\langle p_{\rm T} \rangle$ fitted in 1-15 GeV/c, test pp reference cross section with PowerLawFixed and test $(\mathscr{A} \times \varepsilon)$ with RatioLevy.
19. test $R_{\rm AA}$ with WoodSaxonLike fixed to $2\langle p_{\rm T} \rangle$ fitted in 0.65-15 GeV/c, test pp reference cross section with PowerLawFixed and test $(\mathscr{A} \times \varepsilon)$ with RatioLevy.

20. test R_{AA} with WoodSaxonLike fixed to $2\langle p_{\mathrm{T}}\rangle$ fitted in 1-15 GeV/c, test pp reference cross section with PowerLawFixed and test $(\mathscr{A} \times \varepsilon)$ with RatioLevy.
21. test R_{AA} with WoodSaxonLikeFree fitted in 0.65-15 GeV/c, test pp reference cross section with Levy and test $(\mathscr{A} \times \varepsilon)$ with RatioLevy.
22. test R_{AA} with WoodSaxonLikeFree fitted in 1-15 GeV/c, test pp reference cross section with Levy and test $(\mathscr{A} \times \varepsilon)$ with RatioLevy.
23. test R_{AA} with WoodSaxonLike fixed to $m_{\mathrm{J}/\psi}$ fitted in 0.65-15 GeV/c, test pp reference cross section with Levy and test $(\mathscr{A} \times \varepsilon)$ with RatioLevy.
24. test R_{AA} with WoodSaxonLike fixed to $m_{\mathrm{J}/\psi}$ fitted in 1-15 GeV/c, test pp reference cross section with Levy and test $(\mathscr{A} \times \varepsilon)$ with RatioLevy.
25. test R_{AA} with WoodSaxonLike fixed to $m_{\mathrm{J}/\psi}/2$ fitted in 0.65-15 GeV/c, test pp reference cross section with Levy and test $(\mathscr{A} \times \varepsilon)$ with RatioLevy.
26. test R_{AA} with WoodSaxonLike fixed to $m_{\mathrm{J}/\psi}/2$ fitted in 1-15 GeV/c, test pp reference cross section with Levy and test $(\mathscr{A} \times \varepsilon)$ with RatioLevy.
27. test R_{AA} with WoodSaxonLike fixed to $\langle p_{\mathrm{T}}\rangle$ fitted in 0.65-15 GeV/c, test pp reference cross section with Levy and test $(\mathscr{A} \times \varepsilon)$ with RatioLevy.
28. test R_{AA} with WoodSaxonLike fixed to $\langle p_{\mathrm{T}}\rangle$ fitted in 1-15 GeV/c, test pp reference cross section with Levy and test $(\mathscr{A} \times \varepsilon)$ with RatioLevy.
29. test R_{AA} with WoodSaxonLike fixed to $2\langle p_{\mathrm{T}}\rangle$ fitted in 0.65-15 GeV/c, test pp reference cross section with Levy and test $(\mathscr{A} \times \varepsilon)$ with RatioLevy.
30. test R_{AA} with WoodSaxonLike fixed to $2\langle p_{\mathrm{T}}\rangle$ fitted in 1-15 GeV/c, test pp reference cross section with Levy and test $(\mathscr{A} \times \varepsilon)$ with RatioLevy.

Finally, the number of J/ψ from hadronic production for $p_{\mathrm{T}} < 0.3$ GeV/c and for each centrality class is obtained as the average of the various parametrization results. The associated statistical uncertainty comes from the statistical uncertainty on $N_{\mathrm{J}/\psi}(1-8$ GeV/$c)$. The systematic uncertainty is the quadratic sum of the average of each individual systematic uncertainty and of the standard deviation of the parametrization results. The number of hadronic J/ψ from hadronic production used to extract the excess are reported in table 17.

test	Syst. Uncorr. on $R(p_{\mathrm{T}})$ (%)	Syst. Uncorr. on $N_{\mathrm{J}/\psi}(1-8\ \mathrm{GeV}/c)(\%)$	Total Syst. Uncorr. (%)	$N^{\mathrm{J}/\psi}_{hadro}$ $\pm(stat.)\pm(syst.)$
1	5.80	2.60	6.36	$2611\pm24\pm166$
2	5.81	2.60	6.37	$2597\pm24\pm165$
3	5.41	2.60	6.01	$2747\pm25\pm165$
4	5.50	2.60	6.08	$2755\pm25\pm168$
5	6.08	2.60	6.61	$2811\pm26\pm186$
6	6.54	2.60	7.04	$2840\pm26\pm200$
7	5.77	2.60	6.33	$2787\pm25\pm176$
8	6.02	2.60	6.56	$2807\pm26\pm184$
9	5.54	2.60	6.12	$2558\pm23\pm157$
10	5.55	2.60	6.13	$2548\pm23\pm156$
11	4.01	2.60	4.79	$2409\pm22\pm115$
12	4.03	2.60	4.80	$2396\pm22\pm115$
13	3.43	2.60	4.30	$2535\pm23\pm109$
14	3.55	2.60	4.41	$2543\pm23\pm112$
15	4.40	2.60	5.12	$2594\pm24\pm133$
16	5.01	2.60	5.65	$2621\pm24\pm148$
17	3.96	2.60	4.74	$2572\pm23\pm122$
18	4.31	2.60	5.04	$2590\pm24\pm131$
19	3.64	2.60	4.48	$2360\pm21\pm106$
20	3.65	2.60	4.48	$2351\pm21\pm105$
21	3.79	2.60	4.60	$2478\pm23\pm114$
22	3.81	2.60	4.61	$2465\pm22\pm114$
23	3.18	2.60	4.11	$2607\pm24\pm107$
24	3.31	2.60	4.22	$2615\pm24\pm110$
25	4.21	2.60	4.95	$2668\pm24\pm132$
26	4.85	2.60	5.50	$2696\pm25\pm148$
27	3.75	2.60	4.57	$2646\pm24\pm121$
28	4.12	2.60	4.87	$2664\pm24\pm130$
29	3.39	2.60	4.28	$2428\pm22\pm104$
30	3.40	2.60	4.28	$2419\pm22\pm104$
Total				$2591\pm24\pm192$

Table 14: Number of hadronic J/ψ for $p_{\mathrm{T}} < 0.3$ GeV$/c$ for each combination of the hadronic parametrization in the centrality class 30-50%.

test	Syst. Uncorr. on $R(p_{\rm T})$ (%)	Syst. Uncorr. on $N_{\rm J/\psi}(1-8$ GeV/$c)$(%)	Total Syst. Uncorr. (%)	$N^{\rm J/\psi}_{hadro}$ $\pm(stat.)\pm(syst.)$
1	7.35	2.65	7.81	$8523 \pm 62 \pm 666$
2	8.19	2.65	8.61	$8401 \pm 61 \pm 723$
3	5.18	2.65	5.81	$8888 \pm 65 \pm 517$
4	5.21	2.65	5.85	$8899 \pm 65 \pm 520$
5	5.77	2.65	6.35	$9716 \pm 71 \pm 617$
6	6.12	2.65	6.67	$9903 \pm 72 \pm 660$
7	5.52	2.65	6.12	$9456 \pm 69 \pm 579$
8	5.70	2.65	6.28	$9560 \pm 69 \pm 601$
9	5.25	2.65	5.88	$7719 \pm 56 \pm 454$
10	5.27	2.65	5.90	$7672 \pm 56 \pm 452$
11	5.99	2.65	6.55	$7852 \pm 57 \pm 514$
12	7.00	2.65	7.48	$7739 \pm 56 \pm 579$
13	2.92	2.65	3.94	$8189 \pm 59 \pm 323$
14	2.98	2.65	3.99	$8199 \pm 60 \pm 327$
15	3.89	2.65	4.71	$8955 \pm 65 \pm 422$
16	4.39	2.65	5.12	$9127 \pm 66 \pm 468$
17	3.50	2.65	4.39	$8715 \pm 63 \pm 382$
18	3.77	2.65	4.61	$8810 \pm 64 \pm 406$
19	3.06	2.65	4.04	$7112 \pm 52 \pm 288$
20	3.09	2.65	4.07	$7069 \pm 51 \pm 288$
21	5.84	2.65	6.42	$8080 \pm 59 \pm 518$
22	6.87	2.65	7.36	$7964 \pm 58 \pm 586$
23	2.64	2.65	3.74	$8426 \pm 61 \pm 315$
24	2.71	2.65	3.79	$8436 \pm 61 \pm 319$
25	3.69	2.65	4.54	$9212 \pm 67 \pm 418$
26	4.20	2.65	4.97	$9388 \pm 68 \pm 467$
27	3.27	2.65	4.21	$8966 \pm 65 \pm 377$
28	3.56	2.65	4.43	$9064 \pm 66 \pm 402$
29	2.77	2.65	3.83	$7320 \pm 53 \pm 281$
30	2.81	2.65	3.86	$7276 \pm 53 \pm 281$
Total				$8488 \pm 62 \pm 904$

Table 15: Number of hadronic J/ψ for $p_{\rm T} < 0.3$ GeV/c for each combination of the hadronic parametrization in the centrality class 10-30%.

test	Syst. Uncorr. on $R(p_{\mathrm{T}})$ (%)	Syst. Uncorr. on $N_{\mathrm{J}/\psi}(1-8$ GeV$/c)(\%)$	Total Syst. Uncorr. (%)	$N^{\mathrm{J}/\psi}_{hadro}$ $\pm(stat.)\pm(syst.)$
1	7.59	2.69	8.05	$9025\pm89\pm727$
2	8.57	2.69	8.98	$8890\pm87\pm799$
3	5.12	2.69	5.78	$9311\pm91\pm539$
4	5.14	2.69	5.80	$9314\pm91\pm540$
5	5.67	2.69	6.27	$10558\pm104\pm662$
6	5.92	2.69	6.50	$10767\pm106\pm700$
7	5.46	2.69	6.09	$10238\pm101\pm623$
8	5.61	2.69	6.22	$10360\pm102\pm644$
9	5.22	2.69	5.87	$7932\pm78\pm466$
10	5.24	2.69	5.89	$7892\pm78\pm464$
11	6.25	2.69	6.80	$8308\pm82\pm565$
12	7.41	2.69	7.89	$8183\pm80\pm645$
13	2.74	2.69	3.84	$8572\pm84\pm329$
14	2.78	2.69	3.86	$8574\pm84\pm331$
15	3.68	2.69	4.55	$9723\pm95\pm443$
16	4.05	2.69	4.86	$9915\pm97\pm482$
17	3.35	2.69	4.30	$9428\pm93\pm405$
18	3.57	2.69	4.47	$9540\pm94\pm426$
19	2.93	2.69	3.97	$7300\pm72\pm290$
20	2.96	2.69	3.99	$7264\pm71\pm290$
21	6.11	2.69	6.67	$8550\pm84\pm571$
22	7.29	2.69	7.77	$8422\pm83\pm655$
23	2.45	2.69	3.64	$8821\pm87\pm321$
24	2.49	2.69	3.66	$8824\pm87\pm323$
25	3.47	2.69	4.39	$10003\pm98\pm439$
26	3.86	2.69	4.70	$10200\pm100\pm480$
27	3.12	2.69	4.12	$9700\pm95\pm399$
28	3.36	2.69	4.30	$9815\pm96\pm422$
29	2.64	2.69	3.76	$7516\pm74\pm283$
30	2.67	2.69	3.79	$7479\pm73\pm283$
Total				$9014\pm89\pm1103$

Table 16: Number of hadronic J/ψ for $p_{\mathrm{T}}<0.3$ GeV$/c$ for each combination of the hadronic parametrization in the centrality class 0-10%.

Centrality class	$N^{raw}_{\rm J/\psi}$	$N^{hadro}_{\rm J/\psi}$	$N^{excess}_{\rm J/\psi}$	$N^{coh}_{\rm J/\psi}$
0-10%	$8351 \pm 762 \pm 312$	$9014 \pm 89 \pm 1103$	$-663 \pm 767 \pm 1146$	$\sim$
10-30%	$9624 \pm 571 \pm 278$	$8488 \pm 62 \pm 904$	$1136 \pm 574 \pm 946$	$\sim$
30-50%	$4280 \pm 225 \pm 105$	$2591 \pm 24 \pm 192$	$1689 \pm 226 \pm 219$	$1462 \pm 197 \pm 195$
50-70%	$2763 \pm 98 \pm 68$	$674 \pm 8 \pm 40$	$2089 \pm 98 \pm 79$	$1808 \pm 88 \pm 88$
70-90%	$1758 \pm 57 \pm 32$	$138 \pm 3 \pm 9$	$1620 \pm 57 \pm 33$	$1402 \pm 52 \pm 52$

Table 17: Number of J/ψ from hadronic production obtained with a parametrization of the hadronic contribution at low $p_{\rm T}$ and the corresponding number of J/ψ in excess for $p_{\rm T} < 0.3$ GeV/c.

9 J/ψ coherent photoproduction cross section

Considering the coherent photoproduction of J/ψ as the underlying production process of the excess, the number of coherently photoproduced J/ψ in $0 < p_{\rm T} < 0.3$ GeV/c can be evaluated as :

$$N^{\rm J/\psi}_{\rm coh} = \frac{N^{\rm J/\psi}_{\rm excess}}{1 + f_{\rm I} + f_{\rm D}} = \frac{N^{\rm J/\psi}_{\rm raw} - N^{\rm J/\psi}_{\rm hadro}}{1 + f_{\rm I} + f_{\rm D}} \tag{25}$$

where $f_{\rm I}$ is the fraction of J/ψ from incoherent photoproduction in $0 < p_{\rm T} < 0.3$ GeV/c and $f_{\rm D}$ the fraction of J/ψ from the feed down of coherently photoproduced ψ(2S) in $0 < p_{\rm T} < 0.3$ GeV/c.
The significance of the excess reaches 24.5σ in the most peripheral class, 16.6σ and 5.4σ in the centrality class 50-70% and 30-50%, respectively. In central events, the excess is compatible with zero within the uncertainties. For this reason, the number of coherent J/ψ in these intervals has not been calculated.

Values of $f_{\rm I}$ and $f_{\rm D}$ are provided by an UPC analysis in which the absence of a hadronic contribution makes easier the extraction of each photoproduced contribution. The method is similar as the one employed in [11] with some adjustments to match as closely as possible the triggers and kinematic intervals used in the analysis.

Previous values were taken in the paper of coherent J/ψ photoproduction at $\sqrt{s_{\rm NN}} = 5.02$ TeV in ultraperipheral collisions [12]. These values were extracted applying a $p_{\rm T}$ cut at 0.25 GeV/c : $f_{\rm D} = 0.055 \pm 0.01$ and $f_{\rm I} = 0.055 \pm 0.001$.
Update : For preliminary results, we used the values of $f_{\rm I}$ and $f_{\rm D}$ provided by an UPC analysis based on the CMUP6 trigger class. $f_{\rm D} = 0.0664 \pm 0.0114$ and $f_{\rm I} = 0.0888 \pm 0.0338$. Since the systematic uncertainties are not yet evaluated, we took the difference observed between the new values with the previous ones (i.e. from the UPC paper) as the systematic uncertainties on the fractions.

Table 17 shows the results of the number of J/ψ in excess and the number of J/ψ obtained with eq. 25 considering the coherent photoproduction as the underlying physics mechanism. We assumed that the fractions $f_{\rm I}$ and $f_{\rm D}$ are not centrality dependent. **We are currently in contact with theorists to provide a possible aditional systematic uncertainty on this assumption.**

Finally, the coherent J/ψ coherent photoproduction cross section is calculated as:

$$\frac{{\rm d}\sigma^{\rm J/\psi}_{\rm coh}}{{\rm d}y} = \frac{N^{\rm J/\psi}_{\rm coh}}{BR_{\rm J/\psi \to \mu^+\mu^-} \times (\mathscr{A} \times \varepsilon)^{\rm J/\psi}_{\rm coh} \times \mathscr{L}_{\rm int} \times \Delta y} \tag{26}$$

where $BR = 5.961 \pm 0.033$ % [6] is the branching ratio of J/ψ decaying into dimuon, $(\mathscr{A} \times \varepsilon)^{\rm J/\psi}_{\rm coh}$ is

the acceptance efficiency correction of the detector for coherent J/ψ photoproduction evaluated using STARLIGHT simulation as described in 7 and $\mathscr{L}_{\rm int} = 758.7 \pm 38.4\ \mu{\rm b}^{-1}$ is the integrated luminosity on the three periods reported in table 1.

9.1 Systematic uncertainties

The systematic uncertainties on the J/ψ coherent photoproduction cross section as function of the centrality reported in table 18 are discussed in this section.

Tracking Efficiency and Trigger Efficiency and Matching
The systematic uncertainties on the tracking, trigger and matching efficiency are the same as those discussed in section 8.1.
Only the systematic uncertainty on the MC inputs is different due to the MC production used for the measurement of the acceptance efficiency. In the case of the coherent photoproduction cross section, we use embedded STARLIGHT signal simulations. The associated systematic uncertainty therefore comes from the $p_{\rm T}$ shape for coherent J/ψ used by the STARLIGHT generator. This uncertainties has been estimated as 0.1% by the UPC analysis [12].

The raw number of J/ψ in excess
The systematic uncertainty on $N^{J/\psi}_{\rm excess}$ contains

- the uncertainty on the raw signal extraction as discussed in 6 and reported in table 4.
- the average of the uncertainties on the each parametrization σ_R.
- the dispersion of the results from the various parametrizations as discussed in 8.5.

The fractions $f_{\rm I}$ and $f_{\rm D}$
The systematic uncertainties on $f_{\rm I}$ and $f_{\rm D}$ are not yet evaluated, we took the difference observed between the new values with the previous ones (i.e. from the UPC paper) as the systematic uncertainties on the fractions. Finally, an additional systematic uncertainty could be added on the assumption that $f_{\rm I}$ and $f_{\rm D}$ are not centrality dependent.

Others
The systematic uncertainty on the integrated luminosity is discussed section 5.

The systematic uncertainty on the centrality limits is the same used in 8.1.

9.2 Results

The J/ψ coherent photoproduction cross section has been evaluated for 3 centrality classes (30-50%, 50-70% and 70-90%) for $-4 < y < -2.5$. The systematic uncertainties considered in the calculation are listed table 18 and results are quoted below as ${\rm d}\sigma^{J/\psi}_{\rm coh}/{\rm d}y \pm$ stat (%) $\pm$ uncor. syst (%) $\pm$ cor. syst (%).

$$ {\rm d}\sigma^{J/\psi}_{\rm coh}/{\rm d}y(30-50\%) = (176.02 \pm 23.66(13.44\%) \pm 22.9(13.01\%) \pm 12.79(7.27\%))\ \mu{\rm b} $$

$$ {\rm d}\sigma^{J/\psi}_{\rm coh}/{\rm d}y(50-70\%) = (215.48 \pm 10.43(4.84\%) \pm 9.21(4.27\%) \pm 15.65(7.27\%))\ \mu{\rm b} $$

Source	Value
BR	0.5*
$N_{\rm excess}^{\rm J/\psi}$	2 - 12.97
$f_{\rm I}$	2.9*
$f_{\rm D}$	1*
MCH	3* + 0 - 0.5
MTR	2.8* + 0 - 0.5
Matching	1*
$p_{\rm T}$ shape for coherent J/ψ	0.1*
Centrality limits	0.9 - 3.5
$\mathscr{L}_{\rm int}$	5*
Total	7.27* + 4.1 - 13

Table 18: Systematic uncertainties on the J/ψ coherent photoproduction cross section versus centrality in %. The values marked with an * correspond to uncertainties correlated over the centrality.

$$\mathrm{d}\sigma_{\rm coh}^{\rm J/\psi}/\mathrm{d}y(70-90\%) = (166.22 \pm 6.15(3.7\%) \pm 6.74(4.06\%) \pm 12.08(7.27\%))\ \mu\mathrm{b}$$

The J/ψ coherent photoproduction cross section is shown in Fig 29 as a function of $\langle N_{\rm part} \rangle$. Empty boxes correspond to the uncorrelated systematic uncertainties. The correlated systematic uncertainty over the centrality amounts 4.84% and is quoted is the legend.

The cross section from this analysis is shown as function of y together with preliminary result at mid-rapidity [13] on figure 30 for the centrality class 50-70% (70-90%) on top (bottom). It should be noted that mid-rapidity analysis only used the 2015 data sample. The coherent photoproduction cross section is compared with theoritical calculations that used an effective description based on UPC dipole models. The GG-hs and GS-hs calculations are based on energy dependent hot-spot models extended to the nuclear case using the Glauber-Gribov formalism and using geometric scaling to obtain the nuclear saturation scale, respectively [14]. In the GBW calculation, the light cone colour dipole formalism was used while the IIM calculation is based on the Color Glass Consensate approach [15]. The models are able to qualitatively describe the magnitude of the cross section at mid-rapidity and forward rapidity in peripheral events.

The cross section measured at 5.02 TeV are also compared to the ALICE results from Run-1 data in Pb–Pb collisions at 2.76 TeV [16] on figure 31. In a future version of the analysis note, these results will be compared with models. The magnitude of the increase of the cross section can be compared to theoretical expectations. We will also be able to see if these new results as a function of centrality can help to favour one of the scenarios considered to maintain the condition of coherence in hadronic collisions. These scenarios imply either the whole nucleus or only the spectators for coherence both for the photon emitter or for the pomeron emitter [17]. According to this model, some scenarios are able to describe the increase of the cross section in the centrality class 50-70% with respect to 70-90%.

Finally, the results from this analysis are compared to those from preliminary results at the same center-of-mass energy but only using the 2015 data sample [18]. The comparison is shown top figure 32. Results are compatible within the large systematic uncertainties. The statistical uncertainty was reduced by a factor of ~ 1.4 and the full systematic uncertainty was reduced by a factor of ~ 4. We can see that new

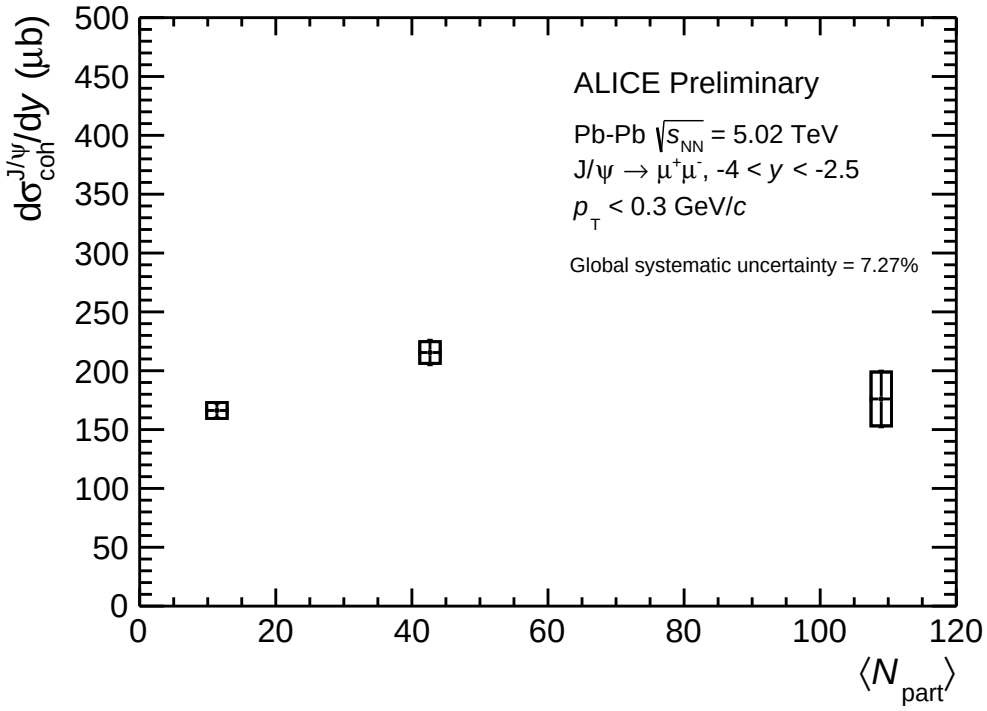

Fig. 29: J/ψ coherent photoproduction cross section as function of $\langle N_{\rm part} \rangle$ at forward rapidity in Pb–Pb collisions at $\sqrt{s_{\rm NN}} = 5.02$ TeV.

results are systematically larger with respect to previous preliminary results. The previous preliminary results used $f_{\rm I}$ and $f_{\rm D}$ fractions at 2.76 TeV (both values are a factor of 2 larger w.r.t. 5.02 TeV). A systematic uncertainty of 20% was added on the assumption that fractions are not energy dependent. By using the same fractions to compute the coherent photoproduction cross section, (bottom figure 32) the results are compatible.

Additionnal figures for preliminary results

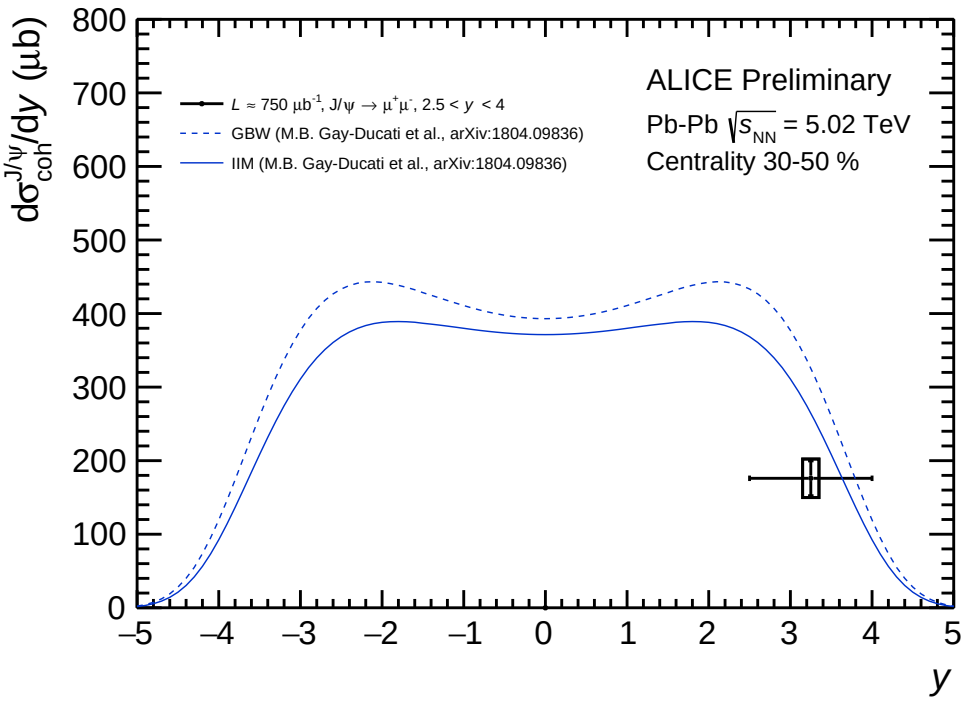
ALICE Preliminary
Pb-Pb $\sqrt{s_{\mathrm{NN}}}$ = 5.02 TeV
Centrality 30-50 %
$L \approx 750\ \mu b^{-1}$, $J/\psi \to \mu^+\mu^-$, $2.5 < y < 4$
GBW (M.B. Gay-Ducati et al., arXiv:1804.09836)
IIM (M.B. Gay-Ducati et al., arXiv:1804.09836)
$d\sigma^{J/\psi}_{coh}/dy$ (μb)
y

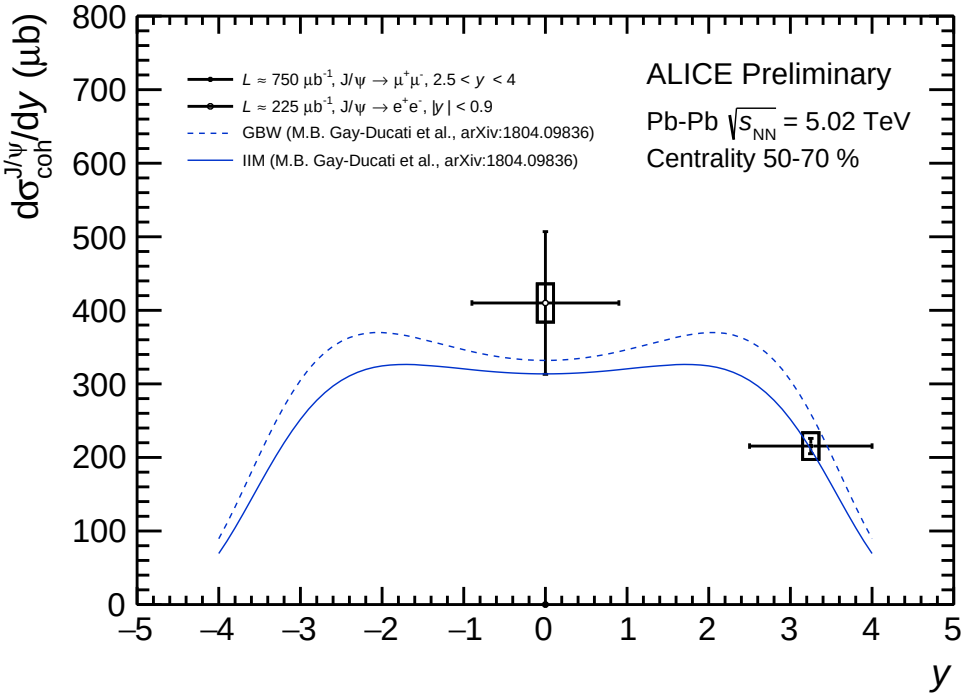
ALICE Preliminary
Pb-Pb $\sqrt{s_{\mathrm{NN}}}$ = 5.02 TeV
Centrality 50-70 %
$L \approx 750\ \mu b^{-1}$, $J/\psi \to \mu^+\mu^-$, $2.5 < y < 4$
$L \approx 225\ \mu b^{-1}$, $J/\psi \to e^+e^-$, $|y| < 0.9$
GBW (M.B. Gay-Ducati et al., arXiv:1804.09836)
IIM (M.B. Gay-Ducati et al., arXiv:1804.09836)
$d\sigma^{J/\psi}_{coh}/dy$ (μb)
y

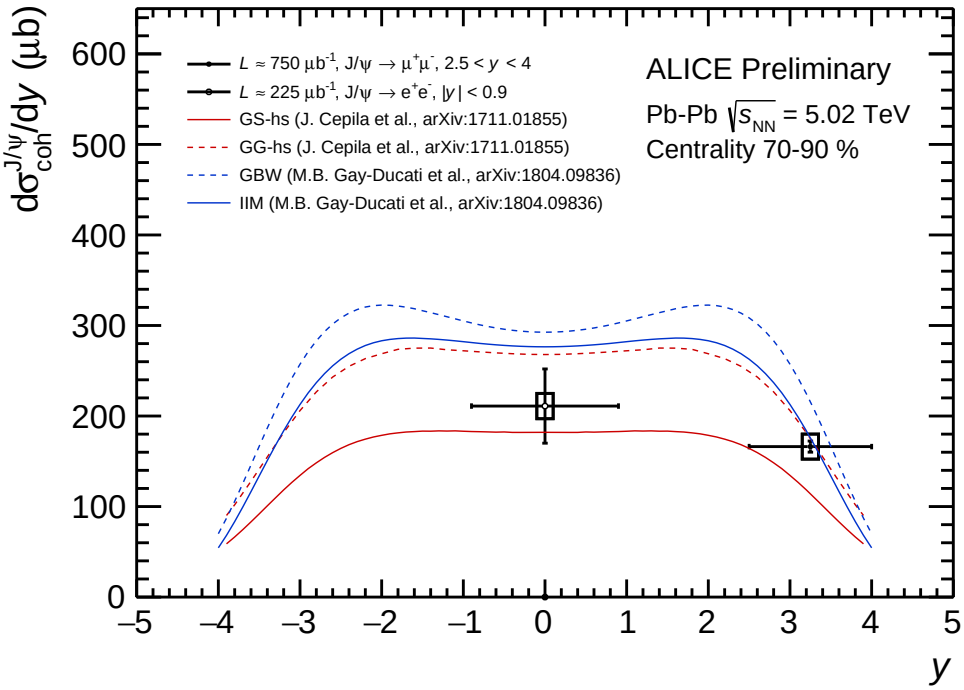

Fig. 30: J/ψ coherent photoproduction cross section as function of y in Pb–Pb collisions at $\sqrt{s_{\rm NN}} = 5.02$ TeV for the centrality class 30-50%, 50-70% and 70-90% on top, middel and bottom, respectively. Results are compared to theoritical calculations [14, 15]. Preliminary results at mid-rapidity only used the 2015 data sample [13].

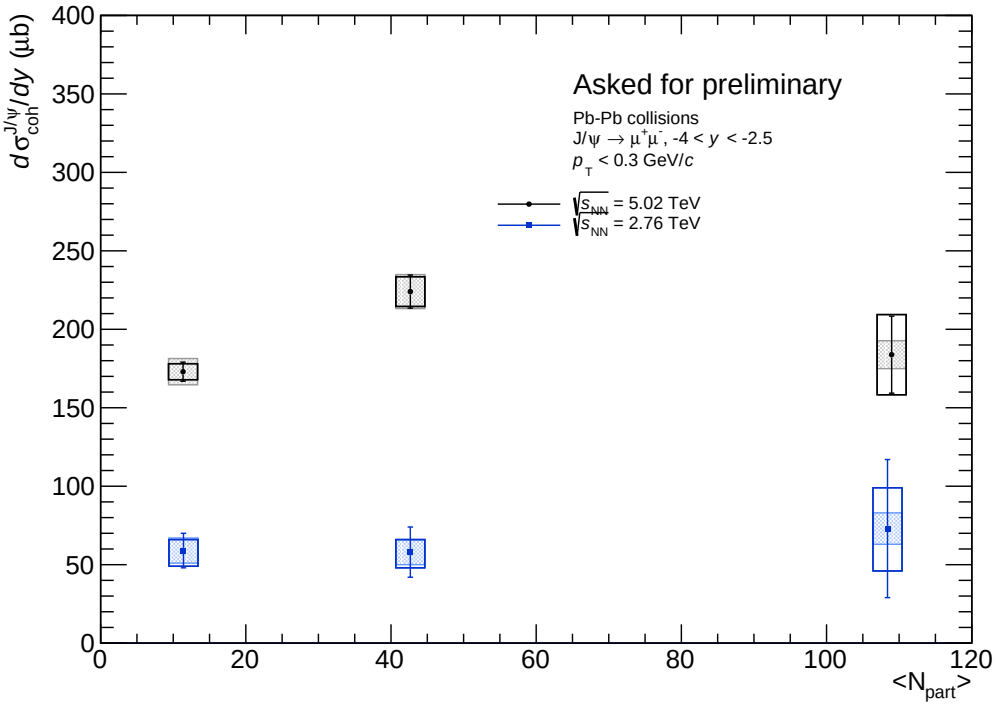

Fig. 31: J/ψ coherent photoproduction cross section as function of $\langle N_{\mathrm{part}} \rangle$ at forward rapidity in Pb–Pb collisions at $\sqrt{s_{\mathrm{NN}}} = 5.02$ TeV and at $\sqrt{s_{\mathrm{NN}}} = 2.76$ TeV [16].

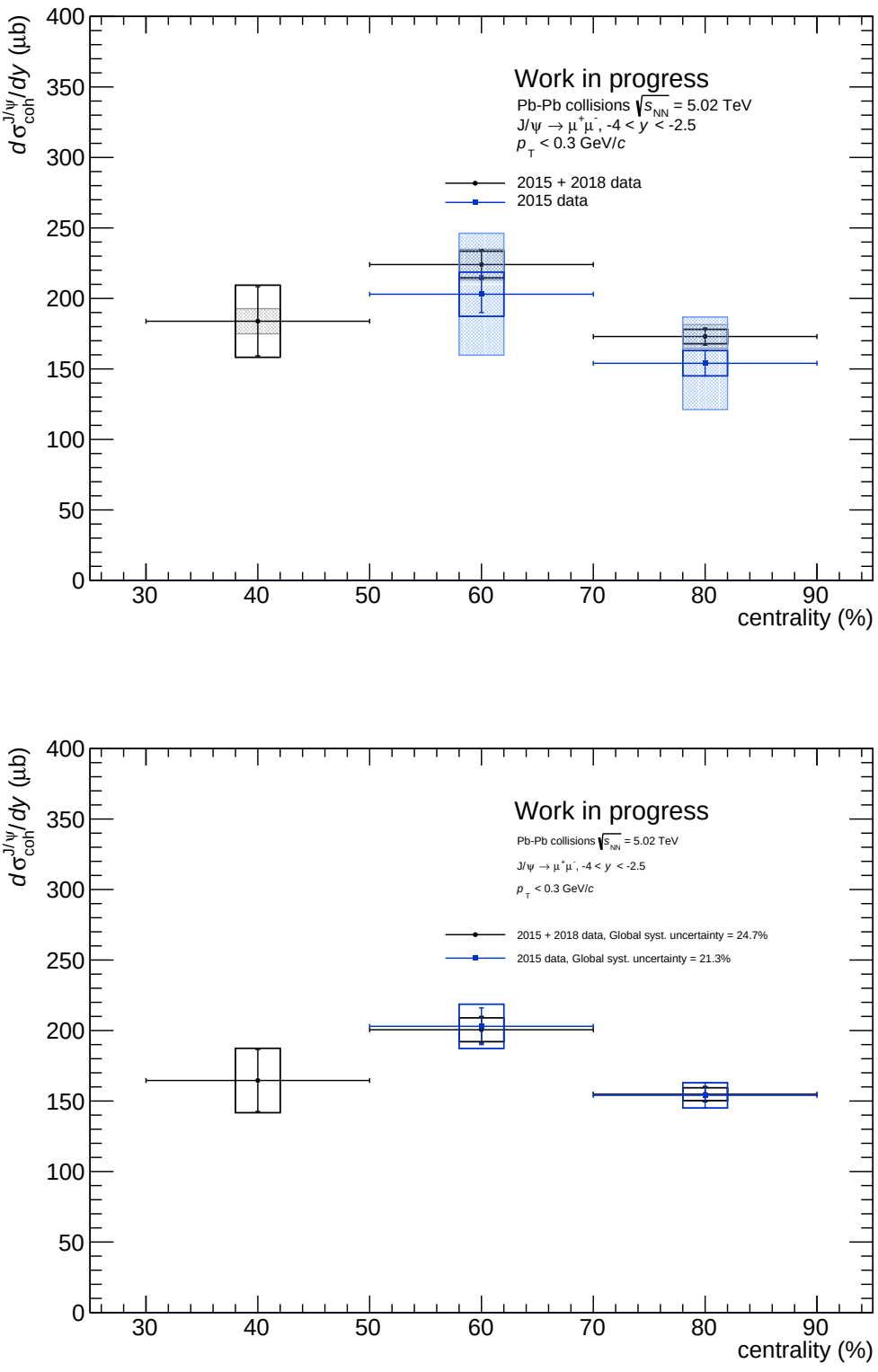

Fig. 32: Top : J/ψ coherent photoproduction cross section from this analysis compared to preliminary results on 2015 data sample [18]. Bottom : Cross section measured using the same f_{I} and f_{D} fractions to correct the excess.

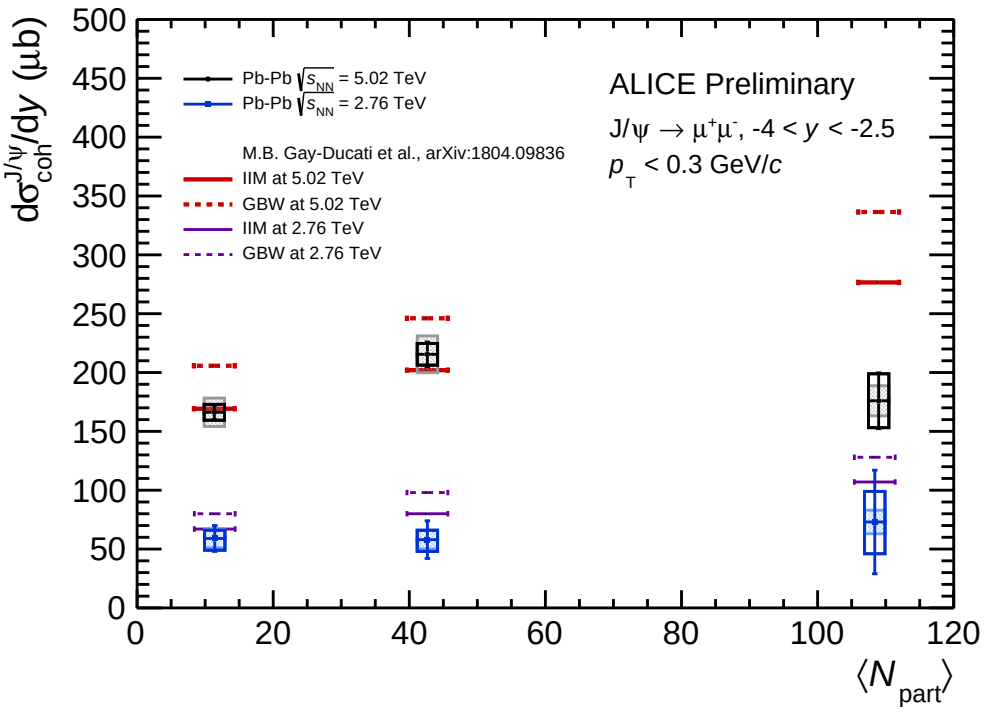

Fig. 33: J/ψ coherent photoproduction cross section as function of $\langle N_{\mathrm{part}} \rangle$ at forward rapidity in Pb–Pb collisions at $\sqrt{s_{\mathrm{NN}}} = 5.02$ TeV and at $\sqrt{s_{\mathrm{NN}}} = 2.76$ TeV [16]. Results are compared to theoritical calculations [15].

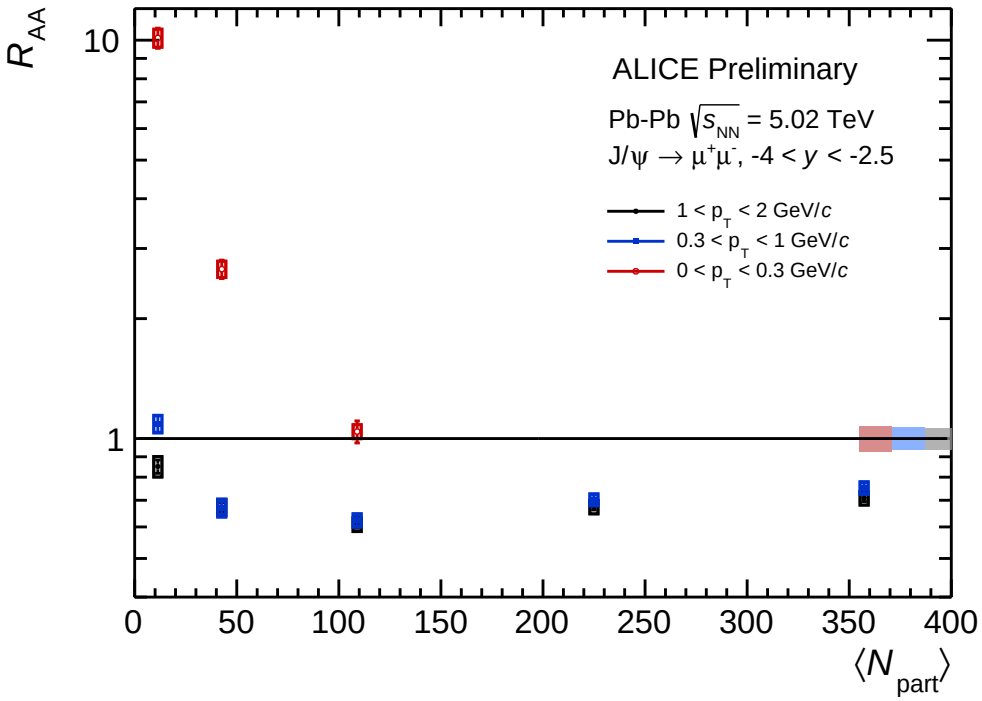

Fig. 34: J/ψ nuclear modification factor distribution as a function of $\langle N_{\rm part}\rangle$ in $-4 < y < -2.5$. The quoted errors are statistical and uncorrelated systematic uncertainty. The correlated over centrality systematic uncertainties are represented by a box at the unity.

A Run lists

244918	244980	244982	244983	245064	245066	245068	245145	245146
245151	245152	245231	245232	245233	245253	245259	245343	245345
245346	245347	245353	245401	245407	245409	245410	245446	245450
245496	245501	245504	245505	245507	245535	245540	245542	245543
245554	245683	245692	245700	245705	245729	245731	245738	245752
245759	245766	245775	245785	245793	245829	245831	245833	245949
245952	245954	245963	245996	246001	246003	246012	246036	246037
246042	246048	246049	246053	246087	246089	246113	246115	246148
246151	246152	246153	246178	246181	246182	246217	246220	246222
246225	246272	246275	246276	246390	246391	246392	246424	246428
246431	246433	246434	246487	246488	246493	246495	246675	246676
246750	246751	246755	246757	246758	246759	246760	246763	246765
246804	246805	246806	246807	246808	246809	246844	246845	246846
246847	246851	246855	246859	246864	246865	246867	246871	246930
246937	246942	246945	246948	246949	246980	246982	246984	246989
246991	246994							

Table A.1: Run list LHC15o

295584	295585	295586	295587	295588	295589	295612	295615	295665
295666	295667	295668	295671	295673	295675	295676	295677	295714
295716	295717	295718	295719	295723	295725	295753	295754	295755
295758	295759	295762	295763	295786	295788	295791	295816	295818
295819	295822	295825	295826	295829	295831	295854	295855	295856
295859	295860	295861	295863	295881	295908	295909	295910	295913
295936	295937	295941	295942	295943	295945	295947	296061	296062
296063	296065	296066	296068	296123	296128	296132	296133	296134
296135	296142	296143	296191	296192	296194	296195	296196	296197
296198	296241	296242	296243	296244	296246	296247	296269	296270
296273	296279	296280	296303	296304	296307	296309	296312	296376
296377	296378	296379	296380	296381	296383	296414	296419	296420
296423	296424	296433	296472	296509	296510	296511	296514	296516
296547	296548	296549	296550	296551	296552	296553	296615	296616
296618	296619	296622	296623					

Table A.2: Run list LHC18q

296690	296691	296694	296749	296750	296752	296781	296784	296785
296786	296787	296791	296793	296794	296799	296836	296838	296839
296848	296849	296850	296851	296852	296890	296894	296899	296900
296903	296930	296931	296932	296934	296935	296938	296941	296966
296967	296968	296969	296971	296975	296976	296979	297029	297031
297035	297085	297117	297118	297119	297123	297124	297128	297129
297132	297133	297193	297194	297196	297218	297219	297221	297222
297278	297310	297312	297315	297317	297363	297366	297367	297372
297379	297380	297405	297408	297413	297414	297415	297441	297442
297446	297450	297451	297452	297479	297481	297483	297512	297537
297540	297541	297542	297544	297558	297588	297590	297595	

Table A.3: Run list LHC18r

B Fit Functions

Power Law

The power law has 4 parameters if the parameter D is not fixed.

$$f(p_{\mathrm{T}}) = N \times \frac{p_{\mathrm{T}}}{\left(1+\left(\frac{p_{\mathrm{T}}}{\langle p_{\mathrm{T}}\rangle}\right)^{D}\right)^{n}} \tag{B.1}$$

Levy Function

The Levy function has 3 free parameters, le mass m is fixed to the J/ψ mass.

$$f(p_{\mathrm{T}}) = N \times \frac{p_{\mathrm{T}}(n-1)(n-2)}{nT \times (nT + m(n-2))} \times \left(1 + \frac{\sqrt{m^2 p_{\mathrm{T}}^2} - m}{nT}\right)^{-n} \tag{B.2}$$

UA1 Function

$$\begin{aligned} &\text{for } p_{\mathrm{T}} \leq p_{\mathrm{T}}* \qquad f(p_{\mathrm{T}}) = N \times p_{\mathrm{T}} \times exp\left(-\frac{\sqrt{p_{\mathrm{T}}^2+m^2}}{T}\right) \\ &\text{for } p_{\mathrm{T}} > p_{\mathrm{T}}* \qquad f(p_{\mathrm{T}}) = N \times p_{\mathrm{T}}\left(1+\frac{p_{\mathrm{T}}}{p_{\mathrm{T0}}}\right)^{-n} \end{aligned} \tag{B.3}$$

Wood-Saxon like function

$$f(p_{\mathrm{T}}) = R_{\mathrm{AA}}^{0}\left(1 + \frac{\Delta R_{\mathrm{AA}}}{1+\exp\left(\frac{\mathrm{p_T}-\mathrm{p_T^0}}{\sigma \mathrm{p_T}}\right)}\right) \tag{B.4}$$

C Tails set for signal extraction

		0-0.3 GeV/c	0.3-1 GeV/c	0.3-0.65 GeV/c	0.65-1 GeV/c	1-8 GeV/c
CB Extended	α_L	0.8374	0.8519	0.8391	0.8615	0.9629
	n_L	5.2199	5.1445	5.2508	5.0695	3.8195
	α_R	2.3261	2.3228	2.3531	2.3024	2.2411
	n_R	3.3130	3.2138	3.1621	3.2483	2.9928
NA60	α_L	-0.7307	-0.6251	-0.5086	-0.5772	-0.8920
	$p1_L$	0.0050	0.0045	0.0049	0.0041	0.0033
	$p2_L$	0.5156	0.5071	0.5291	0.4937	0.4657
	$p3_L$	0.2542	0.2468	0.2564	0.2398	0.2291
	α_R	2.7208	2.5762	2.3614	2.3699	2.5835
	$p1_R$	0.0047	0.0066	0.0087	0.0079	0.0047
	$p2_R$	0.5524	0.6351	0.7466	0.7063	0.5574
	$p3_R$	0.2417	0.2772	0.3193	0.3038	0.2486

Table C.1: Tails from embedding simulations

		1-2 GeV/c	2-3 GeV/c	3-4 GeV/c	4-5 GeV/c
CB Extended	α_L	0.9031	0.9576	0.9870	1.0282
	n_L	4.5206	3.7199	3.4040	3.3088
	α_R	2.2809	2.2245	2.2442	2.2231
	n_R	3.0589	3.0278	2.8653	2.9864
NA60	α_L	-0.8386	-0.8839	-0.9159	-0.9174
	$p1_L$	0.0037	0.0031	0.0033	0.0033
	$p2_L$	0.4702	0.4517	0.4660	0.4731
	$p3_L$	0.2315	0.2234	0.2308	0.2328
	α_R	2.5907	2.5843	2.5686	2.2577
	$p1_R$	0.0051	0.0055	0.0045	0.0058
	$p2_R$	0.5779	0.5742	0.5564	0.6588
	$p3_R$	0.2553	0.2577	0.2489	0.2851

		5-6 GeV/c	6-7 GeV/c	7-8 GeV/c	8-9 GeV/c
CB Extended	α_L	1.1001	1.1555	1.2143	1.2072
	n_L	3.2623	3.2112	3.2187	3.2742
	α_R	2.1688	1.9898	1.9583	1.9227
	n_R	2.9832	3.2413	3.1981	2.8138
NA60	α_L	-1.0958	-1.1620	-1.0435	-1.3990
	$p1_L$	0.0035	0.0040	0.0037	0.0031
	$p2_L$	0.4844	0.5136	0.5199	0.4599
	$p3_L$	0.2368	0.2484	0.2456	0.2240
	α_R	2.2726	2.3981	1.7852	2.0206
	$p1_R$	0.0053	0.0031	0.0051	0.0046
	$p2_R$	0.6260	0.4842	0.6591	0.5977
	$p3_R$	0.2732	0.2182	0.2823	0.2669

		8-10 GeV/c	10-12 GeV/c	12-15 GeV/c	0.3-15 GeV/c
CB Extended	α_L	1.2118	1.1697	1.2524	0.9474
	n_L	3.2383	3.4044	3.5375	3.9884
	α_R	1.9481	1.7962	1.7904	2.2536
	n_R	3.0116	2.9175	2.4443	2.9881
NA60	α_L	-1.1203	-0.9780	-1.1602	-0.6341
	$p1_L$	0.0036	0.0037	0.0039	0.0033
	$p2_L$	0.5132	0.5248	0.5268	0.4772
	$p3_L$	0.2434	0.2470	0.2470	0.2314
	α_R	1.9348	1.7940	1.5407	2.1135
	$p1_R$	0.0048	0.0037	0.0045	0.0072
	$p2_R$	0.6209	0.5621	0.6200	0.7289
	$p3_R$	0.2718	0.2503	0.2769	0.3113

Table C.2: Tails from embedding simulations

		0-0.3 GeV/c		0.3-1 GeV/c
		coherent J/ψ	incoherent J/ψ	incoherent J/ψ
CB Extended	α_L	0.8096	0.8597	0.9068
	n_L	135.747	12.76	8.0909
	α_R	2.3248	2.3387	2.3203
	n_R	7.3228	4.2698	3.4396
NA60	α_L	-0.3421	-0.4578	-0.6001
	$p1_L$	0.1865	0.2011	0.2090
	$p2_L$	1.2562	1.1764	1.0602
	$p3_L$	0.1534	0.0789	0.0311
	α_R	2.1151	2.2534	2.2904
	$p1_R$	0.0990	0.1654	0.1791
	$p2_R$	1.6543	1.4355	1.3589
	$p3_R$	0.4629	0.1397	0.1068

Table C.3: Tails from STARLIGHT simulations

		0-1 GeV/c		1-8 GeV/c	
CB Extended		$2.2 < m_{\mu\mu} < 4.5$	$2.4 < m_{\mu\mu} < 4.7$	$2.2 < m_{\mu\mu} < 4.5$	$2.4 < m_{\mu\mu} < 4.7$
quad VWG	α_L	0.874	0.860	0.877	0.844
	n_L	5.830	9.799	8.942	18.489
	α_R	1.980	1.994	1.891	1.872
	n_R	21.225	21.419	21.540	21.990
Pol2/Pol3	α_L	0.891	0.939	0.890	0.843
	n_L	6.641	6.125	8.735	18.866
	α_R	1.953	1.957	3.043	1.885
	n_R	21.823	30.825	15.323	21.901
		8-15 GeV/c		0-15 GeV/c	
CB Extended		$2.2 < m_{\mu\mu} < 4.5$	$2.4 < m_{\mu\mu} < 4.7$	$2.2 < m_{\mu\mu} < 4.5$	$2.4 < m_{\mu\mu} < 4.7$
quad VWG	α_L	1.011	0.993	0.882	0.869
	n_L	8.658	12.843	10.657	15.203
	α_R	1.326	1.320	1.838	1.836
	n_R	12.011	12.637	30.757	28.427
Pol2/Pol3	α_L	1.011	1.041	0.891	0.910
	n_L	9.917	5.761	8.345	6.863
	α_R	1.299	1.333	1.833	1.844
	n_R	30.680	11.040	20.105	35.608

Table C.4: Tails from pp data at 13 TeV

D Results signal extraction

0-90%

p_{T} (GeV/c)	$N^{raw}_{\mathrm{J}/\psi}$	$\mathrm{d}N_{\mathrm{J}/\psi}/\mathrm{d}p_{\mathrm{T}}$
0-0.3	27532 ± 978 ± 626	91774 ± 3260 ± 2087
0.3-1	162340 ± 2555 ± 2832	231915 ± 3651 ± 4046
0.3-0.65	67045 ± 1747 ± 1484	191558 ± 4992 ± 4240
0.65-1	96171 ± 1916 ± 1723	274775 ± 5475 ± 4923
1-2	274988 ± 2675 ± 6871	274988 ± 2676 ± 6872
2-3	202664 ± 1945 ± 6306	202664 ± 1946 ± 6306
3-4	117950 ± 1173 ± 4081	117950 ± 1174 ± 4082
4-5	64611 ± 798 ± 1878	64612 ± 798 ± 1878
5-6	35594 ± 493 ± 764	35594 ± 494 ± 764
6-7	19394 ± 312 ± 434	19394 ± 312 ± 434
7-8	10650 ± 215 ± 246	10650 ± 216 ± 246
8-9	6023 ± 147 ± 81	6024 ± 148 ± 82
9-10	3454 ± 118 ± 119	3454 ± 118 ± 120
10-12	3509 ± 109 ± 71	1755 ± 55 ± 36
12-15	1916 ± 90 ± 33	639 ± 30 ± 12
0-15 (sum)	931501 ± 12716 ± 24717	
0-15 (fit)	940392 ± 4619 ± 22432	

Table D.1: Number of J/ψ obtained in each p_{T} range in the centrality class 0-90% by combining the results of the various tests. The quoted uncertainties are statistical and systematic

0-10%

p_{T} (GeV/c)	$N^{raw}_{\mathrm{J}/\psi}$	$\mathrm{d}N_{\mathrm{J}/\psi}/\mathrm{d}p_{\mathrm{T}}$
0-0.3	8519 ± 771 ± 283	28397 ± 2570 ± 944
0.3-1	68751 ± 1854 ± 1442	98216 ± 2649 ± 2060
0.3-0.65	28274 ± 1275 ± 975	80783 ± 3643 ± 2786
0.65-1	40819 ± 1456 ± 770	116626 ± 4160 ± 2200
1-2	115505 ± 1971 ± 3014	115506 ± 1972 ± 3014
2-3	82025 ± 1430 ± 2332	82026 ± 1430 ± 2332
3-4	44022 ± 842 ± 1528	44022 ± 842 ± 1528
4-5	22053 ± 573 ± 644	22054 ± 574 ± 644
5-6	11791 ± 345 ± 255	11792 ± 346 ± 256
6-7	5850 ± 204 ± 133	5850 ± 204 ± 134
7-8	3200 ± 146 ± 70	3200 ± 146 ± 70
8-9	1827 ± 97 ± 26	1828 ± 98 ± 26
9-10	1067 ± 78 ± 30	1068 ± 78 ± 30
10-12	1004 ± 69 ± 23	502 ± 35 ± 12
12-15	542 ± 77 ± 27	181 ± 26 ± 10
0-15 (sum)	366498 ± 9334 ± 10110	
0-15 (fit)	370453 ± 3335 ± 9128	

Table D.2: Number of J/ψ obtained in each p_{T} range in the centrality class 0-10% by combining the results of the various tests. The quoted uncertainties are statistical and systematic

10-30%

p_{T} (GeV/c)	$N^{raw}_{\mathrm{J}/\psi}$	$\mathrm{d}N_{\mathrm{J}/\psi}/\mathrm{d}p_{\mathrm{T}}$
0-0.3	9840 ± 583 ± 254	32800 ± 1944 ± 847
0.3-1	66379 ± 1657 ± 1210	94828 ± 2368 ± 1729
0.3-0.65	27092 ± 1026 ± 484	77406 ± 2932 ± 1383
0.65-1	39344 ± 1237 ± 672	112412 ± 3535 ± 1921
1-2	112970 ± 1629 ± 2993	112970 ± 1630 ± 2994
2-3	83586 ± 1208 ± 2494	83586 ± 1208 ± 2494
3-4	48732 ± 725 ± 1613	48732 ± 726 ± 1614
4-5	26806 ± 491 ± 744	26806 ± 492 ± 744
5-6	14570 ± 308 ± 300	14570 ± 308 ± 300
6-7	8152 ± 197 ± 184	8152 ± 198 ± 184
7-8	4325 ± 136 ± 125	4326 ± 136 ± 126
8-9	2443 ± 96 ± 28	2444 ± 96 ± 28
9-10	1324 ± 93 ± 26	1324 ± 94 ± 26
10-12	1504 ± 72 ± 29	752 ± 36 ± 15
12-15	836 ± 78 ± 24	279 ± 26 ± 8
0-15 (sum)	381524 ± 7879 ± 9970	
0-15 (fit)	383663 ± 2940 ± 8939	

Table D.3: Number of J/ψ obtained in each p_{T} range in the centrality class 10-30% by combining the results of the various tests. The quoted uncertainties are statistical and systematic

30-50%

p_{T} (GeV/c)	$N^{raw}_{\mathrm{J}/\psi}$	$\mathrm{d}N_{\mathrm{J}/\psi}/\mathrm{d}p_{\mathrm{T}}$
0-0.3	4372 ± 230 ± 87	14574 ± 767 ± 290
0.3-1	20591 ± 644 ± 449	29416 ± 921 ± 642
0.3-0.65	8689 ± 448 ± 154	24826 ± 1280 ± 440
0.65-1	11935 ± 454 ± 300	34100 ± 1298 ± 858
1-2	35643 ± 693 ± 879	35644 ± 694 ± 880
2-3	28588 ± 482 ± 817	28588 ± 482 ± 818
3-4	18378 ± 321 ± 556	18378 ± 322 ± 556
4-5	11340 ± 223 ± 314	11340 ± 224 ± 314
5-6	6608 ± 149 ± 153	6608 ± 150 ± 154
6-7	3855 ± 91 ± 92	3856 ± 92 ± 92
7-8	2197 ± 80 ± 64	2198 ± 80 ± 64
8-9	1223 ± 60 ± 18	1224 ± 60 ± 18
9-10	732 ± 62 ± 14	732 ± 62 ± 14
10-12	738 ± 70 ± 15	370 ± 36 ± 8
12-15	395 ± 44 ± 12	132 ± 15 ± 4
0-15 (sum)	134693 ± 3407 ± 3475	
0-15 (fit)	135593 ± 1198 ± 3353	

Table D.4: Number of J/ψ obtained in each p_{T} range in the centrality class 30-50% by combining the results of the various tests. The quoted uncertainties are statistical and systematic

50-70%

p_{T} (GeV/c)	$N^{raw}_{\mathrm{J}/\psi}$	$\mathrm{d}N_{\mathrm{J}/\psi}/\mathrm{d}p_{\mathrm{T}}$
0-0.3	2820 ± 99 ± 57	9400 ± 330 ± 190
0.3-1	5580 ± 194 ± 187	7972 ± 278 ± 268
0.3-0.65	2353 ± 127 ± 49	6723 ± 363 ± 140
0.65-1	3119 ± 147 ± 69	8912 ± 420 ± 198
1-2	10008 ± 244 ± 243	10008 ± 244 ± 244
2-3	7863 ± 172 ± 215	7864 ± 172 ± 216
3-4	5628 ± 129 ± 167	5628 ± 130 ± 168
4-5	3592 ± 89 ± 107	3592 ± 90 ± 108
5-6	2193 ± 69 ± 55	2194 ± 70 ± 56
6-7	1383 ± 49 ± 31	1384 ± 50 ± 32
7-8	743 ± 35 ± 21	744 ± 36 ± 22
8-10	698 ± 60 ± 11	350 ± 30 ± 6
10-12	243 ± 33 ± 5	122 ± 17 ± 3
12-15	159 ± 19 ± 6	54 ± 7 ± 2
0-15 (sum)	40802 ± 1272 ± 1036	
0-15 (fit)	40873 ± 439 ± 977	

Table D.5: Number of J/ψ obtained in each p_{T} range in the centrality class 50-70% by combining the results of the various tests. The quoted uncertainties are statistical and systematic

	70-90%	
p_{T} (GeV/c)	$N^{raw}_{\mathrm{J}/\psi}$	$\mathrm{d}N_{\mathrm{J}/\psi}/\mathrm{d}p_{\mathrm{T}}$
0-0.3	1785 ± 56 ± 25	5950 ± 187 ± 84
0.3-1	1518 ± 65 ± 21	2169 ± 93 ± 31
0.3-0.65	750 ± 52 ± 15	2143 ± 149 ± 43
0.65-1	779 ± 63 ± 17	2226 ± 180 ± 49
1-2	2108 ± 76 ± 72	2108 ± 76 ± 72
2-3	1508 ± 55 ± 41	1508 ± 56 ± 42
3-4	1083 ± 46 ± 32	1084 ± 46 ± 32
4-5	728 ± 36 ± 20	728 ± 36 ± 20
5-6	414 ± 27 ± 11	414 ± 28 ± 12
6-7	252 ± 20 ± 5	252 ± 20 ± 6
7-8	155 ± 16 ± 3	156 ± 16 ± 4
8-10	135 ± 15 ± 6	68 ± 8 ± 4
10-12	50 ± 8 ± 3	26 ± 4 ± 2
0-12 (sum)	9747 ± 470 ± 250	
0-12 (fit)	9758 ± 148 ± 229	

Table D.6: Number of J/ψ obtained in each p_{T} range in the centrality class 70-90% by combining the results of the various tests. The quoted uncertainties are statistical and systematic

	$N^{raw}_{\mathrm{J}/\psi}$		
y	0-10%	10-30%	30-50%
4-3.75	$15186 \pm 499 \pm 562$	$17145 \pm 472 \pm 732$	$6429 \pm 200 \pm 240$
3.75-3.5	$54056 \pm 1138 \pm 1217$	$55092 \pm 906 \pm 1199$	$20287 \pm 387 \pm 343$
3.5-3.25	$86443 \pm 1605 \pm 1728$	$91821 \pm 1319 \pm 1717$	$31962 \pm 559 \pm 601$
3.25-3	$99776 \pm 1756 \pm 1997$	$103394 \pm 1538 \pm 2098$	$35935 \pm 633 \pm 681$
3-2.75	$82142 \pm 1675 \pm 2155$	$80290 \pm 1452 \pm 2070$	$28150 \pm 566 \pm 799$
2.75-2.5	$24417 \pm 966 \pm 1407$	$26871 \pm 895 \pm 1382$	$8194 \pm 326 \pm 411$

y	50-70%	70-90%
4-3.75	$2074 \pm 93 \pm 91$	$384 \pm 35 \pm 10$
3.75-3.5	$5936 \pm 151 \pm 112$	$1369 \pm 56 \pm 28$
3.5-3.25	$9226 \pm 198 \pm 197$	$1997 \pm 70 \pm 41$
3.25-3	$10323 \pm 218 \pm 241$	$2052 \pm 70 \pm 38$
3-2.75	$8054 \pm 194 \pm 204$	$1684 \pm 63 \pm 45$
2.75-2.5	$2475 \pm 112 \pm 123$	$451 \pm 56 \pm 25$

Table D.7: Number of J/ψ obtained in each y range and p_{T} from 0.3 to 15 GeV/c. The quoted uncertainties are statistical and systematic.

E Results differential pp cross

p_{T} (GeV/c)	$\frac{\mathrm{d}^2\sigma}{\mathrm{d}p_{\mathrm{T}}\mathrm{d}y} \pm stat(\%) \pm syst(\%)$
0-0.3	$2.27 \cdot 10^{-1} \pm 7.79 \cdot 10^{-3}$ (3.4) $\pm 1.26 \cdot 10^{-2}$ (5.6)
0.3-1	$8.52 \cdot 10^{-1} \pm 1.08 \cdot 10^{-2}$ (1.3) $\pm 4.33 \cdot 10^{-2}$ (5.1)
1-2	$1.24 \pm 1.10 \cdot 10^{-2}$ (0.9) $\pm 5.93 \cdot 10^{-2}$ (4.8)
2-3	$9.26 \cdot 10^{-1} \pm 9.02 \cdot 10^{-3}$ (1.0) $\pm 4.03 \cdot 10^{-2}$ (4.4)
3-4	$5.41 \cdot 10^{-1} \pm 6.42 \cdot 10^{-3}$ (1.2) $\pm 2.28 \cdot 10^{-2}$ (4.2)
4-5	$2.74 \cdot 10^{-1} \pm 4.08 \cdot 10^{-3}$ (1.5) $\pm 1.12 \cdot 10^{-2}$ (4.1)
5-6	$1.37 \cdot 10^{-1} \pm 2.55 \cdot 10^{-3}$ (1.9) $\pm 5.28 \cdot 10^{-3}$ (3.9)
6-7	$7.05 \cdot 10^{-2} \pm 1.74 \cdot 10^{-3}$ (2.5) $\pm 2.61 \cdot 10^{-3}$ (3.7)
7-8	$3.45 \cdot 10^{-2} \pm 1.17 \cdot 10^{-3}$ (3.4) $\pm 1.32 \cdot 10^{-3}$ (3.8)
8-9	$1.83 \cdot 10^{-2} \pm 8.08 \cdot 10^{-4}$ (4.4) $\pm 6.26 \cdot 10^{-4}$ (3.4)
9-10	$1.07 \cdot 10^{-2} \pm 6.31 \cdot 10^{-4}$ (5.9) $\pm 3.84 \cdot 10^{-4}$ (3.6)
8-10	$1.45 \cdot 10^{-2} \pm 7.20 \cdot 10^{-4}$ (5.0) $\pm 5.05 \cdot 10^{-4}$ (3.5)
10-12	$4.59 \cdot 10^{-3} \pm 2.73 \cdot 10^{-4}$ (5.9) $\pm 1.63 \cdot 10^{-4}$ (3.6)
12-15	$1.55 \cdot 10^{-3} \pm 1.26 \cdot 10^{-4}$ (8.1) $\pm 5.26 \cdot 10^{-5}$ (3.4)

Table E.1: J/ψ differential cross section measured by ALICE in pp collisions at $\sqrt{s_{\mathrm{NN}}} = 5.02$ TeV [5]. The quoted errors are statistical and uncorrelated systematic uncertainty. The correlated over p_{T} systematic uncertainty (not included) is 1.9%. The value obtained in $8 < p_{\mathrm{T}} < 10$ GeV/c in estimated as the average of the two correponding finer bins.

F Results J/ψ acceptance efficiency

0-10%

p_{T} (GeV/c)	$(\mathscr{A} \times \varepsilon)_{\mathrm{J}/\psi} \pm stat(\%) \pm syst(\%)$
0-0.3	0.1398 ± 0.0009 (0.6)
0.3-1	0.1255 ± 0.0003 (0.2)
0.3-0.65	0.1318 ± 0.0005 (0.3)
0.65-1	0.1215 ± 0.0004 (0.3)
1-2	0.1088 ± 0.0002 (0.2)
2-3	0.1113 ± 0.0002 (0.2)
3-4	0.1341 ± 0.0004 (0.3)
4-5	0.1737 ± 0.0006 (0.4)
5-6	0.2219 ± 0.0011 (0.5)
6-7	0.2627 ± 0.0018 (0.7)
7-8	0.3008 ± 0.0027 (0.9)
8-9	0.3248 ± 0.0039 (1.2)
9-10	0.3604 ± 0.0055 (1.5)
10-12	0.3778 ± 0.0059 (1.6)
12-15	0.4404 ± 0.0087 (2.0)

Table F.1: $(\mathscr{A} \times \varepsilon)^{\mathrm{J}/\psi}_{\mathrm{AA}}(\Delta y, \Delta p_{\mathrm{T}})$ in 0-10% integrated in rapidity. The quoted errors are statistical.

10-30%

p_{T} (GeV/c)	$(\mathscr{A} \times \varepsilon)_{\mathrm{J}/\psi} \pm stat(\%) \pm syst(\%)$
0-0.3	0.1432 ± 0.0009 (0.6)
0.3-1	0.1302 ± 0.0003 (0.2)
0.3-0.65	0.1359 ± 0.0005 (0.3)
0.65-1	0.1265 ± 0.0004 (0.3)
1-2	0.1124 ± 0.0002 (0.2)
2-3	0.1165 ± 0.0002 (0.2)
3-4	0.1415 ± 0.0004 (0.3)
4-5	0.1835 ± 0.0006 (0.3)
5-6	0.2280 ± 0.0010 (0.4)
6-7	0.2750 ± 0.0015 (0.6)
7-8	0.3130 ± 0.0023 (0.7)
8-9	0.3397 ± 0.0033 (1.0)
9-10	0.3581 ± 0.0045 (1.3)
10-12	0.3972 ± 0.0049 (1.2)
12-15	0.4390 ± 0.0072 (1.6)

Table F.2: $(\mathscr{A} \times \varepsilon)^{\mathrm{J}/\psi}_{\mathrm{AA}}(\Delta y, \Delta p_{\mathrm{T}})$ in 10-30% integrated in rapidity. The quoted errors are statistical.

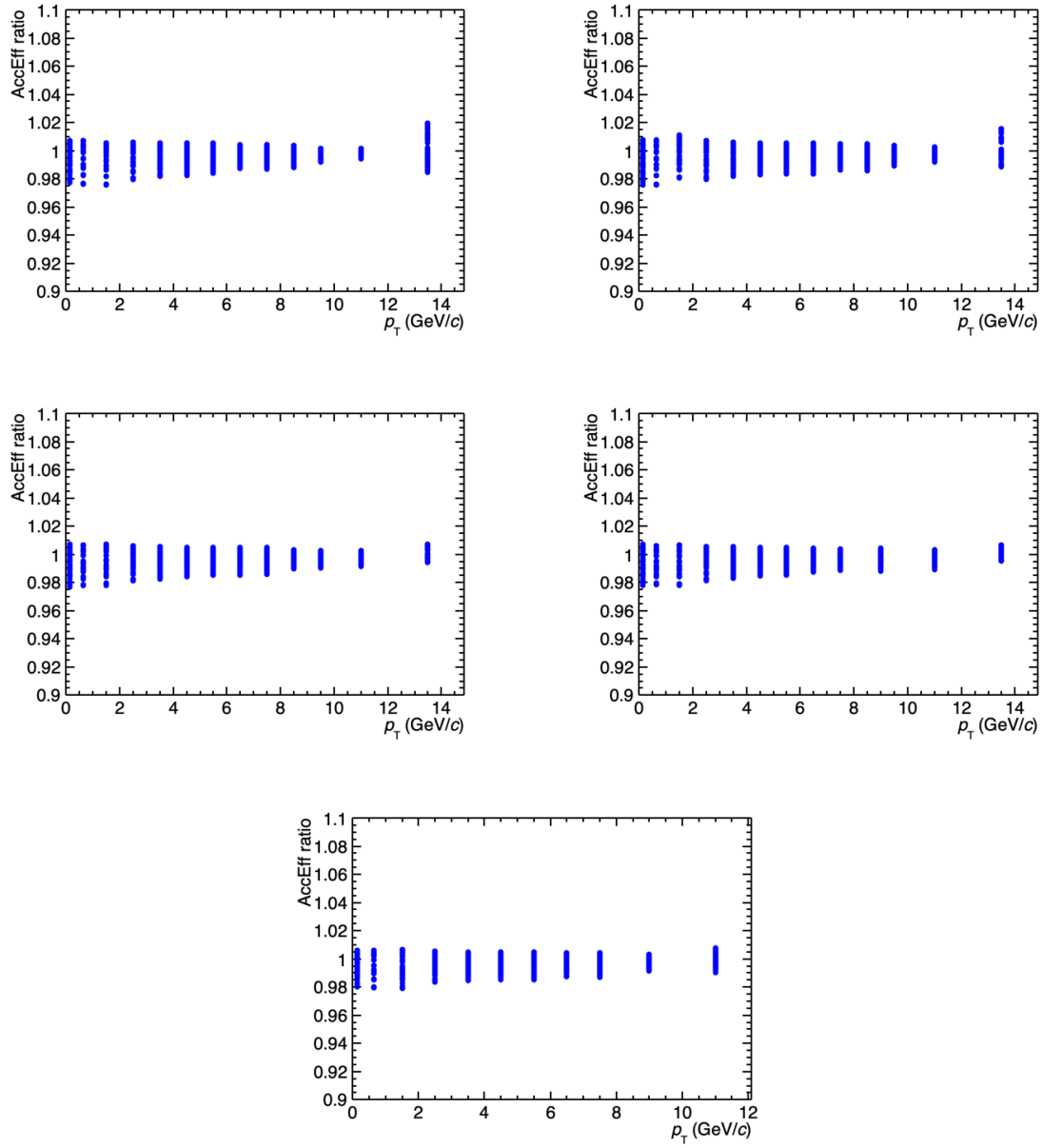

Fig. F.1: Variations of the $(\mathscr{A} \times \varepsilon)$ over the mean value using a combined p_T-y tuning as a function of p_T.

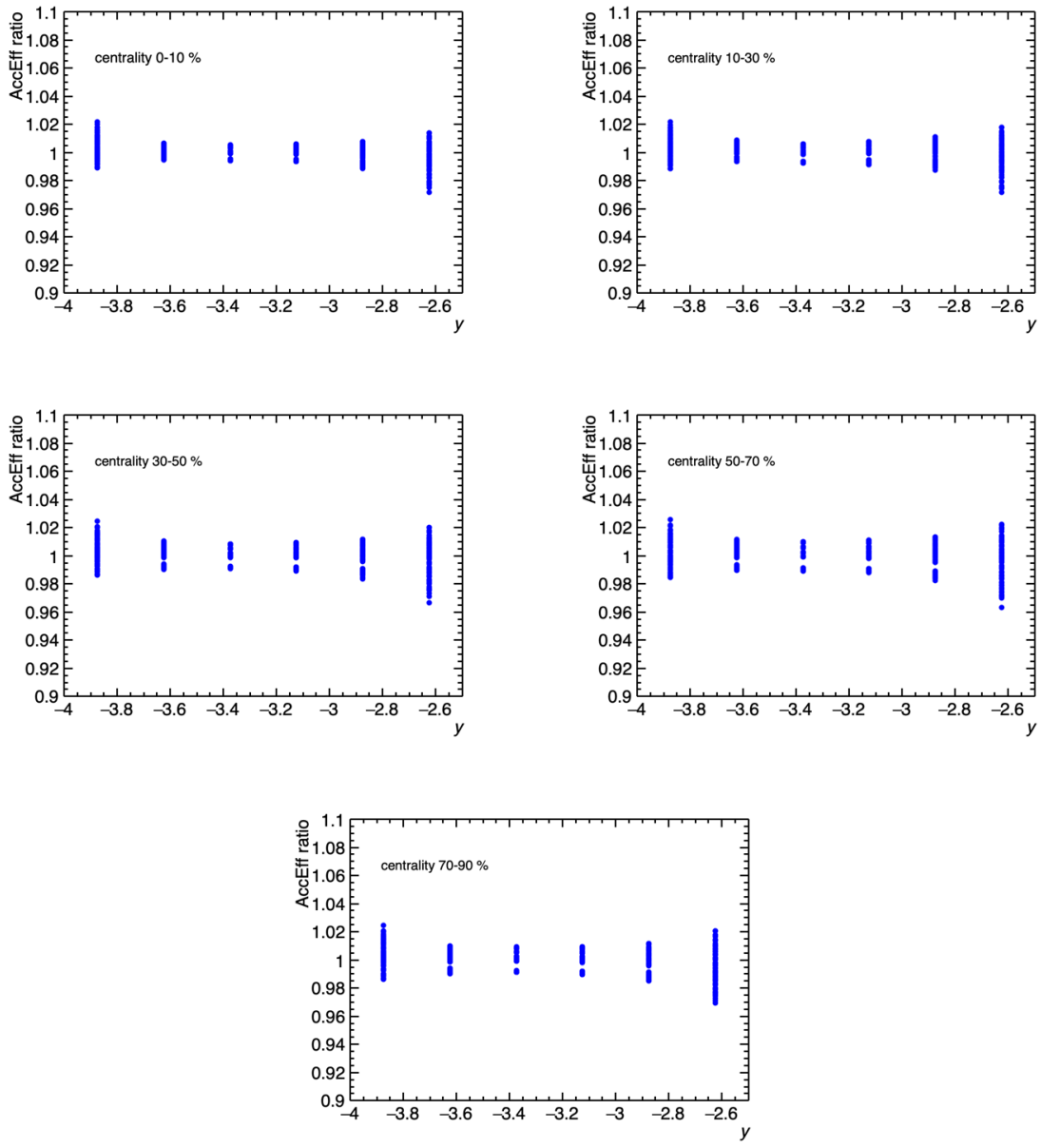

Fig. F.2: Variations of the $(\mathscr{A} \times \varepsilon)$ over the mean value using a combined p_{T}-y tuning as a function of y.

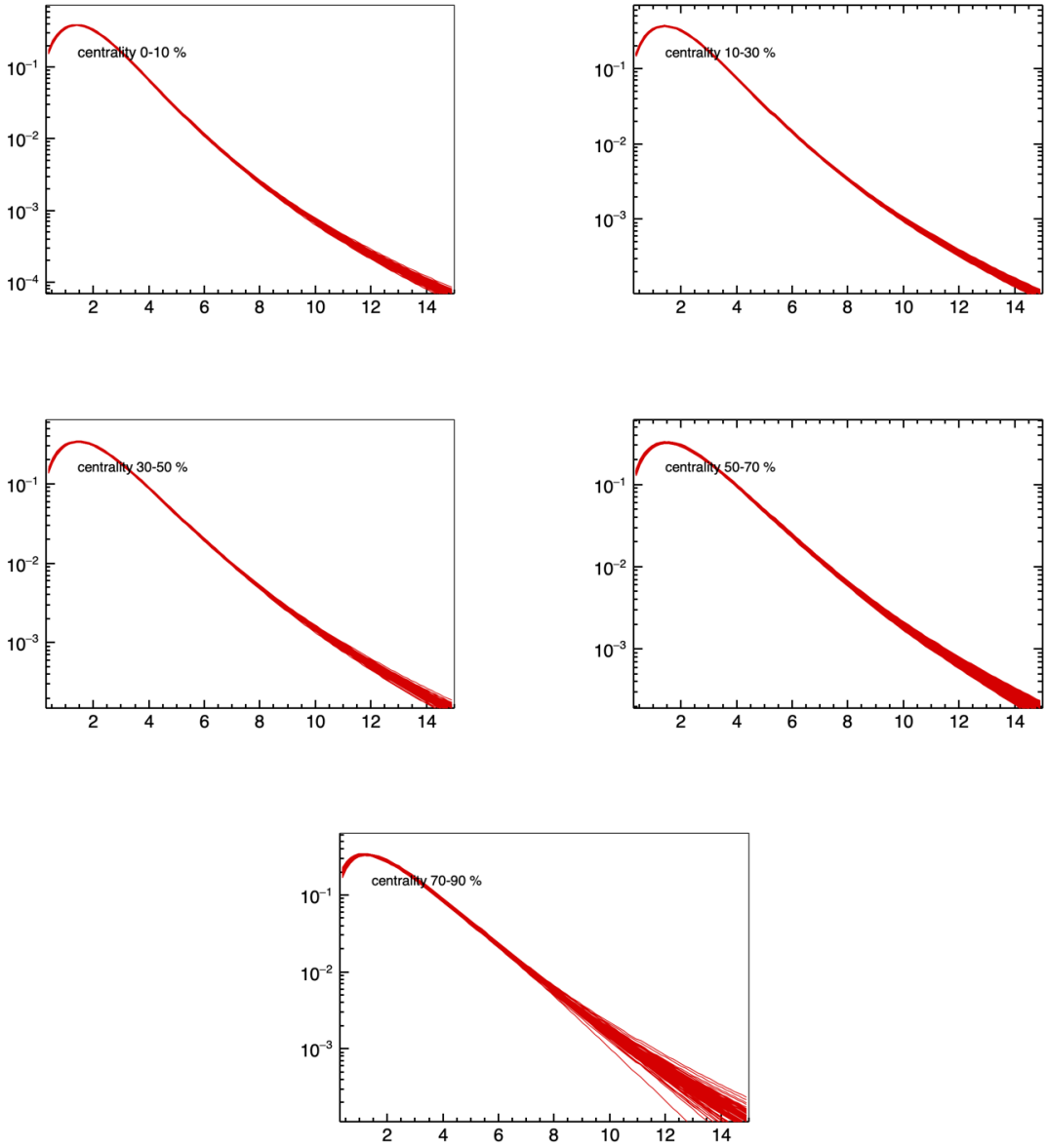

Fig. F.3: Variations of the generation functions by letting each data point fluctuate within its statistical uncertainty.

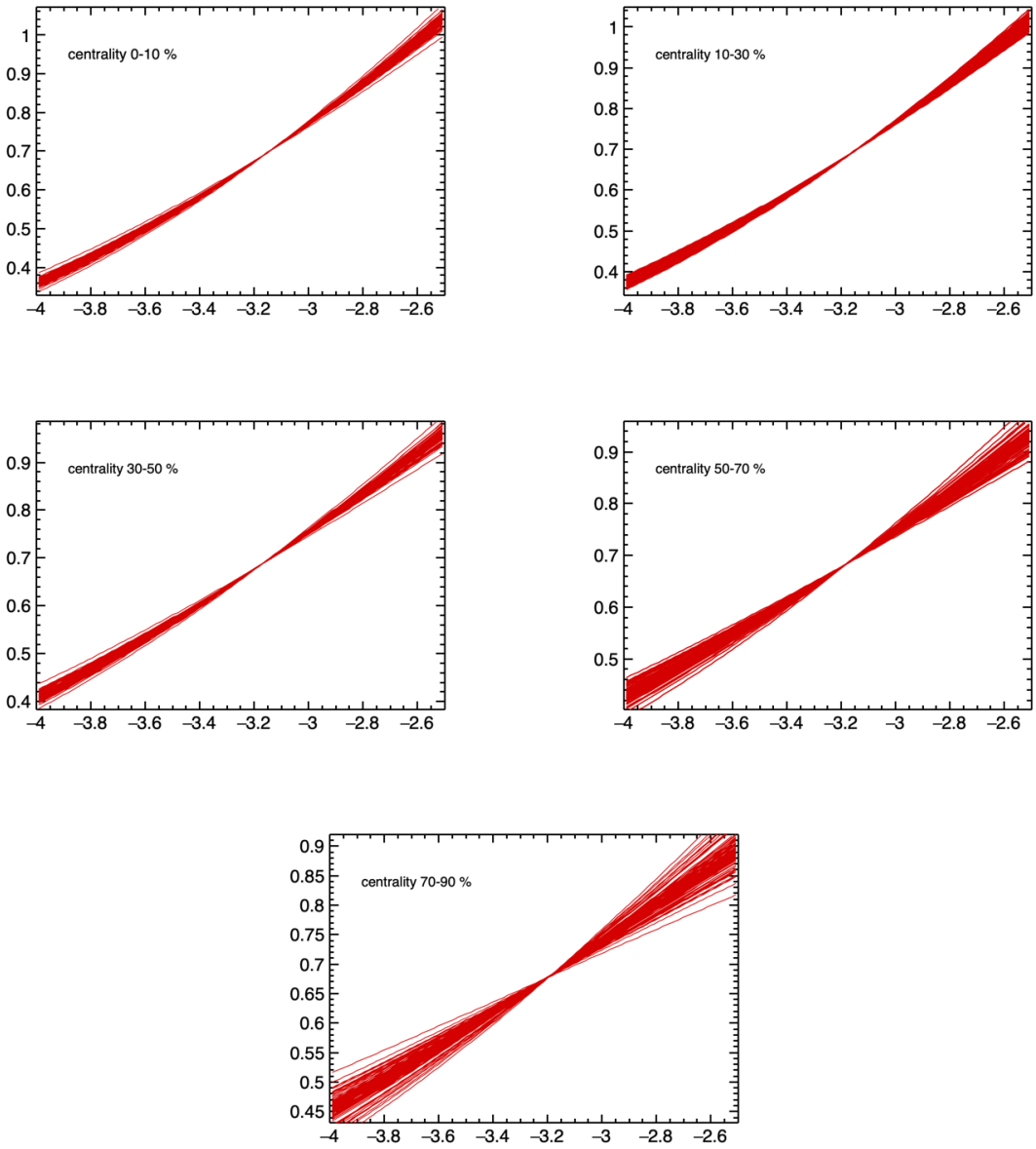

Fig. F.4: Variations of the generation functions by letting each data point fluctuate within its statistical uncertainty.

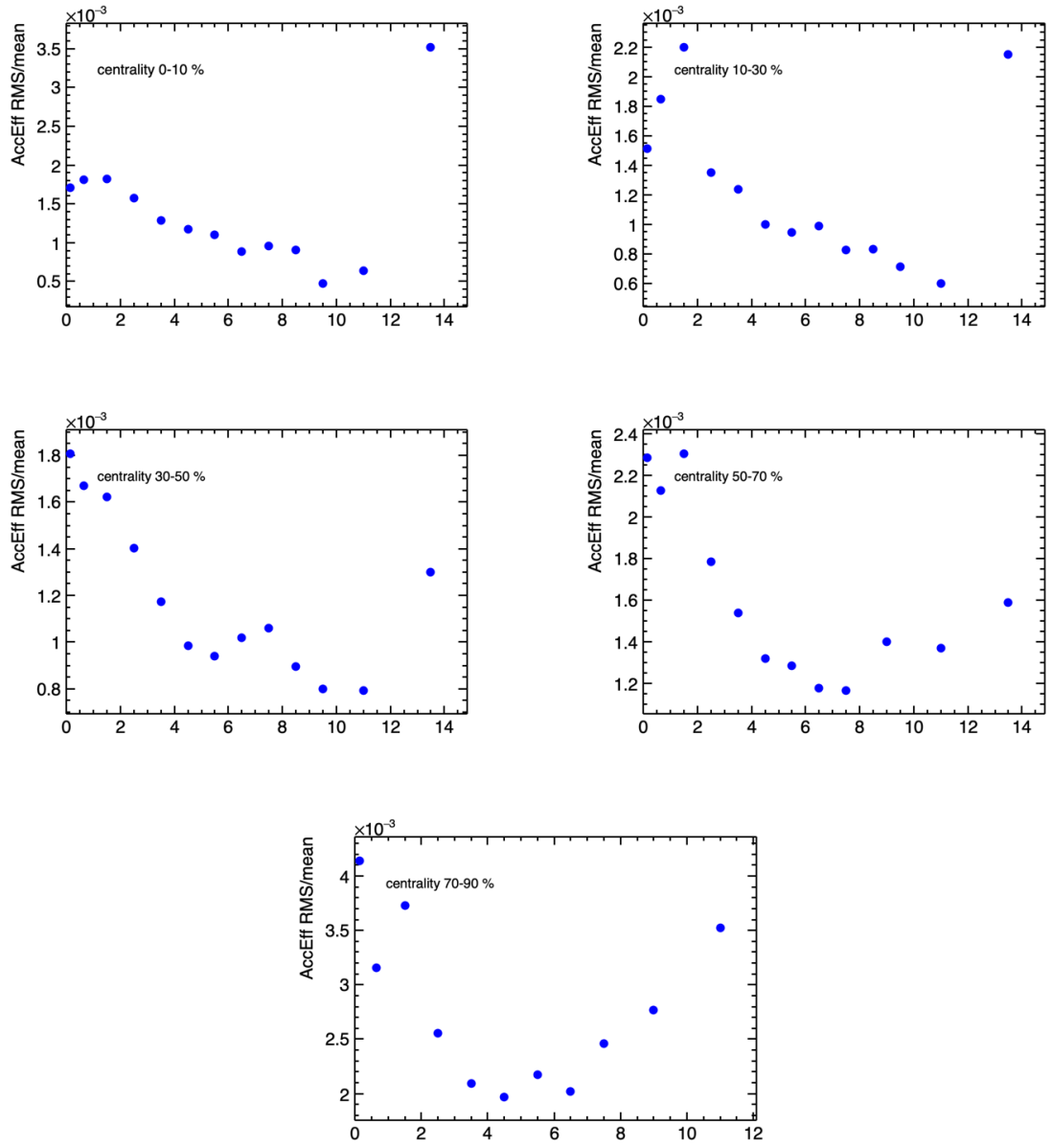

Fig. F.5: RMS of the dispersion on the $(\mathscr{A} \times \varepsilon)$ after weighting with generation functions including the fluctuations within their statistical uncertainties.

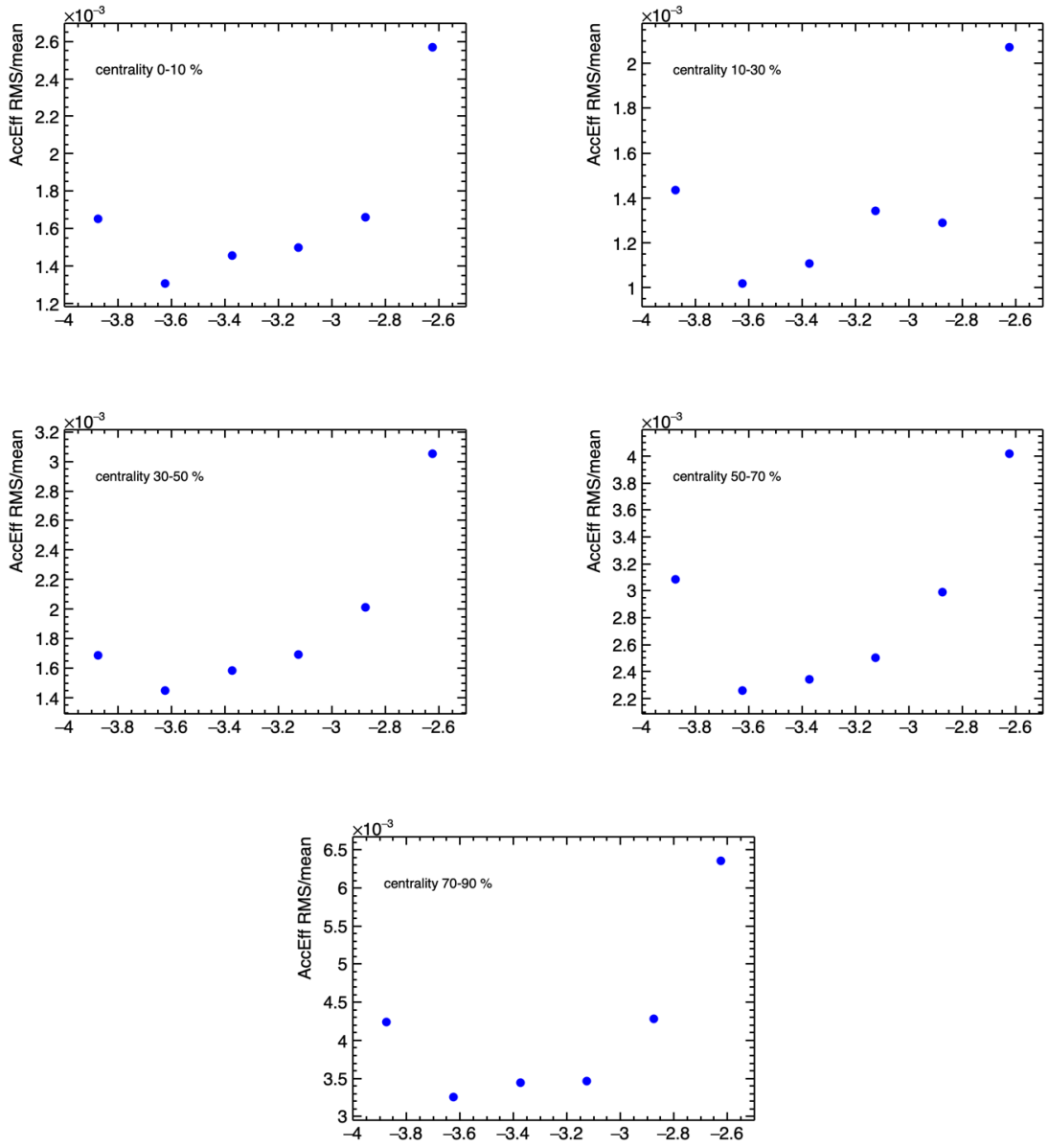

Fig. F.6: RMS of the dispersion on the $(\mathscr{A} \times \varepsilon)$ after weighting with generation functions including the fluctuations within their statistical uncertainties.

30-50%

p_{T} (GeV/c)	$(\mathscr{A} \times \varepsilon)_{\mathrm{J}/\psi} \pm stat(\%) \pm syst(\%)$
0-0.3	0.1483 ± 0.0016 (1.1)
0.3-1	0.1345 ± 0.0005 (0.4)
0.3-0.65	0.1418 ± 0.0008 (0.6)
0.65-1	0.1298 ± 0.0006 (0.5)
1-2	0.1161 ± 0.0003 (0.3)
2-3	0.1205 ± 0.0004 (0.3)
3-4	0.1475 ± 0.0006 (0.4)
4-5	0.1897 ± 0.0009 (0.5)
5-6	0.2384 ± 0.0015 (0.6)
6-7	0.2822 ± 0.0022 (0.8)
7-8	0.3275 ± 0.0033 (1.0)
8-9	0.3543 ± 0.0046 (1.3)
9-10	0.3805 ± 0.0064 (1.7)
10-12	0.4160 ± 0.0068 (1.6)
12-15	0.4455 ± 0.0100 (2.2)

Table F.3: $(\mathscr{A} \times \varepsilon)^{\mathrm{J}/\psi}_{\mathrm{AA}}(\Delta y, \Delta p_{\mathrm{T}})$ in 30-50% integrated in rapidity. The quoted errors are statistical.

50-70%

p_{T} (GeV/c)	$(\mathscr{A} \times \varepsilon)_{\mathrm{J}/\psi} \pm stat(\%) \pm syst(\%)$
0-0.3	0.1503 ± 0.0030 (2.0)
0.3-1	0.1362 ± 0.0010 (0.7)
0.3-0.65	0.1433 ± 0.0016 (1.1)
0.65-1	0.1316 ± 0.0012 (0.9)
1-2	0.1184 ± 0.0006 (0.5)
2-3	0.1225 ± 0.0007 (0.6)
3-4	0.1495 ± 0.0011 (0.7)
4-5	0.1918 ± 0.0016 (0.9)
5-6	0.2423 ± 0.0025 (1.0)
6-7	0.2874 ± 0.0038 (1.3)
7-8	0.3197 ± 0.0054 (1.7)
8-10	0.3701 ± 0.0062 (1.7)
10-12	0.4214 ± 0.0111 (2.6)
12-15	0.4423 ± 0.0161 (3.6)

Table F.4: $(\mathscr{A} \times \varepsilon)^{\mathrm{J}/\psi}_{\mathrm{AA}}(\Delta y, \Delta p_{\mathrm{T}})$ in 50-70% integrated in rapidity. The quoted errors are statistical.

70-90%

p_{T} (GeV/c)	$(\mathscr{A} \times \varepsilon)_{\mathrm{J}/\psi} \pm stat(\%) \pm syst(\%)$
0-0.3	0.1522 ± 0.0052 (3.4)
0.3-1	0.1385 ± 0.0019 (1.4)
0.3-0.65	0.1457 ± 0.0029 (2.0)
0.65-1	0.1332 ± 0.0025 (1.8)
1-2	0.1193 ± 0.0014 (1.2)
2-3	0.1233 ± 0.0017 (1.4)
3-4	0.1513 ± 0.0025 (1.6)
4-5	0.1949 ± 0.0038 (1.9)
5-6	0.2422 ± 0.0058 (2.4)
6-7	0.2920 ± 0.0086 (2.9)
7-8	0.3336 ± 0.0126 (3.8)
8-10	0.3721 ± 0.0143 (3.9)
10-12	0.3971 ± 0.0271 (6.8)

Table F.5: $(\mathscr{A} \times \varepsilon)^{\mathrm{J}/\psi}_{\mathrm{AA}}(\Delta y, \Delta p_{\mathrm{T}})$ in 70-90% integrated in rapidity. The quoted errors are statistical.

centrality (%)	$(\mathscr{A} \times \varepsilon)_{\mathrm{J}/\psi} \pm stat(\%)$
0-10	0.1138 ± 0.0002 (0.15)
10-30	0.1190 ± 0.0001 (0.1)
30-50	0.1226 ± 0.0001 (0.1)
50-70	0.1239 ± 0.0001 (0.1)
70-90	0.1245 ± 0.0001 (0.1)

Table F.6: $(\mathscr{A} \times \varepsilon)^{\mathrm{J}/\psi}_{\mathrm{AA}}(\Delta y, \Delta p_{\mathrm{T}})$ from embedding STARLIGHT simulations for $p_{\mathrm{T}} < 0.3$ GeV/c and $-4 < y < -2.5$. The quoted errors are statistical.

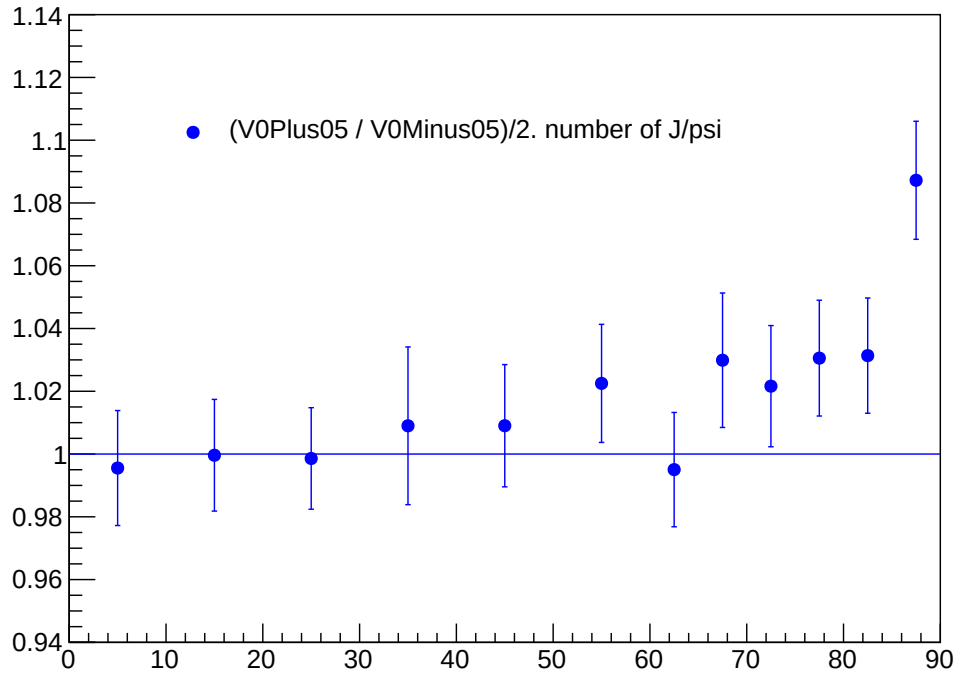

Fig. G.1: Ratio of the number of J/ψ using the centrality estimators V0Mplus05 and V0Mminus05 for the 2015 data sample. The blue star markers are the highest deviation in each centrality class.

G Results J/ψ R_{AA}

0-10%

p_{T} (GeV/c)	$R_{\mathrm{AA}}^{\mathrm{J}/\psi} \pm stat(\%) \pm syst(\%)$
0-0.3	0.74 ± 0.07 (9.7) ± 0.06 (8.1)
0.3-1	0.76 ± 0.02 (3.0) ± 0.05 (7.1)
0.3-0.65	0.77 ± 0.04 (4.6) ± 0.05 (6.9)
0.65-1	0.78 ± 0.03 (3.7) ± 0.05 (6.0)
1-2	0.71 ± 0.01 (1.9) ± 0.05 (6.9)
2-3	0.66 ± 0.01 (2.0) ± 0.04 (6.6)
3-4	0.50 ± 0.01 (2.3) ± 0.03 (6.7)
4-5	0.38 ± 0.01 (3.0) ± 0.02 (6.4)
5-6	0.32 ± 0.01 (3.5) ± 0.02 (5.9)
6-7	0.26 ± 0.01 (4.3) ± 0.02 (5.8)
7-8	0.26 ± 0.01 (5.8) ± 0.01 (5.8)
8-9	0.25 ± 0.02 (7.0) ± 0.01 (5.3)
9-10	0.23 ± 0.02 (9.5) ± 0.01 (5.9)
10-12	0.24 ± 0.02 (9.2) ± 0.01 (5.6)
12-15	0.22 ± 0.04 (16.5) ± 0.02 (7.3)

Table G.1: J/ψ nuclear modification factor in each p_{T} range in the centrality class 0-10% in $-4 < y < -2.5$. The quoted errors are statistical and uncorrelated systematic uncertainty. The correlated over p_{T} systematic uncertainty (not included) is 2.472% in this centrality class.

10-30%

p_{T} (GeV/c)	$R_{\mathrm{AA}}^{\mathrm{J}/\psi} \pm stat(\%) \pm syst(\%)$
0-0.3	0.84 ± 0.06 (6.9) ± 0.07 (7.9)
0.3-1	0.71 ± 0.02 (2.8) ± 0.05 (7.0)
0.3-0.65	0.72 ± 0.03 (3.9) ± 0.05 (6.3)
0.65-1	0.73 ± 0.02 (3.3) ± 0.04 (6.0)
1-2	0.67 ± 0.01 (1.7) ± 0.05 (6.9)
2-3	0.64 ± 0.01 (1.8) ± 0.04 (6.7)
3-4	0.53 ± 0.01 (1.9) ± 0.04 (6.7)
4-5	0.44 ± 0.01 (2.4) ± 0.03 (6.3)
5-6	0.39 ± 0.01 (2.8) ± 0.02 (5.8)
6-7	0.35 ± 0.01 (3.5) ± 0.02 (5.8)
7-8	0.33 ± 0.02 (4.7) ± 0.02 (6.1)
8-9	0.33 ± 0.02 (6.0) ± 0.02 (5.2)
9-10	0.29 ± 0.03 (9.3) ± 0.02 (5.5)
10-12	0.34 ± 0.03 (7.7) ± 0.02 (5.5)
12-15	0.34 ± 0.04 (12.5) ± 0.02 (6.0)

Table G.2: J/ψ nuclear modification factor in each p_{T} range in the centrality class 10-30% in $-4 < y < -2.5$. The quoted errors are statistical and uncorrelated systematic uncertainty. The correlated over p_{T} systematic uncertainty (not included) is 2.377% in this centrality class.

30-50%

p_{T} (GeV/c)	$R_{\mathrm{AA}}^{\mathrm{J}/\psi} \pm stat(\%) \pm syst(\%)$
0-0.3	1.06 ± 0.07 (6.4) ± 0.08 (7.7)
0.3-1	0.63 ± 0.02 (3.4) ± 0.04 (7.1)
0.3-0.65	0.65 ± 0.03 (5.3) ± 0.04 (6.3)
0.65-1	0.64 ± 0.02 (3.9) ± 0.04 (6.2)
1-2	0.61 ± 0.01 (2.2) ± 0.04 (6.9)
2-3	0.63 ± 0.01 (2.0) ± 0.04 (6.6)
3-4	0.57 ± 0.01 (2.1) ± 0.04 (6.5)
4-5	0.54 ± 0.01 (2.5) ± 0.03 (6.3)
5-6	0.50 ± 0.01 (3.0) ± 0.03 (5.9)
6-7	0.48 ± 0.02 (3.5) ± 0.03 (5.9)
7-8	0.48 ± 0.02 (5.1) ± 0.03 (6.1)
8-9	0.46 ± 0.03 (6.7) ± 0.02 (5.3)
9-10	0.44 ± 0.05 (10.5) ± 0.02 (5.5)
10-12	0.47 ± 0.05 (11.3) ± 0.03 (5.5)
12-15	0.47 ± 0.07 (14.0) ± 0.03 (6.1)

Table G.3: J/ψ nuclear modification factor in each p_{T} range in the centrality class 30-50% in $-4 < y < -2.5$. The quoted errors are statistical and uncorrelated systematic uncertainty. The correlated over p_{T} systematic uncertainty (not included) is 2.737% in this centrality class.

50-70%

p_{T} (GeV/c)	$R_{\mathrm{AA}}^{\mathrm{J}/\psi} \pm stat(\%) \pm syst(\%)$
0-0.3	2.72 ± 0.14 (5.3) ± 0.21 (7.7)
0.3-1	0.68 ± 0.03 (3.8) ± 0.05 (7.6)
0.3-0.65	0.70 ± 0.04 (5.6) ± 0.04 (6.4)
0.65-1	0.66 ± 0.03 (4.9) ± 0.04 (6.1)
1-2	0.67 ± 0.02 (2.6) ± 0.05 (6.9)
2-3	0.68 ± 0.02 (2.5) ± 0.04 (6.6)
3-4	0.69 ± 0.02 (2.7) ± 0.04 (6.5)
4-5	0.67 ± 0.02 (3.0) ± 0.04 (6.4)
5-6	0.65 ± 0.02 (3.8) ± 0.04 (6.0)
6-7	0.67 ± 0.03 (4.5) ± 0.04 (5.8)
7-8	0.66 ± 0.04 (6.0) ± 0.04 (6.1)
8-10	0.64 ± 0.06 (10.1) ± 0.03 (5.3)
10-12	0.62 ± 0.09 (15.1) ± 0.03 (5.5)
12-15	0.76 ± 0.11 (14.9) ± 0.05 (6.5)

Table G.4: J/ψ nuclear modification factor in each p_{T} range in the centrality class 50-70% in $-4 < y < -2.5$. The quoted errors are statistical and uncorrelated systematic uncertainty. The correlated over p_{T} systematic uncertainty (not included) is 3.627% in this centrality class.

70-90%

p_{T} (GeV/c)	$R_{\mathrm{AA}}^{\mathrm{J}/\psi} \pm stat(\%) \pm syst(\%)$
0-0.3	10.28 ± 0.59 (5.8) ± 0.78 (7.6)
0.3-1	1.10 ± 0.05 (4.7) ± 0.08 (6.9)
0.3-0.65	1.33 ± 0.10 (7.3) ± 0.08 (6.4)
0.65-1	0.98 ± 0.08 (8.3) ± 0.06 (6.1)
1-2	0.85 ± 0.03 (3.9) ± 0.06 (7.3)
2-3	0.79 ± 0.03 (4.0) ± 0.05 (6.6)
3-4	0.79 ± 0.04 (4.7) ± 0.05 (6.5)
4-5	0.81 ± 0.04 (5.5) ± 0.05 (6.3)
5-6	0.74 ± 0.05 (7.2) ± 0.05 (6.1)
6-7	0.73 ± 0.06 (8.8) ± 0.04 (5.7)
7-8	0.80 ± 0.09 (11.5) ± 0.05 (5.7)
8-10	0.75 ± 0.10 (12.8) ± 0.05 (6.8)
10-12	0.82 ± 0.15 (18.4) ± 0.06 (7.9)

Table G.5: J/ψ nuclear modification factor in each p_{T} range in the centrality class 70-90% in $-4 < y < -2.5$. The quoted errors are statistical and uncorrelated systematic uncertainty. The correlated over p_{T} systematic uncertainty (not included) is 4.562% in this centrality class.

Centrality class	$N^{raw}_{J/\psi}$	$N^{hadro}_{J/\psi}$	$N^{excess}_{J/\psi}$
0-10%	$8351 \pm 762 \pm 312$	$8083 \pm 369 \pm 863$	$268 \pm 847 \pm 918$
10-30%	$9624 \pm 571 \pm 278$	$7760 \pm 293 \pm 874$	$1864 \pm 642 \pm 917$
30-50%	$4280 \pm 225 \pm 105$	$2396 \pm 124 \pm 241$	$1884 \pm 257 \pm 263$
50-70%	$2763 \pm 98 \pm 68$	$660 \pm 45 \pm 60$	$2103 \pm 108 \pm 91$
70-90%	$1758 \pm 57 \pm 32$	$179 \pm 21 \pm 30$	$1579 \pm 61 \pm 44$

Table H.1: Number of J/ψ from hadronic production obtained with the yield parametrization and the corresponding number of J/ψ in excess for $p_T < 0.3$ GeV/c.

H Additionnal check with the corrected yield

The number of hadronic J/ψ can be extracted from a fit of the corrected yield obtained from the formula 20. The corrected yield was fitted with a power law function. We tested several fitting ranges starting from 0, 0.3, 0.65 and 1 GeV/c and going to 15 GeV/c. In central collisions, we considered every tests in the final results whereas in 30-50% and 50-70% the test considering the result in 0-0.3 GeV/c was removed due to a large contribution of the coherent photoproduction and in 70-90% only tests starting at least from 0.65 GeV/c were considered to remove contributions from coherent and incoherent photoproduction. Figure H.1 shows examples of the fit to the J/ψ invariant yield for the five centrality classes. As it was done for the pp cross section obtained from the parametrization, we considered on each point :

- the quadratic sum of the statistical and uncorrelated systematic uncertainties to evaluate the weighted average of the number of hadronic J/ψ and the standard deviation on the results.
- the statistical uncertainty only to get the combined statistical uncertainty.
- the uncorrelated systematic uncertainty only to get the combined systematic uncertainty.

Finally the number of hadronic J/ψ is calculated as the weighted average of all test results. The combined statistical uncertainty is given by the weighted average of the individual statistical uncertainties. And the total uncorrelated systematic uncertainty is given by the quadratic sum of the standard deviation and the combined systematic uncertainty given by the weighted average of the individual systematic uncertainties.

The fit performed in 1 to 15 GeV/c and considering on each point the quadratic sum of the statistical and uncorrelated systematic uncertainties was also used to extract the $\langle p_T \rangle$ of the hadronic J/ψ distribution. We found 2.09 GeV/c, 2.20 GeV/c, 2.35 GeV/c, 2.44 GeV/c and 2.34 GeV/c in the centrality class 0-10%, 10, 30%, 30-50%, 50-70% and 70-90%, respectively.

Table H.1 reports the number of hadronic J/ψ extracted from the fit and the corresponding number of J/ψ in excess evaluated by subtracted the number of hadronic J/ψ to the raw number of J/ψ. The significance of the excess reaches 21.1σ in the most peripheral centrality class. The significance amounts 14.9σ and 5.1σ in the centrality class 50-70% and 30-50%, respectively.

These results are compared to those obtained with the parameterisation method described in section 8. The values are comptible within $\sim 0.7\sigma_{\text{syst}}$.

Centrality class	$N_{\mathrm{J}/\psi}^{\text{excess param}}$	$N_{\mathrm{J}/\psi}^{\text{excess yield}}$
0-10%	$-659 \pm 767 \pm 1145$	$268 \pm 847 \pm 918$
10-30%	$1140 \pm 574 \pm 946$	$1864 \pm 642 \pm 917$
30-50%	$1691 \pm 226 \pm 221$	$1884 \pm 257 \pm 263$
50-70%	$2089 \pm 98 \pm 79$	$2103 \pm 108 \pm 91$
70-90%	$1620 \pm 57 \pm 33$	$1579 \pm 61 \pm 44$

Table H.2: Number of J/ψ from hadronic production obtained with the yield parametrization and compared to the number obtained with the full parametrization for $p_{\mathrm{T}} < 0.3$ GeV/c.

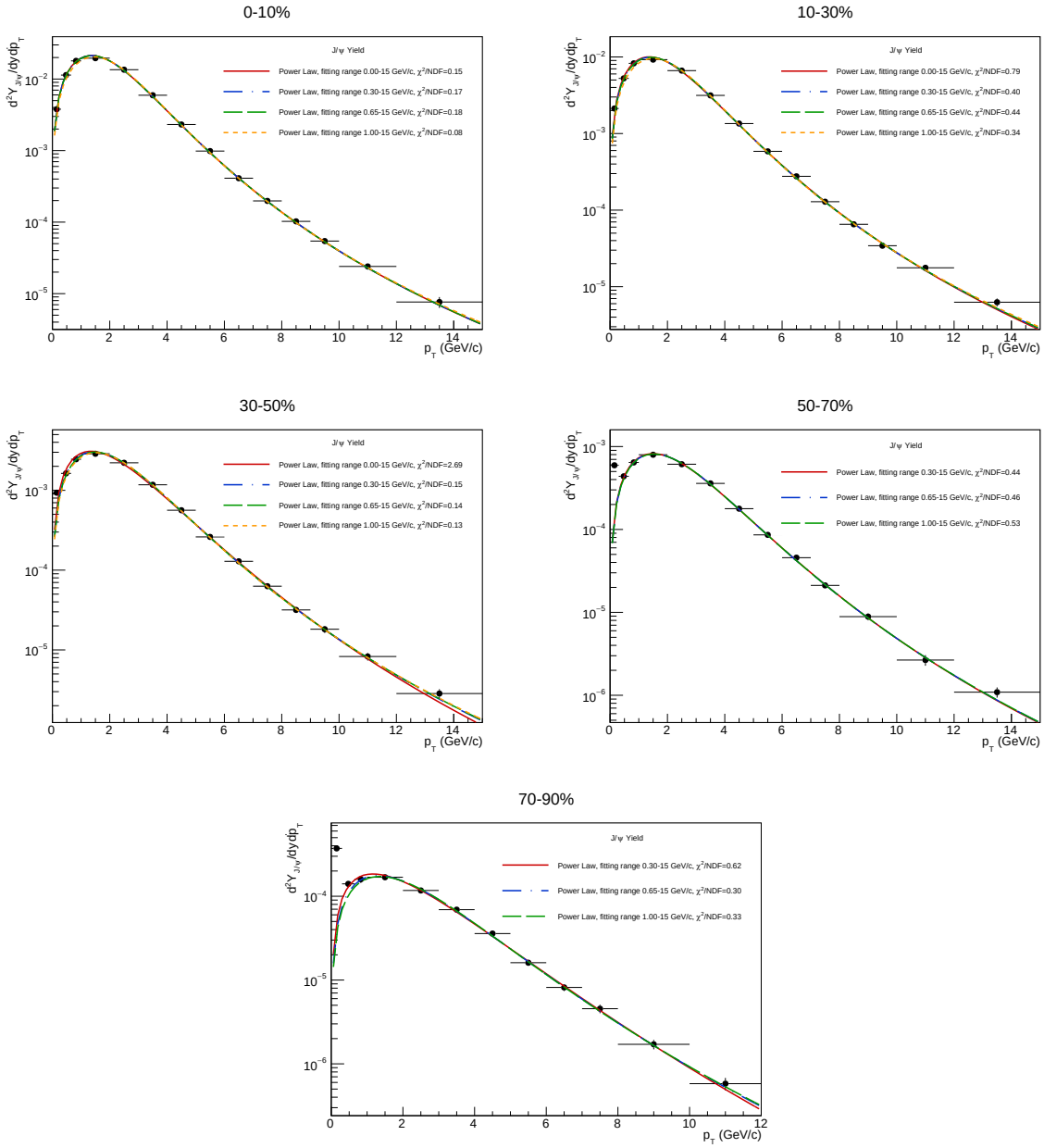

Fig. H.1: Fit of the J/ψ invariant yield as a function of p_{T} with a power law function for the five centrality classes. The uncertainty on each data point is the qadratic sum of the statistical and uncorrelated systematic uncertainty.

References

[1] **ALICE** Collaboration, S. Aziz and N. Valle, "Z boson production in Pb–Pb collisions at $\sqrt{s_{NN}} = 5.02$ TeV,". https://alice-notes.web.cern.ch/node/952.

[2] **ALICE** Collaboration, "Centrality determination in heavy ion collisions,". https://cds.cern.ch/record/2636623.

[3] **ALICE** Collaboration, "Quarkonium signal extraction in ALICE,". http://cds.cern.ch/record/2060096.

[4] **ALICE** Collaboration, A. Morreale, " J/ψ and ψ(2S) cross sections in pp collisions at $\sqrt{s} = 13$ TeV.,". https://alice-notes.web.cern.ch/node/497.

[5] **ALICE** Collaboration, C. Huang and H. Hushnud, "J/ψ production in pp collisions at $\sqrt{s} = 5.02$ TeV with the 2017 data sample,". https://alice-notes.web.cern.ch/node/909.

[6] **Particle Data Group** Collaboration, M. Tanabashi *et al.*, "Review of Particle Physics," *Phys. Rev. D* **98** no. 3, (2018) 030001.

[7] O. Bugnon. https://indico.cern.ch/event/796503/contributions/3359823/attachments/1822060/2980665/MuonTrackingEfficiency_PbPb5TeV.pdf. Presentation in Workshop.

[8] D. Stocco. https://indico.cern.ch/event/482176/contributions/2000604/attachments/1218555/1780620/mtrChEff_2015.pdf. Presentation in Workshop.

[9] **ALICE** Collaboration, C. Huang, "p_{T}-differential production of J/ψ in Pb-Pb collisions at $\sqrt{s} = 5.02$ TeV with the 2015 and 2018 data samples,". https://alice-notes.web.cern.ch/node/981.

[10] **ALICE** Collaboration, R. Arnaldi, "J/ψ production in Pb-Pb collisions at $\sqrt{s} = 5.02$ TeV.,". https://alice-notes.web.cern.ch/node/486.

[11] **ALICE** Collaboration, O. V. Baillie, "Forward J/ψ photoproduction in ultra-peripheral in Pb-Pb collisions at $\sqrt{s} = 5.02$ TeV.,". https://alice-notes.web.cern.ch/node/596.

[12] **ALICE** Collaboration, S. Acharya *et al.*, "Coherent J/ψ photoproduction at forward rapidity in ultra-peripheral Pb-Pb collisions at $\sqrt{s_{\mathrm{NN}}} = 5.02$ TeV" *Phys. Lett. B* **798** (2019) 134926, arXiv:1904.06272 [nucl-ex].

[13] **ALICE** Collaboration, I. C. Arsene, "Low p_{T} J/ψ excess at mid-rapidity in Pb-Pb collisions at $\sqrt{s} = 5.02$ TeV.,". https://alice-notes.web.cern.ch/node/607.

[14] J. Cepila, J. G. Contreras, and M. Krelina, "Coherent and incoherent J$/\psi$ photonuclear production in an energy-dependent hot-spot model," *Phys. Rev. C* **97** no. 2, (2018) 024901, arXiv:1711.01855 [hep-ph].

[15] M. Gay Ducati and S. Martins, "Heavy meson photoproduction in peripheral AA collisions," *Phys. Rev. D* **97** no. 11, (2018) 116013, arXiv:1804.09836 [hep-ph].

[16] **ALICE** Collaboration, J. Adam *et al.*, "Measurement of an excess in the yield of J/ψ at very low p_{T} in Pb-Pb collisions at $\sqrt{s_{\mathrm{NN}}} = 2.76$ TeV," *Phys. Rev. Lett.* **116** no. 22, (2016) 222301, arXiv:1509.08802 [nucl-ex].

[17] W. Zha, S. Klein, R. Ma, L. Ruan, T. Todoroki, Z. Tang, Z. Xu, C. Yang, Q. Yang, and S. Yang, "Coherent J/ψ photoproduction in hadronic heavy-ion collisions," *Phys. Rev. C* **97** no. 4, (2018) 044910, arXiv:1705.01460 [nucl-th].

[18] **ALICE** Collaboration, L. M. Massacrier, "Measurement of an excess in the yield of J/ψ at very low p_{T} in Pb-Pb collisions at $\sqrt{s} = 5.02$ TeV.,". https://alice-notes.web.cern.ch/node/847.